water

MDPI

Article

Application of MODFLOW with Boundary Conditions Analyses Based on Limited Available Observations: A Case Study of Birjand Plain in East Iran

Reza Aghlmand [1] and Ali Abbasi [1,2,*]

[1] Department of Civil Engineering, Faculty of Engineering, Ferdowsi University of Mashhad, Mashhad 9177948974, Iran; rezaaghlmandcivil@gmail.com

[2] Faculty of Civil Engineering and Geosciences, Water Resources Section, Delft University of Technology, Stevinweg 1, 2628 CN Delft, The Netherlands

* Correspondence: a.abbasi@tudelft.nl or aabbasi@um.ac.ir; Tel.: +31-15-2781029

Received: 18 July 2019; Accepted: 9 September 2019; Published: 12 September 2019

Abstract: Increasing water demands, especially in arid and semi-arid regions, continuously exacerbate groundwater resources as the only reliable water resources in these regions. Groundwater numerical modeling can be considered as an effective tool for sustainable management of limited available groundwater. This study aims to model the Birjand aquifer using GMS: MODFLOW groundwater flow modeling software to monitor the groundwater status in the Birjand region. Due to the lack of the reliable required data to run the model, the obtained data from the Regional Water Company of South Khorasan (RWCSK) are controlled using some published reports. To get practical results, the aquifer boundary conditions are improved in the established conceptual method by applying real/field conditions. To calibrate the model parameters, including the hydraulic conductivity, a semi-transient approach is applied by using the observed data of seven years. For model performance evaluation, mean error (ME), mean absolute error (MAE), and root mean square error (RMSE) are calculated. The results of the model are in good agreement with the observed data and therefore, the model can be used for studying the water level changes in the aquifer. In addition, the results can assist water authorities for more accurate and sustainable planning and management of groundwater resources in the Birjand region.

Keywords: groundwater modeling; GMS: MODFLOW; Birjand aquifer; calibration process

1. Introduction

Groundwater is a major source for drinking water, agricultural and industrial uses in arid and semi-arid regions. About 94.8% of Iran has an arid and semi-arid climate with low precipitation and high evapotranspiration rate and therefore, faces water scarcity [1,2]. It is estimated that around 98.7% of freshwater is available as groundwater [3].

Due to less vulnerability to pollution and high reliability, groundwater resources are commonly preferred for drinking water supply [4]. Groundwater is often not affected by short-term drought and therefore, can be considered as a reliable drinking water resource. However, it is difficult to obtain precise knowledge of aquifers because they are not visible like surface waters [5].

Groundwater models are the backbones of water resource planning and management in (semi) arid areas [6]. Nowadays, numerical modeling is considered an important tool for studying groundwater resources [7]. Generally, in groundwater models, a simplified mathematical representation of a groundwater system is solved by a computer program [8]. These models need

varieties of information—including geology, hydrogeology, hydrology, climatology, geography, etc.—to simulate the quantity/quality of the groundwater resources [9]. However, collecting such information, especially in developing countries, is a challenge and suffers from a high degree of uncertainty [10]. Quality of the input data in groundwater models has a significant effect on the model results. In other words, to get the accurate results, accurate input data should be ingested in the model [11]. Accordingly, the input data should be quality controlled and have the required resolution.

In this study, a three-dimensional, block-centered (cell-centered), steady-state, finite difference model, MODFLOW (McDonald and Harbaugh [12]) is employed to quantify groundwater in Birjand plain, South Khorasan, Iran. In recent years, GMS: MODFLOW model (Groundwater Modeling System) has been successfully developed and published in a large number of groundwater quantitative and qualitative studies because of its simple methods, modular program structure, and separate packages to resolve special hydrogeological problems [10,13–30]. This model, with a graphical user interface (GUI), can be integrated with geographic information system (GIS) to provide an appropriate visual environment for groundwater resources evaluation and management [15]. MODFLOW is considered an international standard for simulating and predicting groundwater conditions and groundwater/surface-water interactions [31]. Although MODFLOW has been applied for Birjand Plain in some literature, the real conditions—including source/sinks, recharges, extractions, return flows, soil coverage, etc.—have not been considered in detail. To fill these available gaps in the literature and previous studies conducted about Birjand aquifer, the boundary conditions as well as the input parameters in the model have been improved to reduce the bias of the simulated parameters such as hydraulic head distribution in the aquifer. To reach this aim, the limited available data are investigated and applied in the model effectively. Due to the lack of required data time series (such as head and flow), a semi-transient approach is applied to calibrate the parameters. In the GMS: MODFLOW, there are only two main approaches including steady-state and transient. Using a semi-transient approach allows consideration of the changes of the parameters in the study time period.

In the current research, the available data and the measurements are analyzed regarding their quality. Then, these data are prepared to use in the numerical model of Birjand aquifer. The data has been received from the Regional Water Company of South Khorasan (RWCSK), to construct the aquifer mathematical model.

In addition, the boundary conditions of the model are revised according to the available information. Using the measured values, the required parameters in the model are calibrated using a semi-transient method. Results show that the prepared model can be used in Birjand aquifer investigations and for predictions of the aquifer conditions under different development scenarios in the region.

2. Materials and Methods

2.1. Study Area

According to Iran Water Resources Management Company (IWRMC) [32], the number of deep and semi-deep wells utilized for extracting groundwater has been increased as shown in Figure 1. It should be noted that the shown numbers of wells in Figure 1 include only the authorized wells that have been licensed for exploitation. Unfortunately, the total number of groundwater extracting wells (either with license or without one) in the country is much higher than the available numbers in Figure 1. For the study region, the situation is the same. In Figure 2, the consumption of groundwater in different uses in South Khorasan province is shown. Groundwater is the main source of water supply for all types of uses in this region.

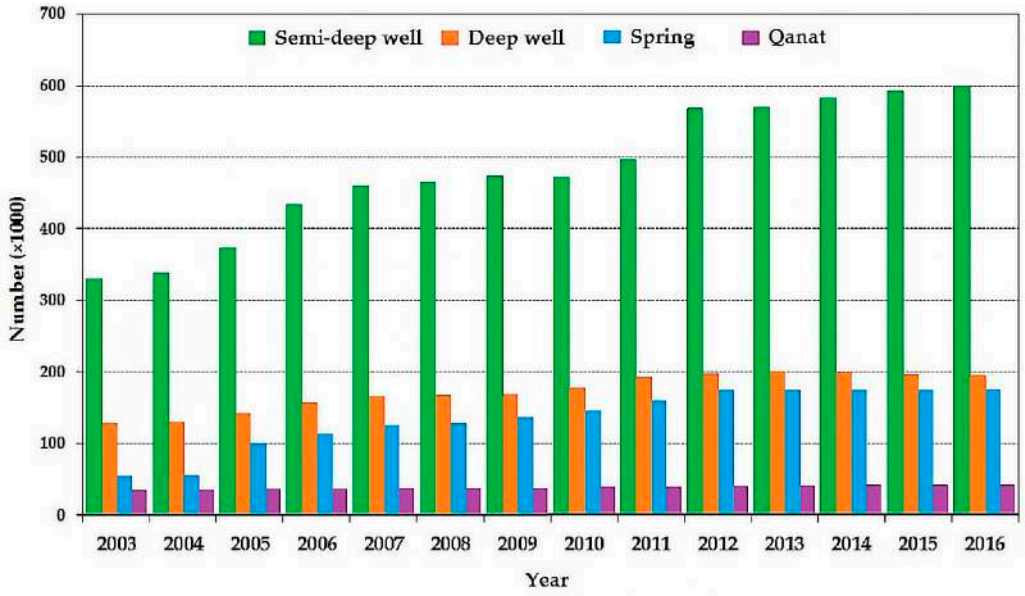

Figure 1. The number of deep and semi-deep wells, qanats, and springs in the period of 2003 to 2016 in Iran [32].

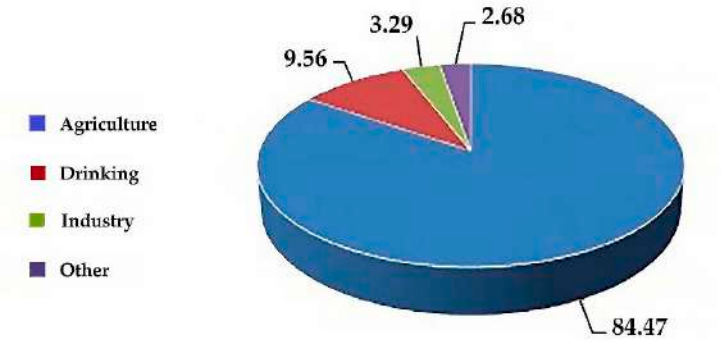

Figure 2. Percentage of groundwater use in different sections in South Khorasan province [33].

Birjand watershed, which includes the Birjand plain and the Birjand aquifer, is located in latitude and longitude of 32°36′ N to 33°8′ N and 58°41′ E to 59°44′ E, respectively. The location of the study region is shown in Figure 3. Birjand aquifer is located in an arid climate. The minimum, maximum, and the average temperatures recorded for the period 1989–2017 are −7.6, 38.3, and 16.6 °C, respectively. Due to the aridity of the region, the average annual precipitation is reported to be about 158 mm and hence, there is no perennial stream in this area. The slope of the ground surface gradually decreases from the eastern part toward the west. The western parts of the study area are almost flat as shown in Figure 3. The length of Birjand aquifer is about 55.0 km and the width in the middle is about 6.0 km. The average long-term temperatures in the eastern and western parts of the Birjand watershed are about 14 and 16 °C, respectively. Also, the average long-term annual precipitation in the easternmost part is about 160 mm, while in the westernmost part of the desired area is about 120 mm. Minimum and maximum annual evaporation occur in the easternmost part (2200 mm) and westernmost part of the watershed (3400 mm), respectively. Due to over-exploitation of Birjand aquifer through both authorized and unauthorized wells in the study area, this aquifer has been declared a prohibited aquifer. About 80% of groundwater discharge in the study area occurs through deep and semi-deep wells and the rest occurs through springs and qanats [34].

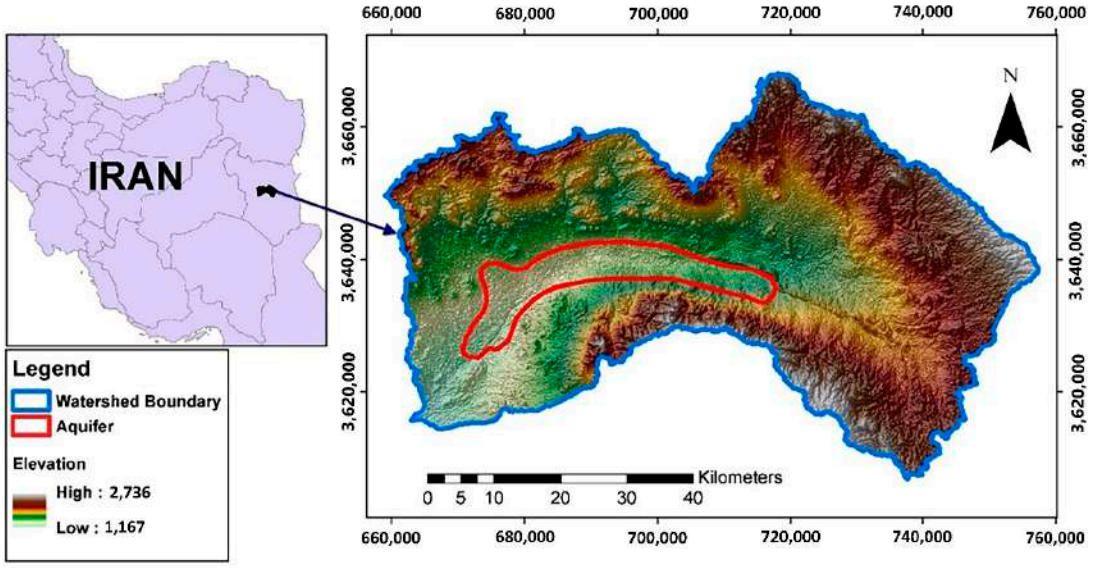

Figure 3. Location of Birjand watershed and Birjand Aquifer in South Khorasan Province, Iran [35].

The groundwater level in Birjand plain, like most other plains in Iran, are continuing to decline due to long-term droughts and excessive extraction, especially by the agriculture sector. Over a 30-year period from 1987 to 2018, the average monthly groundwater level has dropped from 1354.22 m to 1340.51 m (i.e., drawdown about 14.0 m). It means that the water level in Birjand aquifer, as the main source of water supply in the city of Birjand, has declined annually by an average of about 0.45 m over the past 30 years (Figure 4). Consequently, the total deficit of the Birjand groundwater reservoir has been 193.63 million cubic meters (MCM) with an average annual deficit of 6.45 MCM. This situation shows that the Birjand plain has been in a severe water crisis [36].

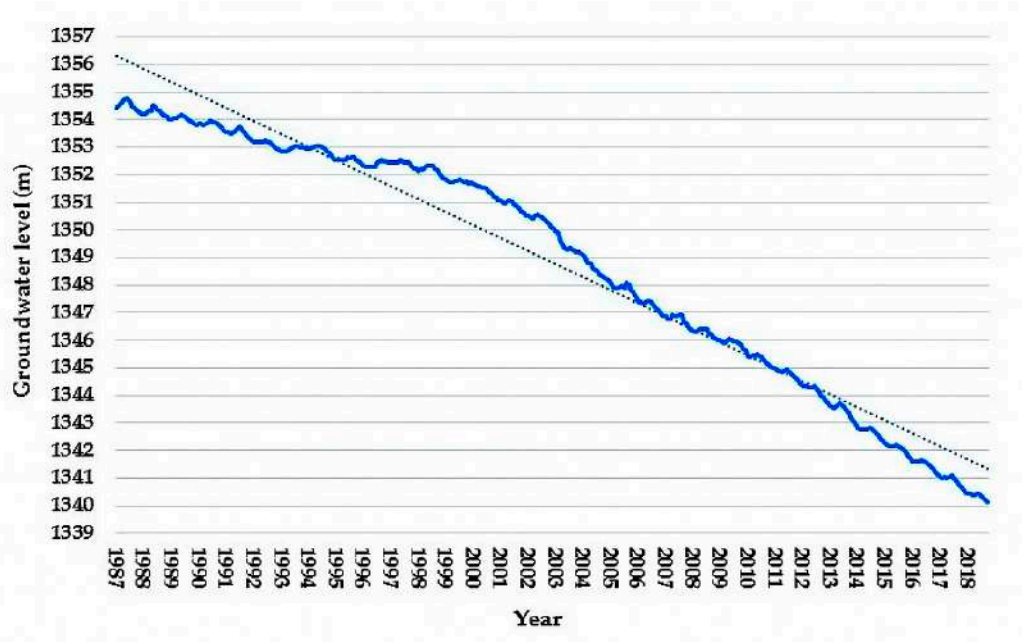

Figure 4. Groundwater hydrograph of Birjand Plain during a 30-year period.

Birjand aquifer is unconfined and in the context of climate change, unconfined aquifers in arid and semi-arid areas compared with ones in wet/rainy areas are more vulnerable. The reason is that the occurrence of droughts in arid and semi-arid areas exacerbates the aquifer's condition through

decreasing in aquifer recharge [37]. This factor, along with other factors such as population growth and increasing demand, leads to a continuous decrease in groundwater resources in these areas.

Investigating the geological maps of the Birjand plain area shows that the Birjand aquifer structure totally is related to the quaternary formation, dating from the quaternary period. The quaternary period began about two and a half million years ago and continues today, and is, in fact, the newest geological period. Therefore, from a geological point of view, the whole body of the Birjand aquifer consists of young deposits (Figure 5). The young quaternary deposits include sediments that are eroded and deposited by rivers in this area and are generally coarse-grained rock material. It should be noted that the young quaternary deposits that cover the whole Birjand aquifer have the highest share (about 25%) among the lithological units of the entire Birjand watershed.

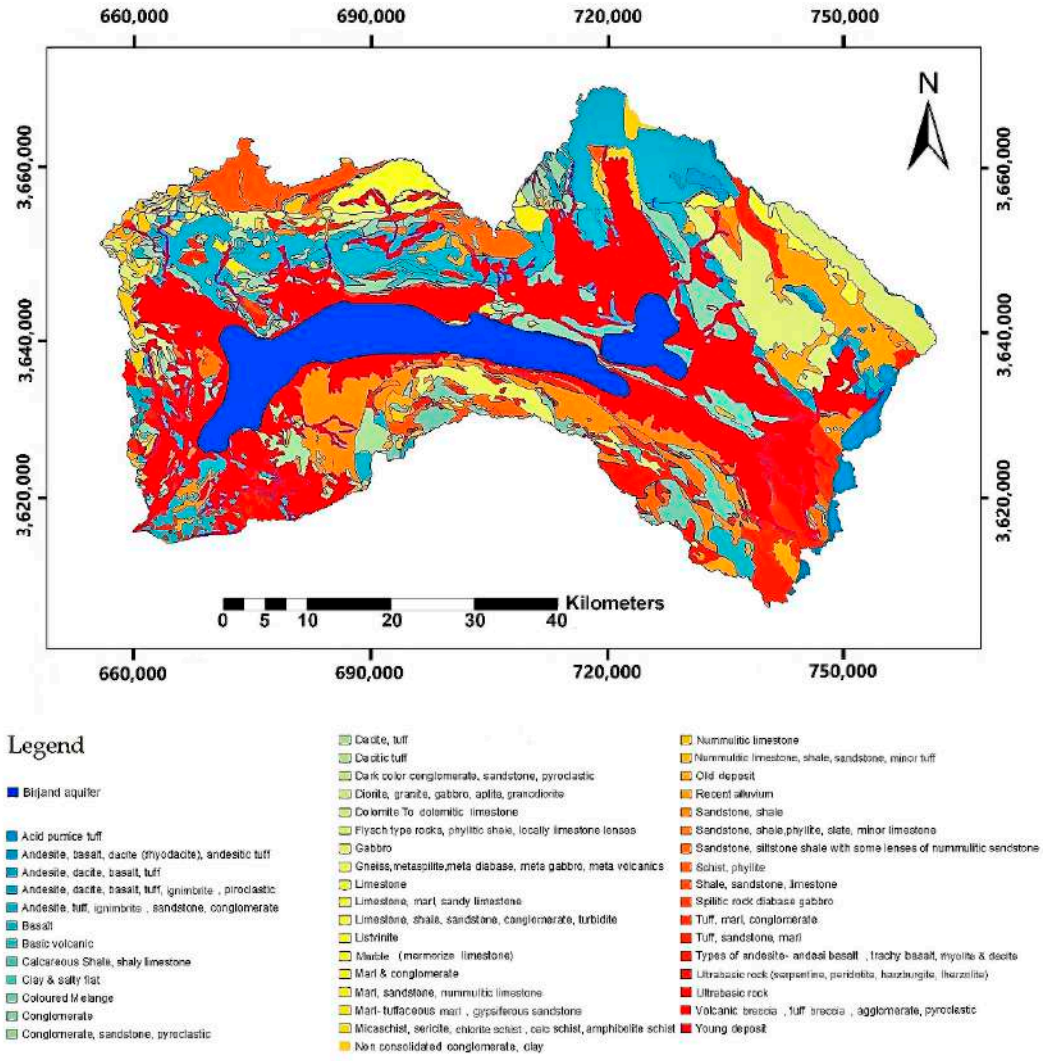

Figure 5. Birjand watershed geological map.

Regarding the soil properties, the southern, eastern, and northern parts of the Birjand watershed are composed of high and relatively high mountains consisting of limestone, metamorphic rock, conglomerate, sandstone, and shale rocks. These areas are generally vegetation-free or with little vegetation. The central parts of the Birjand watershed are related to lowlands with relatively mild slopes. The central parts mainly have very deep soils, consisting of sedimentary rivers. The western part of the Birjand watershed also has relatively high hills, consisting of metamorphic rocks and shale in the north-facing part; and in the central- and south-facing parts: limestone, dolomitic, and

sandstone—generally coarse-grained. These areas are generally vegetation-free or very low on vegetation and have low/very low-deep soils.

As seen in Figure 6, there are two aquifers in the Birjand watershed including Birjand aquifer and Marak aquifer. The areas of the Birjand and Marak aquifers are 277.8 km^2 and 53.72 km^2, respectively. These two aquifers are separated from each other due to the rising bedrock elevation between them.

Figure 6. The study area and the exact location of Birjand and Marak aquifers.

2.2. Groundwater Modeling of Birjand Aquifer

Understanding a groundwater system usually requires drilling a large number of exploratory wells, drilling, and pumping operations, and conducting multiple geophysical experiments and a series of long-term experiments, which are expensive and time-consuming. Unfortunately, in the study area, very few field operations and surveys have been carried out and therefore, modeling the groundwater flow through a mathematical model can be very promising.

There are some groundwater modeling programs which were developed on the basis of various methods. The most famous models (GUIs) are Visual Modular Three-Dimensional Finite-Difference Flow Model (Visual MODFLOW) [38], Finite Element Subsurface Flow System (FEFLOW) [39], Groundwater Modeling System (GMS) [40], etc. FEFLOW, which uses the finite element method for modeling, and GMS and Visual MODFLOW are the most popular software packages applied in groundwater studies [14,19,41–52].

The GMS software is a graphical user interface for many groundwater models such as FEMWATER, SEEP2D, SEAM3D, MT3DMS, MODFLOW (with many packages), RT3D, MODPATH, MODAEM, and SEAWAT. In this study, the MODFLOW model has been chosen due to its high efficiency and its extensive use in groundwater studies. This model simulates the flow in three dimensions using finite difference method for both steady-state and transient conditions. The MODFLOW numerical model is constructed based on the combination of two basic equations—the Darcy equation and the principle of conservation of mass, or mass balance.

2.2.1. Governing Equations

The three-dimensional groundwater flow with constant density through a heterogeneous and anisotropic porous medium can be described by the equation [12]

$$\frac{\partial}{\partial x}\left(K_{xx}\frac{\partial h}{\partial x}\right)+\frac{\partial}{\partial y}\left(K_{yy}\frac{\partial h}{\partial y}\right)+\frac{\partial}{\partial z}\left(K_{zz}\frac{\partial h}{\partial z}\right)\pm W=S_s\frac{\partial h}{\partial t} \quad (1)$$

where K_{xx}, K_{yy}, and K_{zz} are hydraulic conductivity coefficients (L/T) in x, y, and z directions, respectively; h is the pressure head (L); S_s is specific storage (1/L); and W is recharge/discharge rate per unit volume (1/T). The environment is unconfined, isotropic, and heterogeneous ($K_{xx} = K_{yy} = K_{zz} = K$), and hence, the governing equation based on Dupuit assumptions [53] in two-dimensional form can be written as

$$\frac{\partial}{\partial x}\left(Kh\,\frac{\partial h}{\partial x}\right)+\frac{\partial}{\partial y}\left(Kh\,\frac{\partial h}{\partial y}\right)\pm W = S_y\frac{\partial h}{\partial t} \quad (2)$$

where S_y is the specific yield (dimensionless).

Due to the lack of long-term monitoring data for observational/operational wells, amounts of inflow/outflow to/from the Birjand aquifer are unknown and therefore, the simulations are limited to steady-state conditions. Although applying the steady-state groundwater model simulation in Birjand aquifer is a forced choice, we are trying to consider the real-world conditions in the modeling.

2.3. Groundwater Conceptual Model of Birjand Aquifer

The first and most important step in groundwater modeling is constructing the conceptual model of the groundwater system [54], which represent a simplified version of the actual aquifer system. Due to the complexity of the hydrogeological system, as well as the lack of data in the study region, the conceptual model and its structure is applied according to the available data [55]. Establishing the groundwater conceptual model in the study region suffers from many challenges including:

- Lack of adequate knowledge and incomplete information about the physical properties of alluvial deposits of plain, which is the main reservoir of groundwater;
- Lack of adequate and accurate statistics and information on meteorological and climatic parameters and other parameters in the study area for estimating the water balance components;
- Lack of sufficient observation wells and other observations in the area;
- Lack of accurate and adequate statistics and criteria on the method and extent of utilization of Birjand groundwater resource;
- Lack of sufficient exploratory wells in the study plain to understand the physical and geometric characteristics of the aquifer;
- Error in piezometer recorded values;
- Lack of adequate pumping tests in the study area and therefore, lack of sufficient information on the hydrodynamic coefficients of the aquifer;
- Lack of sufficient understanding of the hydraulic behavior of an aquifer's surrounding formations and their relationship with the aquifer, and the consequent lack of proper and precise definition of boundary conditions;
- Lack of sufficient information on the hydraulic connections between surface water (e.g., river or lake) and groundwater resources;
- Lack of sufficient information for calculating agricultural, urban, and industrial backwaters;

The different steps for developing the conceptual model of the Birjand aquifer are described in Figure 7.

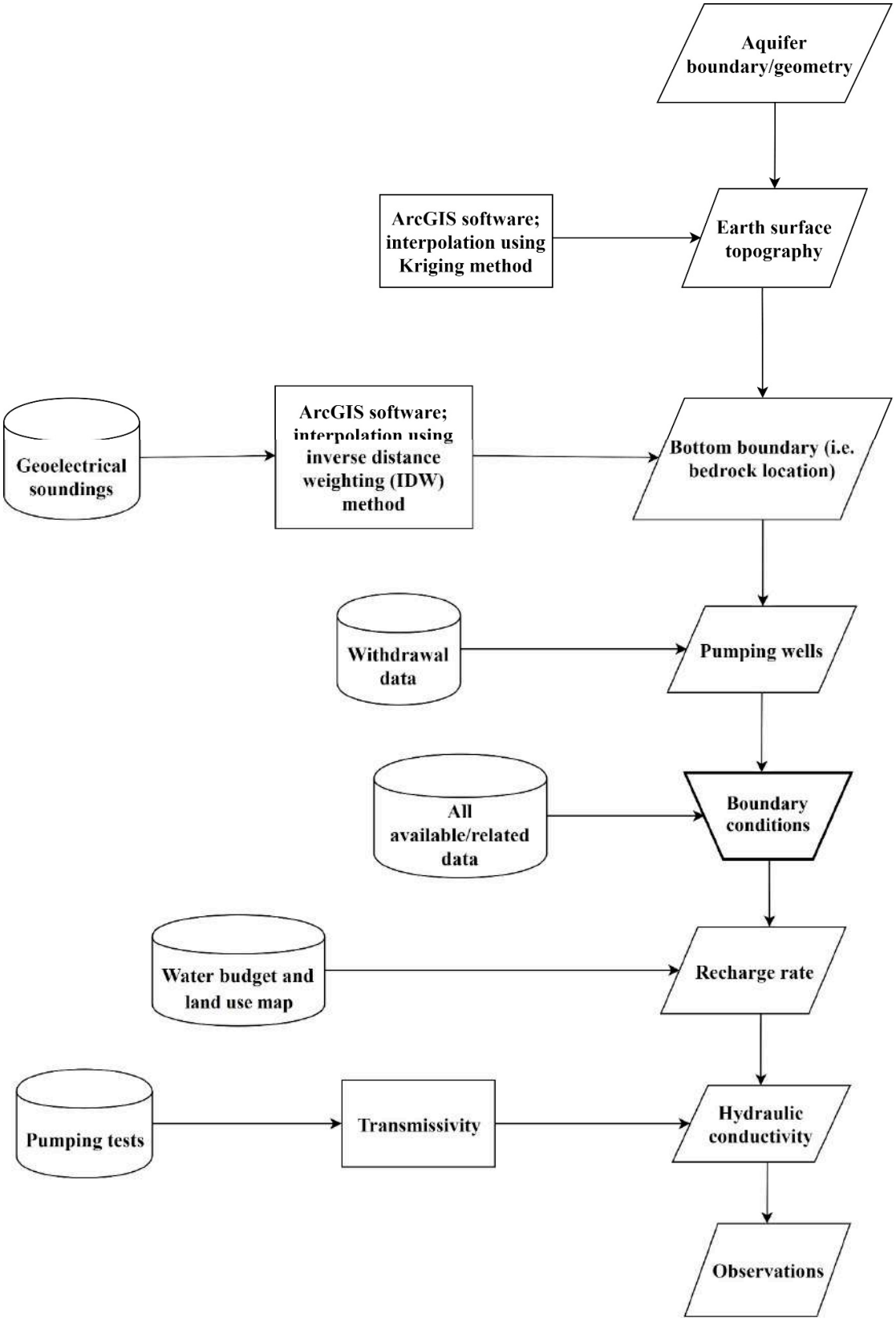

Figure 7. Flowchart of the building the conceptual model of Birjand aquifer.

The aquifer geometry is determined according to the RWCSK data. A comprehensive study (e.g., lithology and geology studies) has been done in this research to be able to model the aquifer

boundaries (i.e., aquifer geometry) accurately in the model [35,56–62]. The bottom boundary (i.e., the bedrock in the aquifer) is also determined using the limited available geophysical study (geoelectrical soundings) carried out in Birjand Plain in 1971 (Figure 8).

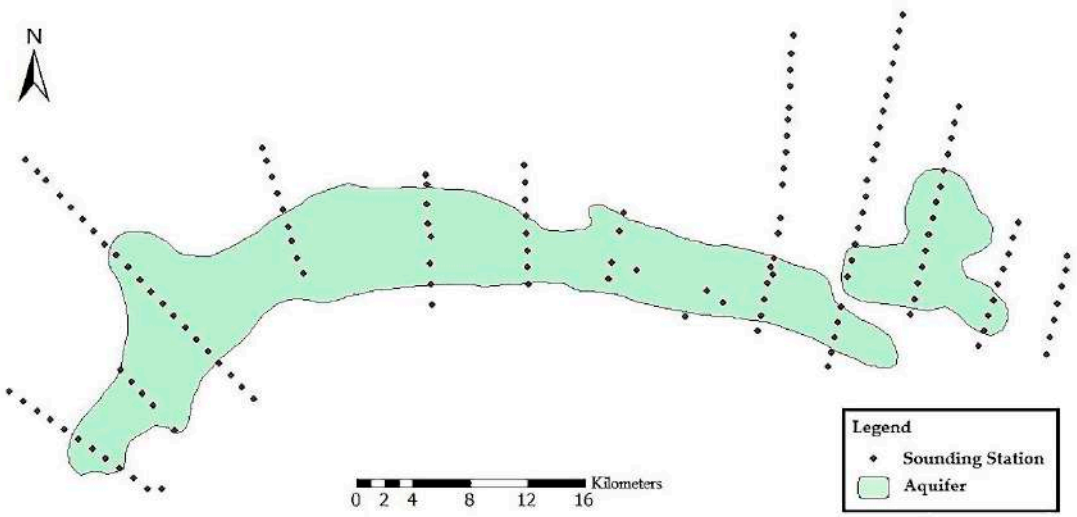

Figure 8. Location of geoelectrical soundings in Birjand aquifer.

To define the sinks and sources in the aquifer model, the positions and amounts of withdrawals/discharges from each well should be determined. There are 187 pumping/extracting wells with recorded data in the study area which are applied in the model (Figure 9). The well data are obtained from RWCSK and their quality are controlled before importing to the model. Of the total wells used in the model, 26 wells are used for drinking water and sanitation, 9 wells for livestock, 26 wells for industry and services, 119 wells for agriculture, and 7 for other uses.

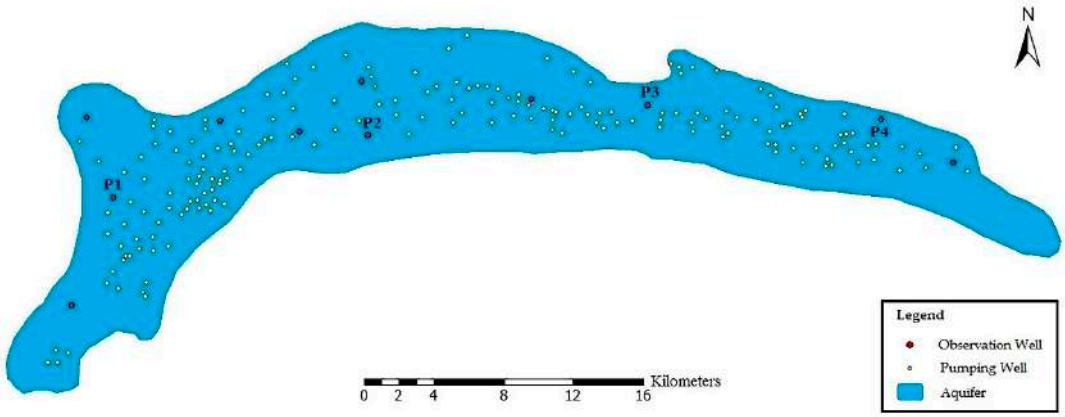

Figure 9. Location of pumping and observation wells (piezometers) in Birjand aquifer. P1, P2, P3, and P4 are for selected piezometers to check the groundwater level changes at the end of calibration and verification processes.

2.3.1. Boundary Conditions

The governing equations of the groundwater flow are solved using the finite difference approach. This requires that the boundary and initial conditions of the problem are described in details in the model [63]. The groundwater budget components of the Birjand aquifer provided by RWCSK are presented in Table 1. This budget can present a good view of the overall status of sinks and sources in the aquifer.

Table 1. Birjand aquifer budget provided by RWCSK [64]. The values are in million cubic meters (MCM) per year.

Inputs (MCM/Year)		Outputs (MCM/Year)	
Lateral underground inflow	25.44	Discharge and extraction (well, qanat, spring)	73.56
Infiltration of precipitation	4.08	Lateral underground outflow	1.15
Infiltration of runoff	4.47	Drainage	0.00
Infiltration of agricultural wastewater	17.87	evapotranspiration	0.00
Infiltration of drinking and industrial wastewaters	14.32	The total volume of discharge	74.71
The total volume of recharge	66.18		

In previous studies, different types of boundary conditions have been used in Birjand aquifer. In the present study, we are trying to apply precise aquifer input/output boundaries using geological surveys and satellite imagery through the Google Earth Pro software.

To find the real-world conditions, a comprehensive investigation of the adjacent areas of the aquifer, geological conditions, lithology maps, the type of soils, and topography of the area has been done. Finally, by using this data, the lateral input boundaries or lateral recharge are defined in the model as follows:

- In the northeast part of the aquifer, there is an exchange of groundwater between Birjand and Marak aquifers (Figure 6). The groundwater flow direction in this area is from the Marak aquifer towards Birjand aquifer (the water levels are higher in the outlet of the Marak aquifer) with the flow rate of about 3.56 million cubic meters per year.
- The second input boundary area to the Birjand aquifer located in the south as shown in Figure 10. The southern parts of the Birjand aquifer have the highest elevations of the land structure in the adjacent areas of the Birjand aquifer. In addition, there are alluvial fans as unconsolidated sedimentary deposits in these parts which, due to having steep slopes, can recharge the aquifer during the precipitation.

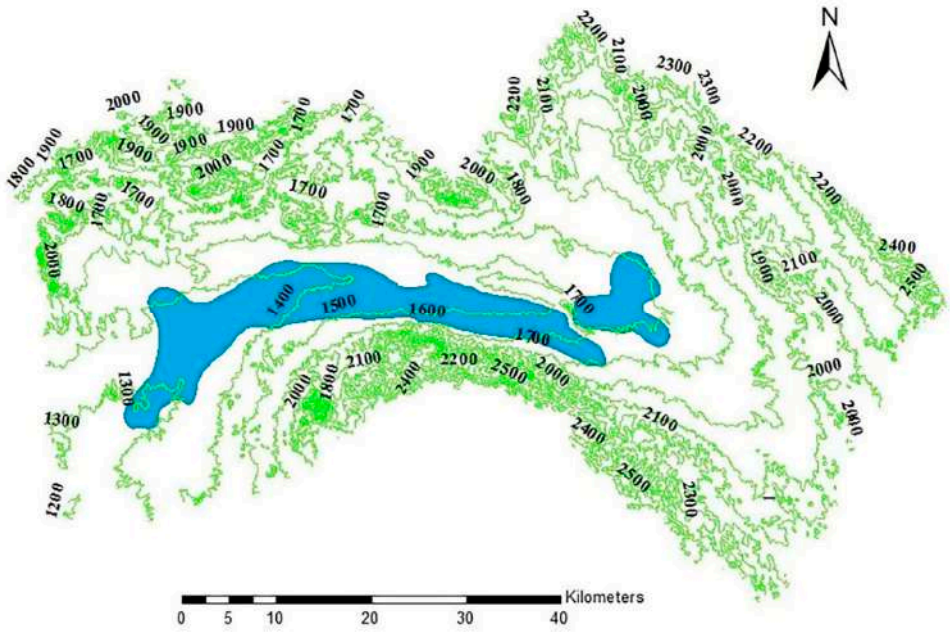

Figure 10. Topography of the Birjand watershed which includes the Birjand aquifer. The numbers represent the elevation in m.s.l.

- There is another lateral input boundary in the northwest of the aquifer, which looks like a camel hump. In this area, there is a large fan-shaped alluvial cone that has been washed out or eroded over the years from high altitudes and dispersed in a large area with a perimeter of about 17.5 km, as shown in Figure 11. Precipitation over this alluvial cone flows through specified paths and then penetrates into this vast area and joins the Birjand aquifer.

Figure 11. Large alluvial fan as an input boundary or lateral recharge, located in the northwest of Birjand aquifer. The blue line shows the groundwater lateral recharge way.

- Lithology, as well as soil type and soil texture investigations in the study region are identified the fourth input boundary. In Figure 6, the southern part of the aquifer and from the central side towards the west of the aquifer, geologically are formed from predominantly sandstone, siltstone, phyllite, slate, and minor limestone, which have very low permeability. As a result, due to the fact that water cannot penetrate rapidly, it becomes runoff and flows downstream, and penetrates as soon as it enters the aquifer's alluvial zone, causing the aquifer recharge. The relatively high slope in this area, which speeds up the runoff from precipitation, as well as the presence of a large mountain above this rock that has average precipitation above the Birjand plain, are some factors that help to recharge the aquifer. The distance between the second and fourth major input areas (both of which are located in the southern part of the Birjand aquifer) mainly is not considered as an input boundary because there are relatively low elevations and slight/gentle slopes between these elevated areas in the southern part. In other words, in the area between these two inputs, the stone structure is far from the aquifer boundary. Due to aridity of this region (high evapotranspiration and small precipitation), the amount of water that penetrates in this area is not transported to the Birjand aquifer.
- There is another input boundary in the northern areas of the Birjand aquifer. There are two large alluvial fans in this area, with a tip distance of about 7.2 km (Figure 12) and at the base, these are located entirely within the aquifer boundary and their distance is reduced by about half. These alluvial fans build a place for penetrating the runoffs to the aquifer and recharging it. In the upstream part of the right (eastern) alluvial fan, there are some human activities, such as leveling the ground, constructing a small earth dam, and farming. Therefore, input flows from this side can be ignored and considered as a no-flow boundary. However, the upstream of the left alluvial fan (western) remains almost virtually undisturbed without any considerable human activities.

Figure 12. Alluvial fans position at the northern boundary of the Birjand aquifer. The blue line shows the groundwater lateral recharge way.

The above mentioned five main input areas are considered as specified head boundary or Dirichlet/first-type boundary conditions in the model. The rest boundaries are considered as no-flow boundaries or Neumann/second-type boundary conditions because there are no hydraulic connections between the aquifer and its neighbors (Figure 13).

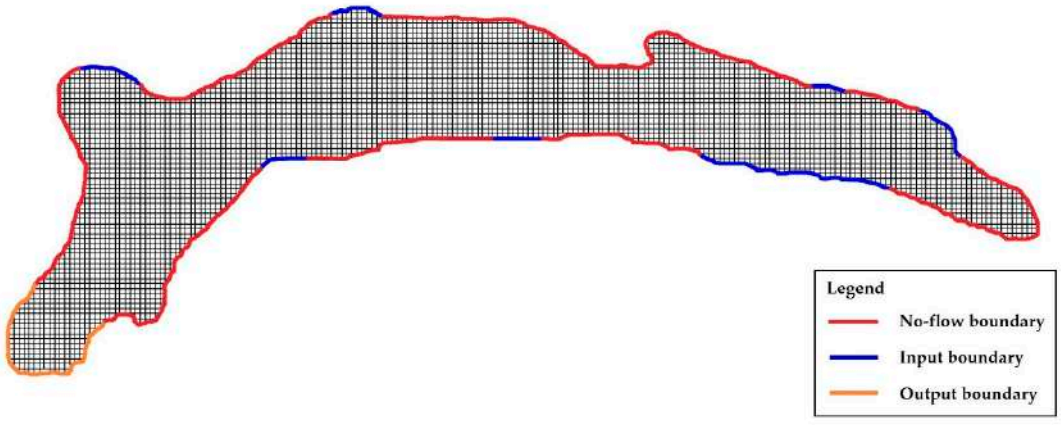

Figure 13. Boundary conditions of the model.

It is assumed that the differences between the ground's surface gradient and the groundwater level gradient are small and therefore, each input boundary's head can be calculated based on the head of the adjacent observation well. Regarding this issue, the distance between the input boundary and adjacent observation well should not be too high.

2.3.2. Model Parameters

One of the most important parameters in a groundwater model is hydraulic conductivity. The hydraulic conductivity values can be calculated based on the transmissivity values (T) obtained from the pumping tests using the equation

$$K = T/B \quad (3)$$

where K represents hydraulic conductivity (m/d); T is transmissivity (m^2/d); and B shows the thickness of the aquifer saturation layer (the difference between groundwater level and bedrock level in each point) (m). Finally, using inverse distance weighting (IDW) interpolation method in GMS, an approximate initial value of the aquifer hydraulic conductivity is obtained.

Calculating the aquifer recharge often is one of the most challenging issues in groundwater studies. According to Table 1, the total amount of aquifer recharge—including the penetration of precipitation, surface runoff, agricultural, drinking, and industry wastewaters—is about 40.74 MCM per year. In this study, this amount of direct recharge distributed in the aquifer conceptual model based on the land use map.

2.3.3. Model Computational Grid

The results of the groundwater model depend on the size of computational grids. In this study, as shown in Figure 14, the grid cell size is 250 × 250 m in horizontal plane uniformly and the height of each cell is equal to alluvial depth in that point (i.e., the difference between earth's surface and bedrock levels). The modeling grid consists of 79 rows and 224 columns. The total number of grid cells is 17,696, including 4088 active cells (all cells inside the aquifer are active) and 13,608 inactive (all cells outside the aquifer are inactive).

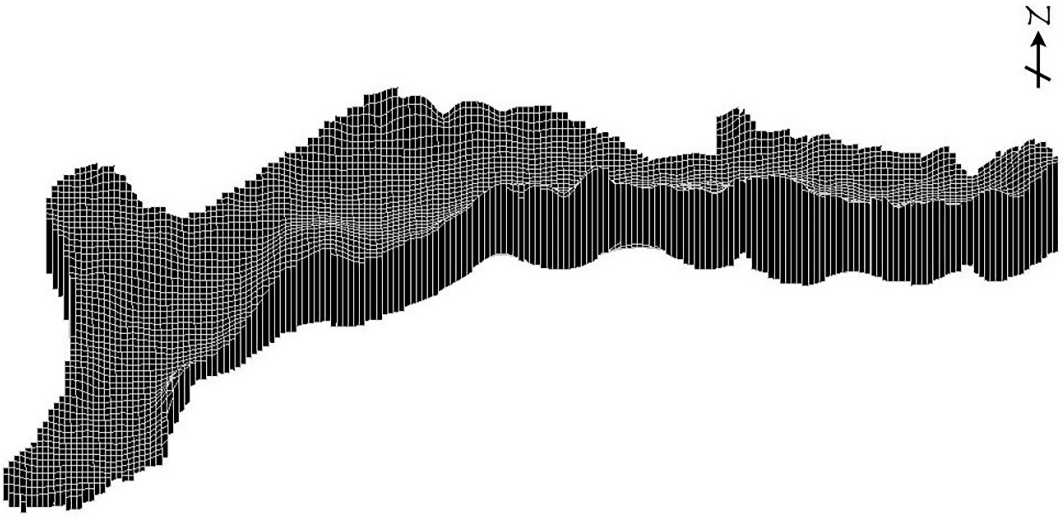

Figure 14. 3-D grid created by GMS: MODFLOW for Birjand groundwater model.

3. Results

3.1. Model Calibration

There are generally two kinds of calibration process; the first one is a trial-and-error process that should be manually changed repeatedly calibration parameters. This method can be considered as a fundamental first step for history matching because it can give the modeler much insight about the site modeled and how parameter changes affect different areas of the model and types of observations [65]. The second type is automated parameter estimation which in many cases can calibrate the model quickly. GMS contains an interface to the mentioned calibration called PEST (Parameter ESTimation) [66]. PEST calibration can be performed in two ways including zonal and pilot point. The first approach (i.e., zonal) is the most common one [67] and is applied in this study.

For calibration, the hydraulic head data of 11 observation wells or piezometers in the study region is imported to model. Using the trial-and-error approach, attempts are made to minimize the

differences between calculated and observed head values. The quality of the calibration is evaluated using some indices including mean error (ME), mean absolute error (MAE), and root mean square error (RMSE) according to the equations

$$\mathrm{ME} = \frac{1}{n}\sum_{i=1}^{n}(h_o\text{-}h_c)_i \quad (4)$$

$$\mathrm{MAE} = \frac{1}{n}\sum_{i=1}^{n}\left|(h_o\text{-}h_c)_i\right| \quad (5)$$

$$\mathrm{RMSE} = \left[\frac{1}{n}\sum_{i=1}^{n}(h_o\text{-}h_c)_i^{\,2}\right]^{0.5} \quad (6)$$

where n is the number of piezometers; h_o and h_c show observed/measured and calculated/simulated head values (m), respectively. Calculation of the above mentioned statistic indices is useful in evaluating the merit of the calibration [68]. It should be noted that the GMS software provides ME, MAE, and RMSE values for each model run. Because both positive and negative residuals are used in calculation, ME value should be close to zero for a good calibration. MAE is calculated using the absolute values of the error (only positive values) and is a measure of the average error in the model. The root mean square error (RMSE) or the standard deviation (RMSD) (due to using the steady state results in calibration RMSE and RMSD are equal) is the average of the squared differences in measured and simulated heads. RMSE is less robust to the effects of outlier residuals. Thus, the RMSE is typically larger than the MAE.

Calibration of the model is performed for steady-state in this study because the time series of groundwater flow are unknown. Instead of transient calibration, a semi-transient calibration approach is applied for Birjand aquifer. In this way, calibration of the model is carried out for seasonal data of the study period (about 7 years) as summarized in Table 2. The main reason for choosing a season as a time step is that the groundwater level changes in all observation wells were insignificant during a season. The average groundwater levels in each piezometer during each season were considered and entered to the model. The results show that there is a good agreement between the input data, calibrated parameters, and the assumption in the study period, and the model can be used beyond this time period.

Table 2. Semi-transient calibration of Birjand groundwater model

Season	Mean Error (m)	Mean Absolute Error (m)	Root Mean Square Error (m)
Spring 2018	−0.04	0.14	0.18
Winter 2018	0.03	0.14	0.19
Autumn 2017	0.00	0.16	0.22
Summer 2017	0.03	0.17	0.20
Spring 2017	0.13	0.17	0.23
Winter 2017	0.14	0.19	0.25
Autumn 2016	0.05	0.22	0.28
Summer 2016	0.02	0.26	0.30
Spring 2016	0.09	0.22	0.27
Winter 2016	0.09	0.23	0.27
Autumn 2015	0.04	0.27	0.33
Summer 2015	0.05	0.28	0.32
Spring 2015	0.16	0.26	0.35
Winter 2015	0.15	0.27	0.31
Autumn 2014	0.05	0.27	0.30
Summer 2014	0.03	0.27	0.30
Spring 2014	0.14	0.26	0.28

Winter 2014	0.12	0.25	0.27
Autumn 2013	0.04	0.27	0.30
Summer 2013	0.13	0.28	0.32
Spring 2013	0.08	0.25	0.27
Winter 2013	0.03	0.27	0.30
Autumn 2012	0.01	0.24	0.31
Summer 2012	−0.01	0.25	0.31
Spring 2012	0.14	0.23	0.30
Winter 2012	0.14	0.24	0.31
Autumn 2011	0.06	0.24	0.33
Summer 2011	0.06	0.25	0.33
Spring 2011	0.13	0.23	0.31

Due to the importance of hydraulic conductivity, model calibration can be used for determining this parameter. Regarding this issue, the Birjand aquifer is divided into 25 polygons or zones as shown in Figure 15.

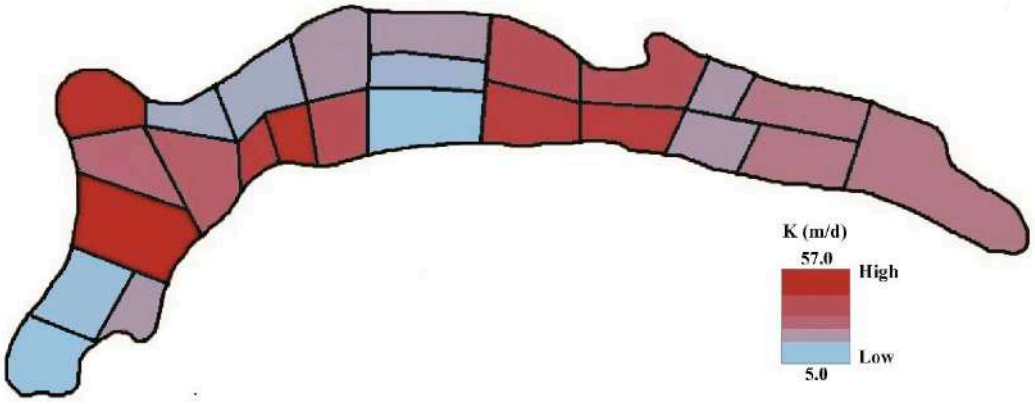

Figure 15. Distribution of hydraulic conductivity values in Birjand aquifer.

To illustrate the difference between observed and calculated head values during the study period, four piezometers were chosen randomly according to Figure 16. The locations of these four selected piezometers are shown in Figure 9. As seen in Figure 16, the groundwater level almost continuously decreases in all selected piezometers in the study area.

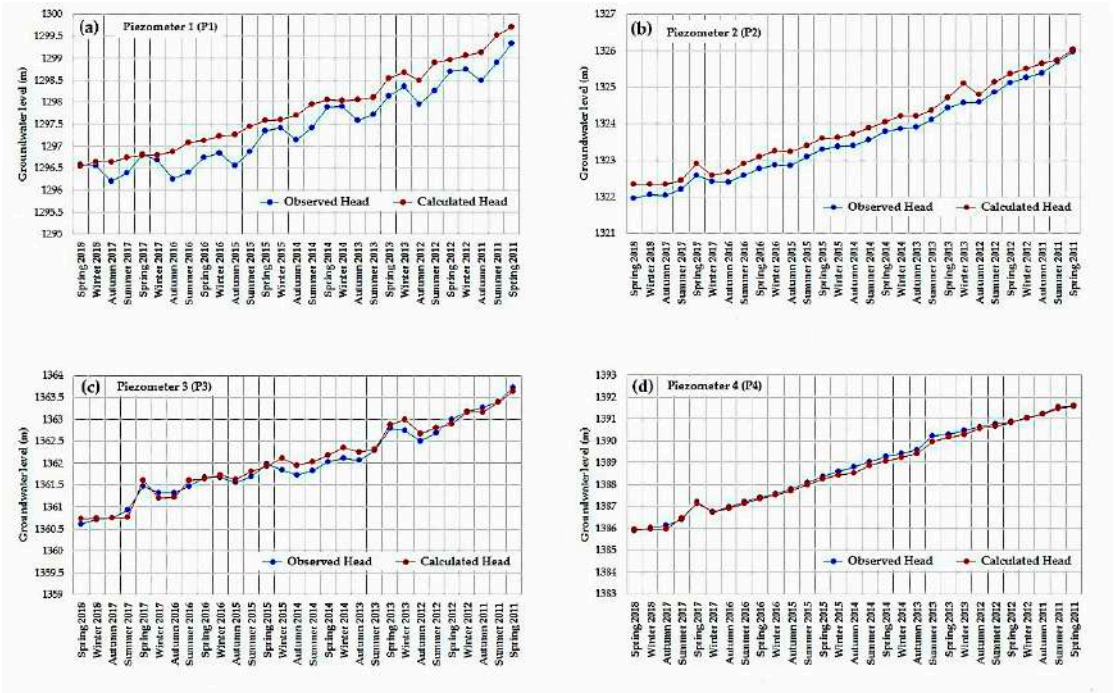

Figure 16. The results of semi-transient calibration of the model, Birjand groundwater level changes as well as observed and calculated head values for the four selected piezometers include (**a**) piezometer 1; (**b**) piezometer 2; (**c**) piezometer 3; and, (**d**) piezometer 4, over a period of about 7 years as seasonal.

As shown in Figure 9, all four piezometers are selected randomly from different areas of the aquifer to investigate groundwater levels. Accordingly, it is clear that P1 and P2 have a relatively big difference between observed and calculated head values. The reason is that these two piezometers are located in the western half of the aquifer. It should be noted that after investigating calibration results for all available piezometers and for all the seasons, we noticed that the difference between the observed and calculated heads in the piezometers of the western parts of the aquifer were a bit higher than the eastern piezometers. Investigation of observation wells data during different months and seasons showed that the temporal variation of the piezometers head values in the western half of the aquifer was more slowly than the piezometers in the eastern half. In other words, the groundwater level decrease over time in the western parts of the aquifer occurs more slowly than the eastern parts; Analysis of piezometer statistics showed that the average annual groundwater level drop in western piezometers was about half of the water level drop in eastern piezometers. Therefore, simultaneous calibration of the entire aquifer is a challenging issue and in this case, it is almost impossible to make the difference between the observed and calculated heads across all piezometers near to zero.

In the present study, all error values reported for model calibration (and model evaluation in the next section) indicate mean values for each error at each season and these errors are general errors of the calibrated/evaluated model that derived from all available piezometers.

3.2. Model Evaluation

After the calibration process, the prepared model should be evaluated to prove the model is reliable in different conditions. In this section, the calibrated parameters for the most recent time (spring 2018) is chosen for evaluating the model results. As shown in Table 3, the agreement between the results of the model and the measurements is promising for both parameters including hydraulic conductivity (K) and recharge (R) and consequently, for the model. Similar to the calibration section, the groundwater level changes in the same four selected piezometers for model evaluation over 7 years are shown in Figure 17. Each red point represents the amount of the head difference and

belongs to a spring season of a specific year that is specified beside each point. P1, P2, P3, and P4 are the selected piezometers as shown in Figure 9.

Table 3. Evaluation results of Birjand groundwater model over a 7-year period

Season.	Mean Error (m)	Mean Absolute Error (m)	Root Mean Square Error (m)
Spring 2017	0.06	0.13	0.20
Spring 2016	0.05	0.19	0.24
Spring 2015	0.06	0.20	0.27
Spring 2014	0.05	0.18	0.23
Spring 2013	0.03	0.19	0.24
Spring 2012	−0.05	0.22	0.28
Spring 2011	−0.03	0.22	0.30

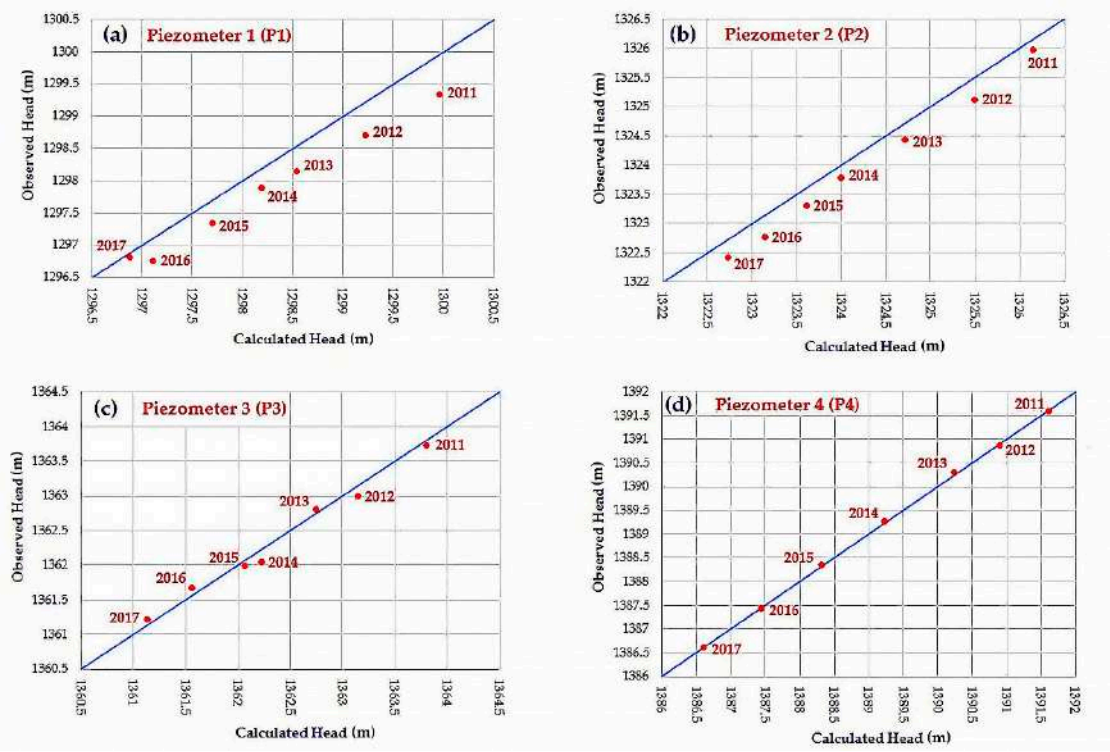

Figure 17. Difference between observed and calculated head values in four selected piezometers include (**a**) piezometer 1; (**b**) piezometer 2; (**c**) piezometer 3; and, (**d**) piezometer 4, at the end of model verification for a 7-year period.

4. Conclusions

Over-exploitation of the groundwater resources in most plains in Iran is common, and continuing the present pressure on these quite precious sources will lead to the occurrence of severe irrecoverable water stress in the country. In this study, the Birjand aquifer in South Khorasan province, Iran is investigated where the groundwater is the main source of water supply. The study area has been explained extensively. One of the major goals of this study is to improve the accuracy of the aquifer model and to overcome the data shortage, especially in the input boundaries. To do this, a semi-transient approach has been used in order to investigate the aquifer model during a period of time. Coupling MODFLOW with ArcGIS using GMS powerful software allows us to simulate the groundwater flow in the desired area. In the previous studies conducted for Birjand region, we noticed a great difference and disagreement in the considered boundary conditions as a

gap of the literature. In the present research, the comprehensive study in the Birjand region caused some important improvements in the Birjand aquifer model, especially in boundary conditions.

The model calibration is done using steady-state and semi-transient approaches. The aquifer model was investigated for 29 seasons and the result presented. In addition, four piezometers were selected randomly from different parts of the aquifer to comprehensively showing the groundwater level changes in the entire area. To quantify the reliability of the model, some evaluation indices—including mean error, mean absolute error, and root mean square error—are calculated. According to these indices, the performance of the model is promising. The approach was used in this study (i.e., semi-transient calibration) can be applied for other regions with a similar problem as well as similar condition. The findings of this study can improve the status of groundwater resource management in the Birjand region and contribute to the sustainable development of this vital resource.

Author Contributions: Conceptualization, A.A.; Formal analysis, R.A.; Methodology, R.A. and A.A.; Project administration, A.A.; Software, R.A.; Supervision, A.A.; Validation, R.A.; Visualization, R.A.; Writing—original draft preparation, R.A.

Funding: This research received no external funding.

Acknowledgments: The authors thank the Regional Water Company of South Khorasan (RWCSK) for the collaborations on providing the data and the information used in this study.

Conflicts of Interest: The authors declare no conflict of interest.

References

1. Sattari, M.T.; Mirabbasi, R.; Sushab, R.S.; Abraham, J. Prediction of Level in Ardebil Plain Using Support Vector Regression and M5 Tree Model. *Groundwater* **2018**, *56*, 636–646.
2. Khalili, K.; Tahoudi, M.N.; Mirabbasi, R.; Ahmadi, F. Investigation of spatial and temporal variability of precipitation in Iran over the last half century. *Stoch. Environ. Res. Risk Assess.* **2016**, *30*, 1205–1221.
3. Rejani, R.; Jha, M.K.; Panda, S.N.; Mull, R. Simulation modeling for efficient groundwater management in balasore coastal basin, India. *Water Resour. Manag.* **2008**, *22*, 23–50.
4. van Engelenburg, J.; Hueting, R.; Rijpkema, S.; Teuling, A.J.; Uijlenhoet, R.; Ludwig, F. Impact of Changes in Groundwater Extractions and Climate Change on Groundwater-Dependent Ecosystems in a Complex Hydrogeological Setting. *Water Resour. Manag.* **2018**, *32*, 259–272.
5. Izady, A.; Abdalla, O.; Joodavi, A.; Chen, M. Groundwater Modeling and Sustainability of a Transboundary Hardrock–Alluvium Aquifer in North Oman Mountains. *Water* **2017**, *9*, 161.
6. Uddameri, V.; Singaraju, S.; Karim, A.; Gowda, P.; Bailey, R.; Schipanski, M. Understanding Climate-Hydrologic-Human Interactions to Guide Groundwater Model Development for Southern High Plains. *J. Contemp. Water Res. Educ.* **2017**, *162*, 79–99.
7. Khadri, S.F.R.; Pande, C. Ground water flow modeling for calibrating steady state using MODFLOW software: A case study of Mahesh River basin, India. *Model. Earth Syst. Environ.* **2016**, *2*, 39.
8. Reilly, T.E.; Harbaugh, A.W. *Guidelines for Evaluating Ground-Water Flow Models*; US Geological Survey, Scientific Investigations Report 2004–5038; USGS: Reston, VA, USA, 2004.
9. Rapantova, N.; Tylcer, J.; Vojtek, D. Numerical modelling as a tool for optimisation of ground water exploitation in urban and industrial areas. *Procedia Eng.* **2017**, *209*, 92–99.
10. Hogeboom, R.H.J.; van Oel, P.R.; Krol, M.S.; Booij, M.J. Modelling the Influence of Groundwater Abstractions on the Water Level of Lake Naivasha, Kenya Under Data-Scarce Conditions. *Water Resour. Manag.* **2015**, *29*, 4447–4463.
11. Baalousha, H. Fundamentals of groundwater modelling. In *Groundwater: Modelling, Management and Contamination*; Konig, L.F., Weiss, J.L., Eds.; Nova Science Publishers, Inc.: New York, NY, USA, 2009; pp. 149–166; ISBN 9781604568325.
12. McDonald, M.G.; Harbaugh, A.W. *A Modular Three-Dimensional Finite-Difference Ground-Water Flow Model*; U.S. Geological Survey, Open File Report 83–875; US Geological Survey: Reston, VA, USA, 1988.
13. Panagopoulos, G. Application of MODFLOW for simulating groundwater flow in the Trifilia karst aquifer, Greece. *Environ. Earth Sci.* **2012**, *67*, 1877–1889.
14. Kushwaha, R.K.; Pandit, M.K.; Goyal, R. MODFLOW Based Groundwater Resource Evaluation and

Prediction in Mendha Sub-Basin, NE Rajasthan. *J. Geol. Soc. India* **2009**, *74*, 449–458.
15. Wang, S.; Shao, J.; Song, X.; Zhang, Y.; Huo, Z.; Zhou, X. Application of MODFLOW and geographic information system to groundwater flow simulation in North China Plain, China. *Environ. Geol.* **2008**, *55*, 1449–1462.
16. Abdulla, F.A.; Al-Khatib, M.A.; Al-Ghazzawi, Z.D. Development of groundwater modeling for the Azraq Basin, Jordan. *Environ. Geol.* **2000**, *40*, 11–18.
17. Gurwin, J.; Lubczynski, M. Modeling of complex multi-aquifer systems for groundwater resources evaluation—Swidnica study case (Poland). *Hydrogeol. J.* **2005**, *13*, 627–639.
18. Lutz, A.; Thomas, J.M.; Pohll, G.; McKay, W.A. Groundwater resource sustainability in the Nabogo Basin of Ghana. *J. Afr. Earth Sci.* **2007**, *49*, 61–70.
19. Jingli, S.; Ling, L.; Yali, C.; Zhaoji, Z. Groundwater Flow Simulation and its Application in Groundwater Resource Evaluation in the North China Plain, China. *Acta Geol. Sin. Engl. Ed.* **2013**, *87*, 243–253.
20. Pisinaras, V.; Petalas, C.; Tsihrintzis, V.A.; Karatzas, G.P. Integrated modeling as a decision-aiding tool for groundwater management in a Mediterranean agricultural watershed. *Hydrol. Process.* **2013**, *27*, 1973–1987.
21. Katpatal, Y.B.; Pophare, A.M.; Lamsoge, B.R. A groundwater flow model for overexploited basaltic aquifer and Bazada formation in India. *Environ. Earth Sci.* **2014**, *72*, 4413–4425.
22. Chakraborty, S.; Maity, P.K.; Das, S. Investigation, simulation, identification and prediction of groundwater levels in coastal areas of Purba Midnapur, India, using MODFLOW. *Environ. Dev. Sustain.* **2019**, 1–13. doi:10.1007/s10668-019-00344-1.
23. Jang, C.S.; Chen, C.F.; Liang, C.P.; Chen, J.S. Combining groundwater quality analysis and a numerical flow simulation for spatially establishing utilization strategies for groundwater and surface water in the Pingtung Plain. *J. Hydrol.* **2016**, *533*, 541–556.
24. Bushira, K.M.; Hernandez, J.R.; Sheng, Z. Surface and groundwater flow modeling for calibrating steady state using MODFLOW in Colorado River Delta, Baja California, Mexico. *Model. Earth Syst. Environ.* **2017**, *3*, 815–824.
25. Habel, S.; Fletcher, C.H.; Rotzoll, K.; El-kadi, A.I. Development of a model to simulate groundwater inundation induced by sea-level rise and high tides in Honolulu, Hawaii. *Water Res.* **2017**, *114*, 122–134.
26. Xu, X.; Huang, G.; Qu, Z.; Pereira, L.S. Using MODFLOW and GIS to Assess Changes in Groundwater Dynamics in Response to Water Yellow River Basin. *Water Resour. Manag.* **2011**, *25*, 2035–2059.
27. Lachaal, F.; Mlayah, A.; Bédir, M.; Tarhouni, J.; Leduc, C. Implementation of a 3-D groundwater flow model in a semi-arid region using MODFLOW and GIS tools: The Zéramdine–Béni Hassen Miocene aquifer system (east-central Tunisia). *Comput. Geosci.* **2012**, *48*, 187–198.
28. El-Zehairy, A.A.; Lubczynski, M.W.; Gurwin, J. Interactions of artificial lakes with groundwater applying an integrated MODFLOW solution. *Hydrogeol. J.* **2018**, *26*, 109–132.
29. Xue, S.; Liu, Y.; Liu, S.; Li, W.; Wu, Y.; Pei., Y. Numerical simulation for groundwater distribution after mining in Zhuanlongwan mining area based on visual MODFLOW. *Environ. Earth Sci.* **2018**, *77*, 400.
30. Chatterjee, R.; Jain, A.K.; Chandra, S.; Tomar, V.; Parchure, P.K.; Ahmed, S. Mapping and management of aquifers suffering from over-exploitation of groundwater resources in Baswa-Bandikui watershed, Rajasthan, India. *Environ. Earth Sci.* **2018**, *77*, 157.
31. United States Geological Survey (USGS). MODFLOW and Related Programs. Available online: https://www.usgs.gov/mission-areas/water-resources/science/modflow-and-related-programs?qt-science_center_objects=0#qt-science_center_objects (accessed on 14 March 2019).
32. Iran Water Resources Management Company. Available online: https://www.wrm.ir (accessed on 23 April 2019).
33. Regional Water Company of South Khorasan. *The National Program on Controlling the Groundwater Exploitation*; Regional Water Company of South Khorasan: Birjand, Iran, 2019.
34. Noor, H. Analysis of Groundwater Resource Utilization and Their Current Condition in Iran. *Iran. J. Rainwater Catchment Syst.* **2017**, *5*, 29–38. (In Persian)
35. Sadeghi-Tabas, S.; Akbarpour, A.; Pourreza-Bilondi, M.; Samadi, S. Toward reliable calibration of aquifer hydrodynamic parameters: Characterizing and optimization of arid groundwater system using swarm intelligence optimization algorithm. *Arab. J. Geosci.* **2016**, *9*, 719.
36. Javan, J.; Fal-Soleiman, M. Water Crisis and Importance of Water Productivity in Agriculture in Dry Area of Iran (Case Study: Birjand Plain). *Geogr. Dev. Iran. J.* **2008**, *6*, 115–138. (In Persian)
37. Sherif, M.M.; Singh, V.P. Effect of climate change on sea water intrusion in coastal aquifers. *Hydrol. Process.*

1999, *13*, 1277–1287.
38. Waterloo Hydrogeologic Company. Available online: https://www.waterloohydrogeologic.com/resources/visual-modflow-flex-resources/introduction-groundwater-modeling-with-visual-modflow (accessed on 2 March 2019).
39. Diersch, H.-J.G. *FEFLOW: Finite Element Modeling of Flow, Mass and Heat Transport in Porous and Fractured Media*; Springer Science & Business Media: Berlin, Germany, 2013.
40. Owen, S.J.; Jones, N.L.; Holland, J.P. A Comprehensive Modeling Environment for the Simulation of Groundwater Flow and Transport. *Eng. Comput.* **1996**, *12*, 235–242.
41. Karimi, L.; Motagh, M.; Entezam, I. Modeling groundwater level fluctuations in Tehran aquifer: Results from a 3D unconfined aquifer model. *Groundw. Sustain. Dev.* **2019**, *8*, 439–449.
42. Nan, T.; Li, K.; Wu, J.; Yin, L. Assessment of groundwater exploitation in an aquifer using the random walk on grid method: A case study at Ordos, China. *Hydrogeol. J.* **2018**, *26*, 1669–1681.
43. Su, X.; Yuan, W.; Du, S.; Cui, G.; Bai, J.; Du, S. Responses of groundwater vulnerability to groundwater extraction reduction in the Hun River Basin, northeastern China. *Hum. Ecol. Risk Assess.* **2017**, *23*, 1121–1139.
44. Meredith, E.; Blais, N. Quantifying irrigation recharge sources using groundwater modeling. *Agric. Water Manag.* **2019**, *214*, 9–16.
45. Qiu, S.; Liang, X.; Xiao, C.; Huang, H.; Fang, Z.; Lv, F. Numerical simulation of groundwater flow in a River Valley Basin in Jilin Urban Area, China. *Water* **2015**, *7*, 5768–5787.
46. Roy, P.K.; Roy, S.S.; Giri, A.; Banerjee, G.; Majumder, A.; Mazumdar, A. Study of impact on surface water and groundwater around flow fields due to changes in river stage using groundwater modeling system. *Clean Technol. Environ. Policy* **2015**, *17*, 145–154.
47. Sobeih, M.M.; El-Arabi, N.E.; Helal, E.E.D.Y.; Awad, B.S. Management of water resources to control groundwater levels in the southern area of the western Nile delta, Egypt. *Water Sci.* **2017**, *31*, 137–150.
48. Moridi, A.; MajdzadehTabatabaie, M.R.; Esmaeelzade, S. Holistic Approach to Sustainable Groundwater Management in Semi- arid Regions. *Int. J. Environ. Res.* **2018**, *12*, 347–355.
49. Hashemi, H.; Berndtsson, R.; Kompani-Zare, M. Steady-State Unconfined Aquifer Simulation of the Gareh-Bygone Plain, Iran. *Open Hydrol. J.* **2012**, *6*, 58–67.
50. Malekinezhad, H.; Banadkooki, F.B. Modeling impacts of climate change and human activities on groundwater resources using MODFLOW. *J. Water Clim. Chang.* **2017**, *9*, 156–177.
51. Jalut, Q.H.; Abbas, N.L.; Mohammad, A.T. Management of groundwater resources in the Al-Mansourieh zone in the Diyala River Basin in Eastern Iraq. *Groundw. Sustain. Dev.* **2018**, *6*, 79–86.
52. He, X.; Sonnenborg, T.O.; Jørgensen, F.; Høyer, A.-S.; Møller, R.R.; Jensen, K.H. Analyzing the effects of geological and parameter uncertainty on prediction of groundwater head and travel time. *Hydrol. Earth Syst. Sci.* **2013**, *17*, 3245–3260.
53. Dupuit, J. *Études Théoriques et Pratiques sur le Mouvement des Eaux Dans les Canaux Découverts et à Travers les Terrains Perméabls*, 2nd ed.; Dunod: Paris, France, 1863.
54. Pholkern, K.; Saraphirom, P.; Cloutier, V.; Srisuk, K. Use of Alternative Hydrogeological Conceptual Models to Assess the Potential Impact of Climate Change on Groundwater Sustainable Yield in Central Huai Luang Basin, Northeast Thailand. *Water* **2019**, *11*, 241.
55. Poeter, E.; Anderson, D. Multimodel Ranking and Inference in Ground Water Modeling. *Ground Water* **2005**, *43*, 597–605.
56. Hamraz, B.S.; Akbarpour, A.; Bilondi, M.P.; Tabas, S.S. On the assessment of ground water parameter uncertainty over an arid aquifer. *Arab. J. Geosci.* **2015**, *8*, 10759–10773.
57. Sadeghi-Tabas, S.; Samadi, S.Z.; Akbarpour, A.; Pourreza-Bilondi, M. Sustainable groundwater modeling using single- and multi-objective optimization algorithms. *J. Hydroinform.* **2017**, *19*, 97–114.
58. Kalantari, M.; Akbarpour, A.; Khatibinia, M. Numerical Modeling of Groundwater Flow in Unconfined Aquifer in Steady State with Isogeometric Method. *Modares Civ. Eng. J.* **2018**, *18*, 195–206. (In Persian)
59. Hassanpour, M.; Khozeymehnezhad, H. Placement of nutrient wells for artificial nutrition and improvement of aquifer quality in Birjand plain using treated wastewater. *Health* **2018**, *4*, 215–226. (In Persian)
60. Mohtashami, A.; Akbarpour, A.; Mollazadeh, M. Development of two-dimensional groundwater flow simulation model using meshless method based on MLS approximation function in unconfined aquifer in transient state. *J. Hydroinform.* **2017**, *19*, 640–652.

61. Roozbahani, A.; Ebrahimi, E.; Banihabib, M.E. A Framework for Ground Water Management Based on Bayesian Network and MCDM Techniques. *Water Resour. Manag.* **2018**, *32*, 4985–5005.
62. Kardan Moghadam, H.; Banihabib, M.E.; Javadi, S. Quantitative Sustainability Analysis of Aquifer System (Case Study: South Khorasan—Birjand Aquifer). *J. Water Soil* **2018**, *31*, 1587–1601. (In Persian)
63. Batu, V. Numerical Flow and Solute Transport Modeling in Aquifers. In *Applied Flow and Solute Transport Modeling in Aquifers: Fundamental Principles and Analytical and Numerical Methods*; CRC Press, Taylor & Francis Group: Boca Raton, FL, USA, 2006; pp. 215–344; ISBN 9780849335747.
64. Regional Water Company of South Khorasan. *Quantifying the Water Resources in Birjand Region, Report Version 3*; Regional Water Company of South Khorasan: Birjand, Iran, 2017.
65. Anderson, M.P.; Woessner, W.W.; Hunt, R.J. *APPLIED GROUNDWATER MODELING: Simulation of Flow and Advective Transport*, 2nd ed.; Academic Press, Elsevier: New York, NY, USA, 2015; ISBN 9780120581030.
66. *GMS 10.4 Tutorial: MODFLOW—Automated Parameter Estimation*; Aquaveo: Provo, Utah, UT, USA, 2018.
67. XMS Wiki: Online help for GMS, SMS, and WMS. Available online: https://www.xmswiki.com/wiki/GMS:Parameters#Parameterizing_the_model (accessed on 25 April 2019).
68. Thangarajan, M. *Groundwater Flow and Mass Transport. Modeling: Theory and Application*; Capital Publishing Company: New Delhi, India, 2007; ISBN 9788185589619.

Journal of Hydrology: Regional Studies 37 (2021) 100885

Contents lists available at ScienceDirect

Journal of Hydrology: Regional Studies

journal homepage: www.elsevier.com/locate/ejrh

Characterization, geostatistical modeling and health risk assessment of potentially toxic elements in groundwater resources of northeastern Iran

Ata Joodavi [a], Reza Aghlmand [b], Joel Podgorski [c], Reza Dehbandi [d], Ali Abbasi [b,e,*]

[a] Department of Water Engineering, Kashmar Higher Education Institute, Kashmar, Iran
[b] Department of Civil Engineering, Faculty of Engineering, Ferdowsi University of Mashhad, Mashhad, Iran
[c] Eawag, Swiss Federal Institute of Aquatic Science and Technology, Department Water Resources and Drinking Water, Dübendorf, Switzerland
[d] Department of Environmental Health, Health Sciences Research Center, Faculty of Health, Mazandaran University of Medical Sciences, Sari, Iran
[e] Faculty of Civil Engineering and Geosciences, Water Resources Section, Delft University of Technology, Stevinweg 1, Delft, 2628 CN, The Netherlands

ARTICLE INFO

Keywords:
Groundwater quality
Health risk assessment
Random forest modelling
Toxic elements
Iran

ABSTRACT

Study region: Northeastern Iran.
Study focus: In northeastern Iran, water needed for municipal and agricultural activities mainly comes from groundwater resources. However, it is subject to substantial anthropogenic and geogenic contamination. We characterize the sources of groundwater contamination by employing an integrated approach that can be applied to the identification of large-scale contamination sources in other regions. An existing dataset of georeferenced water quality parameters from 676 locations in northeast of Iran was analyzed to investigate the geochemical properties of groundwater. Gridding of the parameters graphically illustrates the areas affected by high concentrations of As, Cl^-, Cr, Fe, Mg^{2+}, Na^+, NO_3^-, Se, and SO_4^{2-}. We then identified potential anthropogenic and geogenic contamination sources by employing random forest (RF) regression modeling.
New hydrological insights for the region: Random forest (RF) models show that the major ions, As, Cr, Fe, and Se content of groundwater are mainly determined by geology in the study area. Modeling also links groundwater NO_3^- contamination with sewage discharge into aquifers as well as the application of nitrogenous and animal-waste fertilizers. Areas of high salinity result from evaporate deposits and irrigation return flow. Medium to high non-carcinogenic health risk is found in areas with high concentrations of geogenic As and Cr in groundwater. Our approach can be applied elsewhere to analyze regional groundwater quality and associated health risks as well as identify potential sources of contamination.

1. Introduction

Many parts of Iran, like other arid/semi-arid regions, rely on groundwater to satisfy its drinking, agricultural and industrial water

* Corresponding author at: Department of Civil Engineering, Faculty of Engineering, Ferdowsi University of Mashhad, Mashhad, Iran.
E-mail addresses: atajoodavi@kashmar.ac.ir, atajoodavi@gmail.com (A. Joodavi), rezaaghlmandcivil@gmail.com (R. Aghlmand), joel.podgorski@eawag.ch (J. Podgorski), rezadehbandi65@gmail.com (R. Dehbandi), aabbasi@um.ac.ir, a.abbasi@tudelft.nl (A. Abbasi).

https://doi.org/10.1016/j.ejrh.2021.100885
Received 17 January 2021; Received in revised form 27 July 2021; Accepted 31 July 2021
Available online 6 August 2021

needs (Joodavi et al., 2015; Ashraf et al., 2021). Therefore, poor groundwater quality/groundwater pollution threatens water and food security in Iran. The chemical constituents of groundwater are determined mainly by the physical and chemical properties of an aquifer's saturated and unsaturated zones, residence time and recharge type (Khanoranga and Khalid, 2019). The geochemical conditions of an aquifer can result in high concentrations of various elements that are detrimental for human health such as As, Cd, Cr and F (Appelo and Postma, 2005). Anthropogenic activities can also introduce various pollutants of ions and trace metals to groundwater, for example through agricultural and industrial activities as well as human settlements (Barbieri et al., 2019; Ricolfi et al., 2020).

The presence of different potentially toxic elements (PTEs) in groundwater originating from geological formations and human activities is reported in some of Iran's sub-basins (Baghvand et al., 2010; Amiri et al., 2015; Dehbandi et al., 2017; Rezaei et al., 2018; Dehbandi et al., 2019; Hamidian et al., 2019; Heydarirad et al., 2019; Qasemi et al., 2019; Zendehbad et al., 2019; Sohrabi et al., 2020; Amiri et al., 2021a, b)

Most groundwater quality studies use geochemical methods and approaches to interpret geochemical reactions along groundwater flow paths and to recognize geochemical patterns in an aquifer or a watershed (local-scale studies). However, identifying both the anthropogenic and natural sources of PTEs in groundwater can be challenging in large-scale studies of broad geographical areas where there are different geological and hydrogeological conditions and large gaps in testing locations. As a way to help resolve this, geostatistical models such as logistic regression and random forest have been used to relate various environmental parameters to contaminant concentrations in groundwater and allow to create the groundwater contamination hazard maps (Bretzler et al., 2017; Podgorski and Berg, 2020; Wu et al., 2020).

This study provides a new application of geostatistical models for contamination source identification in groundwater resources through considering multiple parameters (salinity, nitrate and toxic elements) and different pollution sources.

In this paper, we present a combined approach in the large-scale identification of the sources of major ions and toxic elements in groundwater by applying random forest modeling of Razavi Khorasan province, Iran. We first describe our statistical analysis and graphical representation of water chemistry to determine ionic relationships in groundwater. We then investigate the spatial distribution of major and toxic elements and identify possible sources of groundwater contamination. Random forest modeling is then used to find relationships between contamination factors and the concentrations of toxic elements. Finally, we assess the health-risk of drinking groundwater. The findings help to understand water pollution drivers, promote stakeholder involvement, strategically plan for drinking water pollution prevention and manage health threats.

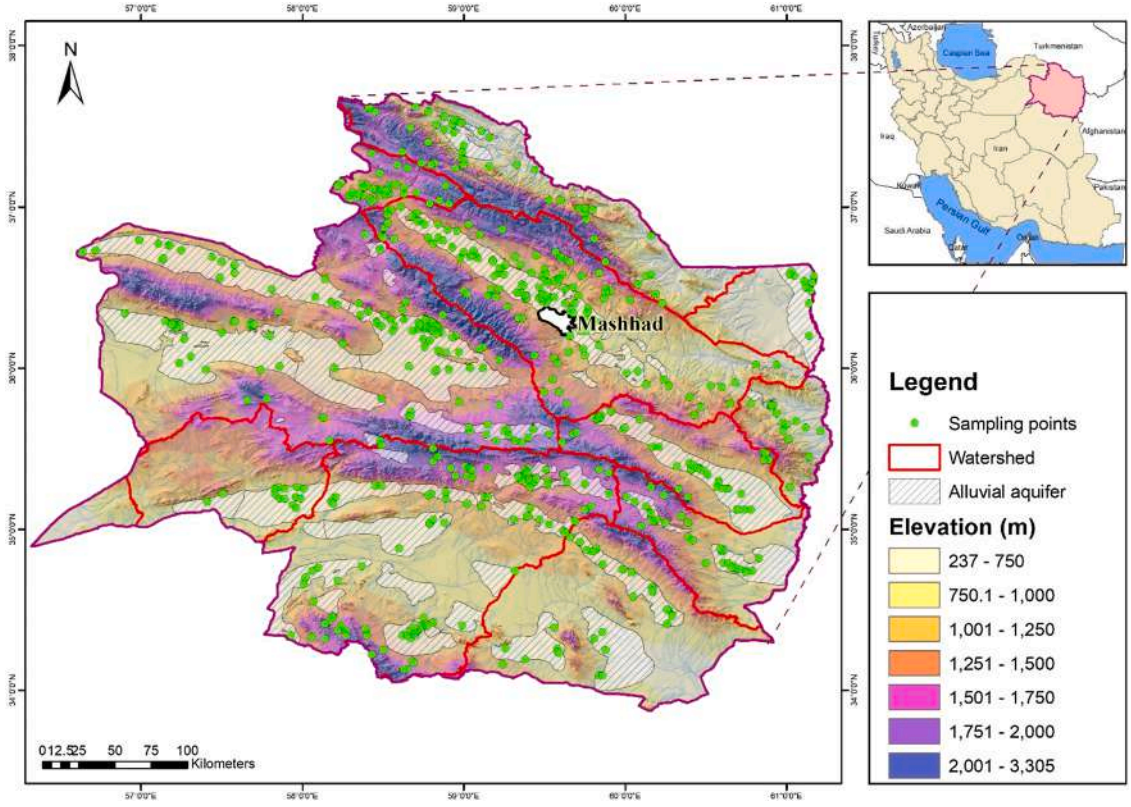

Fig. 1. Groundwater sampling points and topography within the study area of Razavi Khorasan province, Iran.

2. Materials and methods

2.1. Study area

Razavi Khorasan province, located in the northeast of Iran, has a total area of 129,043 km^2 and a population of 6,434,501 (Statistical Center of Iran, 2019). Its climate is arid to semi-arid with rainfall of 209.5 mm/year and mean temperature of 15.9 °C. About 87 % of the water used in Razavi Khorasan province (5,318 MCM) comes from groundwater that is extracted predominantly from alluvial aquifers by 23,727 wells with an average depth of 76 m and an average flow rate of 11.2 L/s. About 86 % of the groundwater withdrawn is used for agriculture, with 7% going to cities and towns used for drinking purposes (Iran Water Resources Management Company, 2019).

The geology of Razavi Khorasan includes unconsolidated Quaternary sediments, different sedimentary (sandstones, conglomerates, carbonate and evaporites), volcano-sedimentary, volcanic, intrusive, and metamorphic rocks and ophiolite series. Deposits of iron, copper, lead, zinc, chromite, aluminum, gold, arsenic, calcite, dolomite and rock salt are also found (Ghorbani, 2013).

The Quaternary sediments are mainly found in alluvial fans and plains and host alluvial aquifers (Fig. 1), which are the main source of fresh water in the study area. The water table depth in the alluvial aquifers varies between 246 m close to foothills to less than five meters in the lower-elevation parts of watersheds with an average of 63 m (Iran Water Resources Management Company, 2019).

2.2. Collection of groundwater geochemistry data sets

This study utilizes an existing dataset of georeferenced concentrations (n = 676) of EC, pH, major cations (Ca^{2+}, K^{+}, Mg^{2+}, Na^{+}), anions (Cl^{-}, HCO_3^{-}, NO_3^{-}, SO_4^{2-}), and trace elements (Al, As, Cr, Cu, Fe, Pb, Se, V, Zn) from public-supply deep wells (n = 610), springs (n = 48) and qanats (n = 18) (Fig. 1). The average depth of sampled wells is 108 m.

The data were collected by the Razavi Khorasan Water and Wastewater Company and the Razavi Khorasan regional water authority (2015–2018) as part of groundwater quality and pollution monitoring in the province (Joodavi, 2018). Sampling and Laboratory analysis methods are presented in the supplementary materials.

All of the measured ions and elements were gridded using the Inverse Distance Weighting (IDW) interpolation method (Hutchinson, 1989) in ArcGIS in order to display their spatial distributions. Relationships among the parameters were analyzed with descriptive statistics, correlation analyses and graphical representations (Piper diagrams and bivariate plots), which were together used to assess the basic hydrogeochemical processes and geochemical reactions.

Furthermore, the saturation states of the groundwater samples with respect to different minerals were calculated using PHREEQC (Parkhurst and Appelo, 2013). The saturation index (SI) of a mineral explains the mineral dissolution/precipitation possibility in the aquifer. $SI < 0$ indicates subsaturation (dissolution) and $SI > 0$ suggests supersaturation (precipitation) (Appelo and Postma, 2005).

2.3. Geostatistical modeling

2.3.1. Selection of target and predictor variables

Based on the geographical distributions of the dissolved ions and elements and their measured concentrations relative to WHO health-based guidelines (World Health Organization-WHO, 2017), the water quality parameters of As, Cr, EC, Fe, NO_3^{-}, and Se were selected as targets for random forest modeling. Predictor variables relating to potential anthropogenic and geogenic contamination sources were identified based on hydrogeochemical analyses as well as previous studies (Shojaat et al., 2003; Esmaeili-Vardanjani et al., 2015; Nematollahi et al., 2016; Taheri et al., 2016; Zirjanizadeh et al., 2016a; Alighardashi and Mehrani, 2017; Qasemi et al., 2018; Vesali Naseh et al., 2018; Hamidian et al., 2019; Zendehbad et al., 2019). Irrigated areas, urban areas, industrial areas, ophiolites and mafic rocks, intermediate to silicic volcanic (granitoid) rocks, carbonate rocks, marl/evaporite/loess, mineral deposits (metal ores) were considered as predictor variables. The attributes of independent variables are shown in Table 1 and the location maps are presented in the supplementary materials.

The main lithologies and metal ore locations, provided in Supplementary Fig. 1, are obtained from geological maps of Razavi Khorasan Province published at 1:250,000 scale (Korehie et al., 2016)

The locations of irrigated, urban and industrial areas were extracted from land use reports provided by Razavi Khorasan Management and Planning Organization (2019). All of the independent variables were available in raster format with province-wide

Table 1
Independent variables used in the RF model. All were available as rasters, which were ranked according to Table 2.

Variable	Source
Distance to irrigated areas	Razavi Khorasan Management and Planning Organization (2019)
Distance to urban areas	Razavi Khorasan Management and Planning Organization (2019)
Distance to industrial areas	Razavi Khorasan Management and Planning Organization (2019)
Distance to ophiolites and mafic	Korehie et al. (2016)
Distance to granitoid rocks	Korehie et al. (2016)
Distance to carbonate rocks	Korehie et al. (2016)
Distance to marl/evaporite/loess	Korehie et al. (2016)
Distance to metal ore deposits	Korehie et al. (2016)

coverage. New rasters were created with buffer zones at distances of 2.5, 5, 7.5 and 10 km around the features of interest. Each buffer distance was assigned a rank value from 1 to 5 according to Table 2.

2.3.2. Random Forest (RF) modeling

RF is an ensemble machine learning technique utilizing decision trees and can be used for classification or regression (Breiman, 2001 and Biau and Scornet, 2016). In regression problems, a continuous response variable is predicted by growing and then averaging many decision trees, which vary by utilizing different randomly selected data rows (with replacement) in each tree and different predictor variables at each branch (Tahmasebi et al., 2020).

Regression RF modelling was implemented using the Microsoft Excel add-in XLSTAT (Addinsoft, 2020). The main parameters of the RF model that must be specified are the number of variables randomly selected at each node (mtry) and the number of trees (ntree). The "mtry" value was set to p/3, in which p is the number of independent variables and "ntree" was set to 1000. The relative importance of the predictor variables in each model was assessed through the RF measure of importance, which gives the average model error when the independent-variable values are randomly sorted.

The predictive ability of the RF models was evaluated by three criteria: coefficient of determination (R^2), normalized root-mean-square error (NRMSE), and the Nash–Sutcliffe coefficient of efficiency (NSE) (Legates and McCabe, 1999), which are defined as follows:

$$NRMSE = \frac{\sqrt{{}^{1}/_{N}\sum_{i=1}^{N}(O_i - P_i)^2}}{O_{\max} - O_{\min}} \tag{1}$$

$$NSE = 1 - \frac{\sum_{i=1}^{N}(O_i - P_i)^2}{\sum_{i=1}^{N}(O_i - \overline{O})^2} \tag{2}$$

where O_i is an observed value, O_{min}, O_{max} *and* $\overline{O}$ are the minimum, maximum and average of the observed values respectively; and P_i is the model predicted value and N is the number of observed data. If a model produces values that are the same as the observations, NRMSE and NSE values are 0 and 1 respectively.

NRMSE shows the square of the differences between the predicted and the observed values in relation to the variability in the observed data. These three criteria together give insight into how well the models predict the observed data.

2.4. Non-carcinogenic health risk assessment

The health risk posed by exposure to the metal(loid)s As, Cr, Cu, Fe, Pb, Se, V, and Zn in groundwater was quantified using the hazard quotient (HQ) method of the USEPA (1999):

$$HQ = CDI/RfD \tag{3}$$

$$CDI = \frac{C \times IR}{BW} \tag{4}$$

where CDI is the dose of metal(loid) intake (mg/kg/day), *RfD* is the reference dose (mg/kg/day), which refers to the maximum acceptable dose of a toxic substance (Table 3), C is the concentration of metal(loid) (mg/L), IR is the ingestion rate of water, which was set to 3.49 for adults and 2.14 L/day for children (Tirkey et al., 2017; Radfard et al., 2019), and BW is body weight, which was taken as 70 kg for adults and 22.3 for children (Fakhri et al., 2015). In this study ingestion of contaminated groundwater was considered as the only exposure route to PTEs (Ravindra et al., 2019).

As the risk assessment is done for multiple metals and metalloids, the hazard index (HI) can be calculated from following equation (Qasemi et al., 2019; Sohrabi et al., 2020):

Table 2
Criteria used to create the ranked raster of independent variables.

Distance (km)	Rank
<2.5	5
2.5–5	4
5–7.5	3
7.5–10	2
>10	1

Table 3
Reference maximum acceptable doses (RfD) for each toxic metal(loid)s (USEPA, 2020).

Chemical Parameter	$RfD_{ingestion}$ (mg/kg/day)
As	0.0003
Cr	0.003
Cu	0.037
Fe	0.3
Pb	0.014
Se	0.005
V	0.009
Zn	0.3

$$HI = \sum_{i=1}^{n} HQ_i \quad (5)$$

An HQ or HI value greater than 1 indicates medium to high chronic health risk (Yousefi et al., 2018), as outlined in Supplementary Table 2.

3. Results

3.1. Groundwater hydrogeochemical characteristics and spatial distribution of physico-chemical parameters

Table 4 provides a statistical summary of the measured major anions, trace elements and other chemical parameters in the 676 data points along with the corresponding WHO guideline concentrations (World Health Organization-WHO, 2017). The gridded maps of these parameters are shown in Fig. 2. The ranking of major cation concentrations is generally $Na^+ > Ca^{2+} > Mg^{2+} > K^+$. The ranking among the major anions is $SO_4^{2-} > Cl^- > HCO_3-$. The measures of EC, SO_4^{2-}, Na^+, Mg^{2+}, and Cr exceed the maximum permissible limits in more than 10 % of the samples.

3.2. Factors controlling the major-ions chemistry in groundwater

Plotting the samples on a Piper diagram (Fig. 3) reveals that 50 % of the samples belongs to the Na-Cl type followed by Ca-Mg-Cl (27 %), Ca-HCO_3 (15 %), Ca-Na-HCO_3 (7 %) and Ca-Cl (2%). The Ca-Mg-HCO_3 water type is mostly found in the northern part of the province where EC values are all less than 1000 μS/cm, which is likely due to the dissolution of carbonates (Supplementary Fig. 6). The predominance of the Na-Cl water type indicates that evaporites such as halite and gypsum/anhydrite strongly affect the groundwater chemistry.

Bivariate plots of ionic constituents of studied samples are presented in Fig. 4. The ratio of (Ca^{2+}+Mg^{2+}) to total cations (Fig. 4a) for

Table 4
Summary of the measured samples. Descriptive statistics of the hydrochemical parameters measured in the 676 groundwater samples in the study area.

Category	Parameter	Unit	Mean ± STDV[1]	UPL[2]	No. of samples exceeds UPL
General	EC	μS/cm	1537.5 ± 1559.2	1500	228 (35 %)
	pH	–	7.8 ± 0.1	8.5	0
Major cations	Ca^{2+}	mg/L	59.5 ± 42.6	200	10 (1 %)
	K^+	mg/L	2.2 ± 1.4	200	0
	Mg^{2+}	mg/L	35.8 ± 23.8	50	122 (18 %)
	Na^+	mg/L	175.8 ± 130.8	200	220 (33 %)
Major anions	Cl^-	mg/L	148.5 ± 144.6	250	110 (16 %)
	HCO_3^-	mg/L	269.7 ± 68.5	500	5 (1 %)
	NO_3^-	mg/L	19.3 ± 15.7	50	18 (2.7 %)
	SO_4^{2-}	mg/L	227.3 ± 184.5	250	237 (35 %)
Trace elements	Al	μg/L	14.2 ± 5.2	200	0
	As	μg/L	3.1 ± 2	10	8 (1 %)
	Fe	μg/L	114.5 ± 108.5	300	43 (6 %)
	Pb	μg/L	2.6 ± 1.2	10	0
	Cr	μg/L	21.9 ± 26.8	50	113 (17 %)
	Cu	μg/L	6.4 ± 4	2000	0
	Se	μg/L	4.8 ± 2.8	10	30 (4 %)
	V	μg/L	12.2 ± 13.9	100	0
	Zn	μg/L	22.8 ± 38.5	3000	0

[1] Standard deviation.
[2] Upper permissible limit (WHO, 2017).

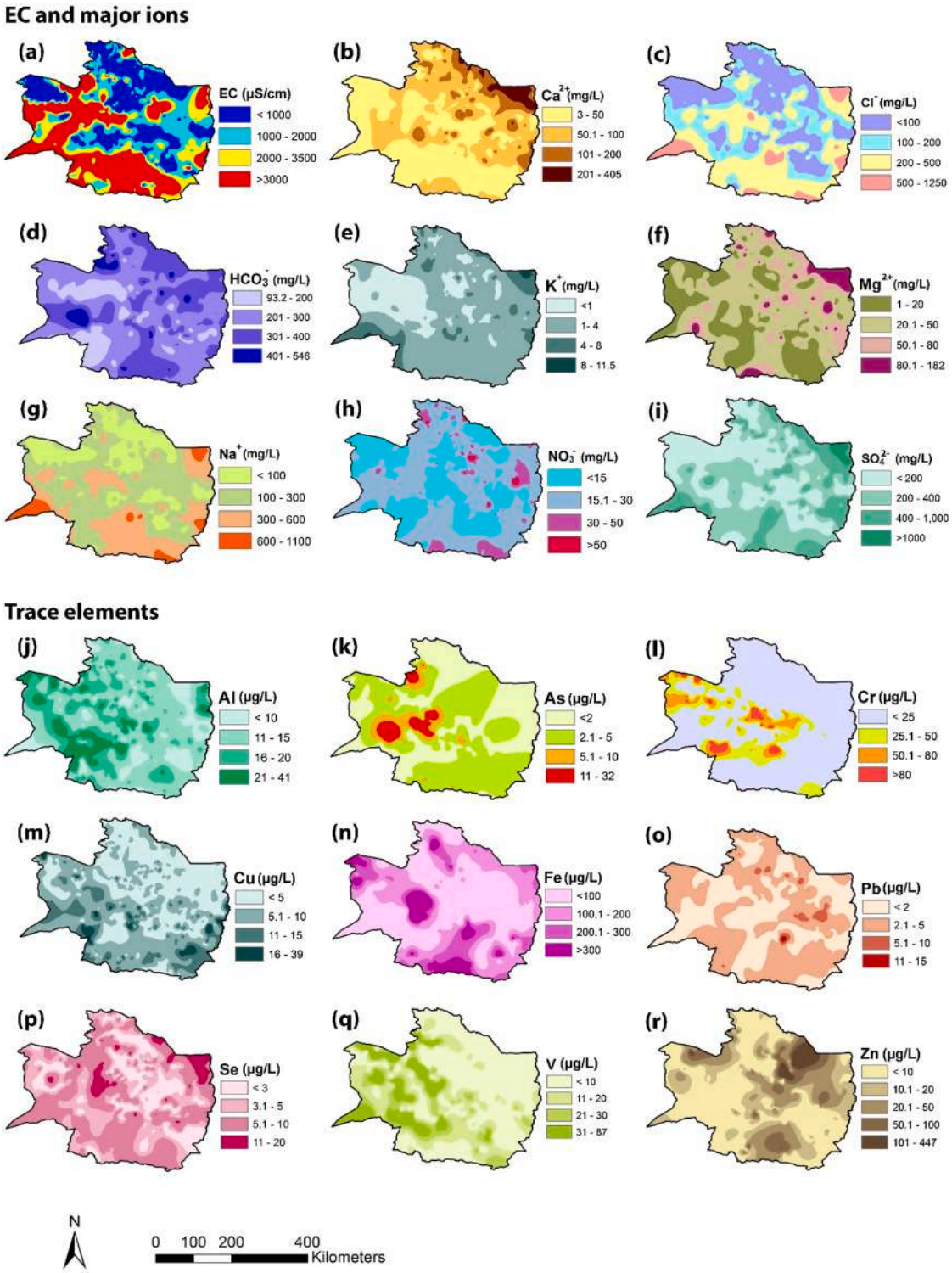

Fig. 2. Gridded maps of the hydrochemical parameters measured in groundwater in Razavi Khorasan province.

all samples is considerably less than one, which implies that other cations, such as Na^+ and K^+, are abundant in groundwater samples. The ratio of $(Ca^{2+} + Mg^{2+})$ to $(HCO_3^- + SO_4^{2-})$ of most samples is less than one (Fig. 4b), which suggests that silicate weathering affects the Ca^{2+} and Mg^{2+} chemistry (Lakshmanan et al., 2003; Dehbandi et al., 2017). The ratio of Ca^{2+} to HCO_3- for groundwater formed in dolomite and calcite aquifers is normally between 1/4 and 1/2 (Ledesma et al., 2014). However, only a few samples in Fig. 4c fall

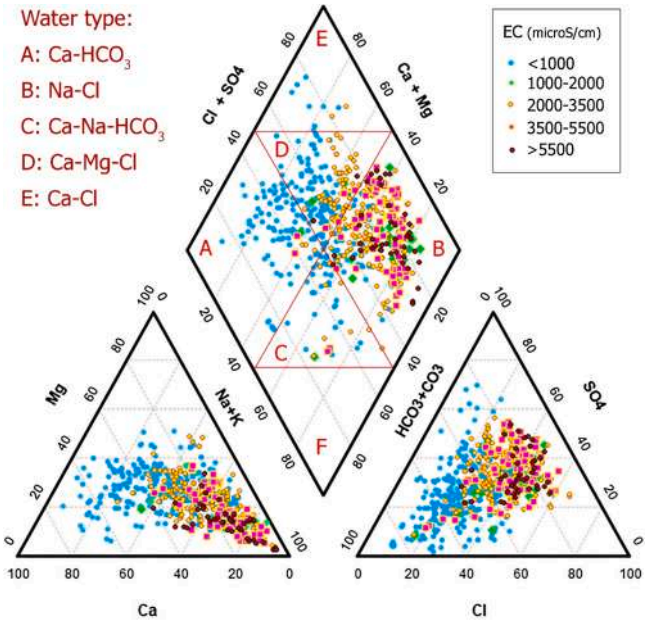

Fig. 3. Piper diagram representing the water types of the 676 groundwater samples.

between these ratios, whereas most are higher. The ratio of some samples of Ca^{2+} vs. SO_4^{2-} (Fig. 4d) is close to one, which suggests that these samples are in contact with gypsum and anhydrite (Wu et al. 2015). Examination of Fig. 4c and d suggests that Ca^{2+} is removed from water by reactions such as cation exchange. The plot of $[(Na^+ + K^+) - Cl^-]$ against $[(Ca^{2+} + Mg^{2+}) - (SO_4^{2-} + HCO_3^-)]$ (Fig. 4e) confirms the cation-exchange process with Na^+ increasing while Ca^{2+} decreases (McLean et al., 2000).

The plot of the Na^+/Cl^- ratio against Cl^- concentrations (Fig. 4f) shows that the ratio increases with decreasing salinity, with the Na^+/Cl^- ratio of the water samples ranging from 0.3 to 8.6. The majority of samples (97 %) has a molar ratio $\geq$1, which indicates that the relative abundance of sodium (Na^+) could be related to ion exchange and/or silicate weathering. This plot also shows that samples with high EC values have a molar ratio equal or close to one, which is a sign of the dissolution of evaporite minerals (Sánchez-Martos et al., 2002; Taherian and Joodavi, 2021). Furthermore, EC is significantly corelated with Na^+, Cl^-, and SO_4^{2+} (Supplementary Table 3).

The HCO_3^-/Cl^- ratio is an indicator of salinization, whereby values greater than one indicate low salinity in carbonate zones. Dissolution of evaporite minerals enriches Cl^- in groundwater, which decreases the HCO_3^-/Cl^- ratio (Fig. 4f). As seen in Fig. 4h, the water samples have a wide range of Ca^{2+}/Na^+ ratios (0.1–10), which are inversely related to salinity. A high Ca^{2+}/Na^+ molar ratio indicates that carbonate dissolution is the dominant process in the aquifer (Ayadi et al., 2018).

Moreover, the saturation index (SI) calculated by PHREEQC indicates that some groundwater samples are saturated with respect to calcite and dolomite (Fig. 5a, b, e), which confirms carbonate dissolution.

On the other hand, all samples are undersaturated with respect to gypsum and halite. SI_{gypsum} and SI_{halite} increase with TDS indicating dissolution of evaporite minerals (Fig. 5c, d). Plotting SI_{halite} versus $SI_{calcite}$ (Fig. 5f) reveals two geochemical evolution trends in the aquifer.

In relatively low salinity groundwater samples, mostly located in the northern areas and close to karst aquifers, the precipitation of Ca^{2+} and the dissolution of evaporite minerals along the groundwater flow path lead to a decrease in $SI_{calcite}$ and increase in SI_{halite} (line I in Fig. 5f). In contrast, far from carbonate formations, for example in the northeast off the study area, the dissolution of evaporites and carbonate minerals in marl and loess formations causes a simultaneous increases in $SI_{calcite}$ and SI_{halite}, EC (line ii in Fig. 5f).

3.3. *Geostatistical modelling*

Random forest (RF) regression models were used to help identify potential sources and processes of groundwater contamination. Based on the water quality assessment described above, six parameters (As, Cr, EC, Fe, NO_3^-, Se) were modeled using the variables listed in Table 1. The model results are plotted against the observations in Fig. 6, which also includes the model-performance measures (R^2, NRMSE and NSE).

The performance of the models are generally considered acceptable, as NSE and R^2 for all models are greater than 0.5 (Zhou et al., 2019). The variables' importance in each regression model indicates the strength of the relationship between a contaminant and its potential sources (Fig. 7).

The EC model confirms that high salinity is found where evaporate deposits are found (Fig. 7a and Supplementary Fig. 1) and/or

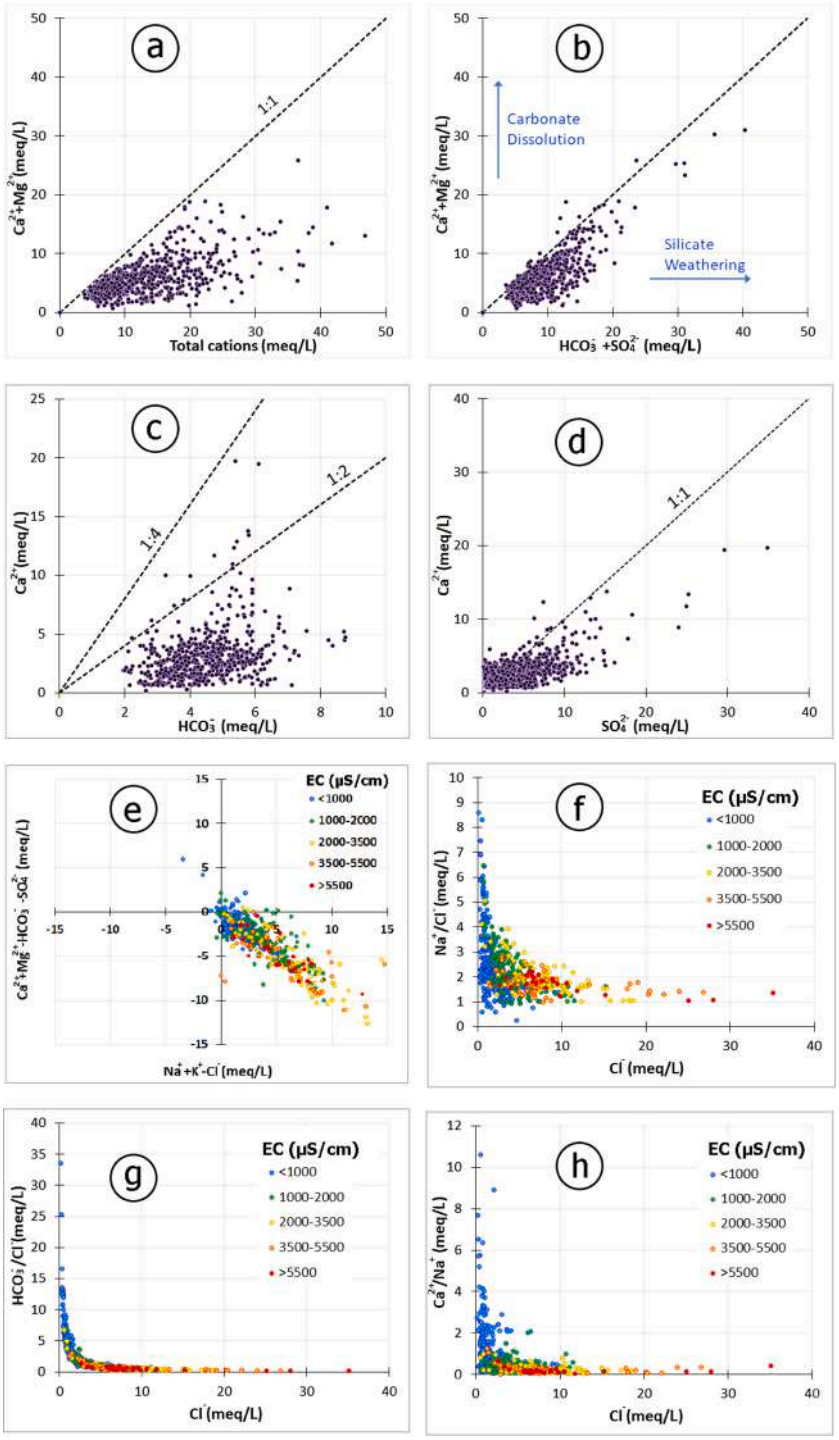

Fig. 4. Relationships between major ions showing geochemical reactions.

considerable evapotranspiration has taken place. Evaporites can exist as geological formations, such as marl, halite, gypsum, loess or salt flats (pans), and their dissolution can considerably increase groundwater salinity (Sánchez-Martos et al., 2002). Furthermore, evapotranspiration from irrigated fields can increase soil and irrigation return-flow salinity (Foster et al., 2018).

The NO_3^- model shows that nitrate in groundwater is associated primarily with urban areas followed by agricultural activities (Fig. 7c). In the study area, human sewage in cities as well as many rural areas is traditionally discharged into absorbing wells, which leads to high levels of nitrate in groundwater (Qasemi et al., 2018; Zendehbad et al., 2019). Furthermore, there are about 752,500 ha of

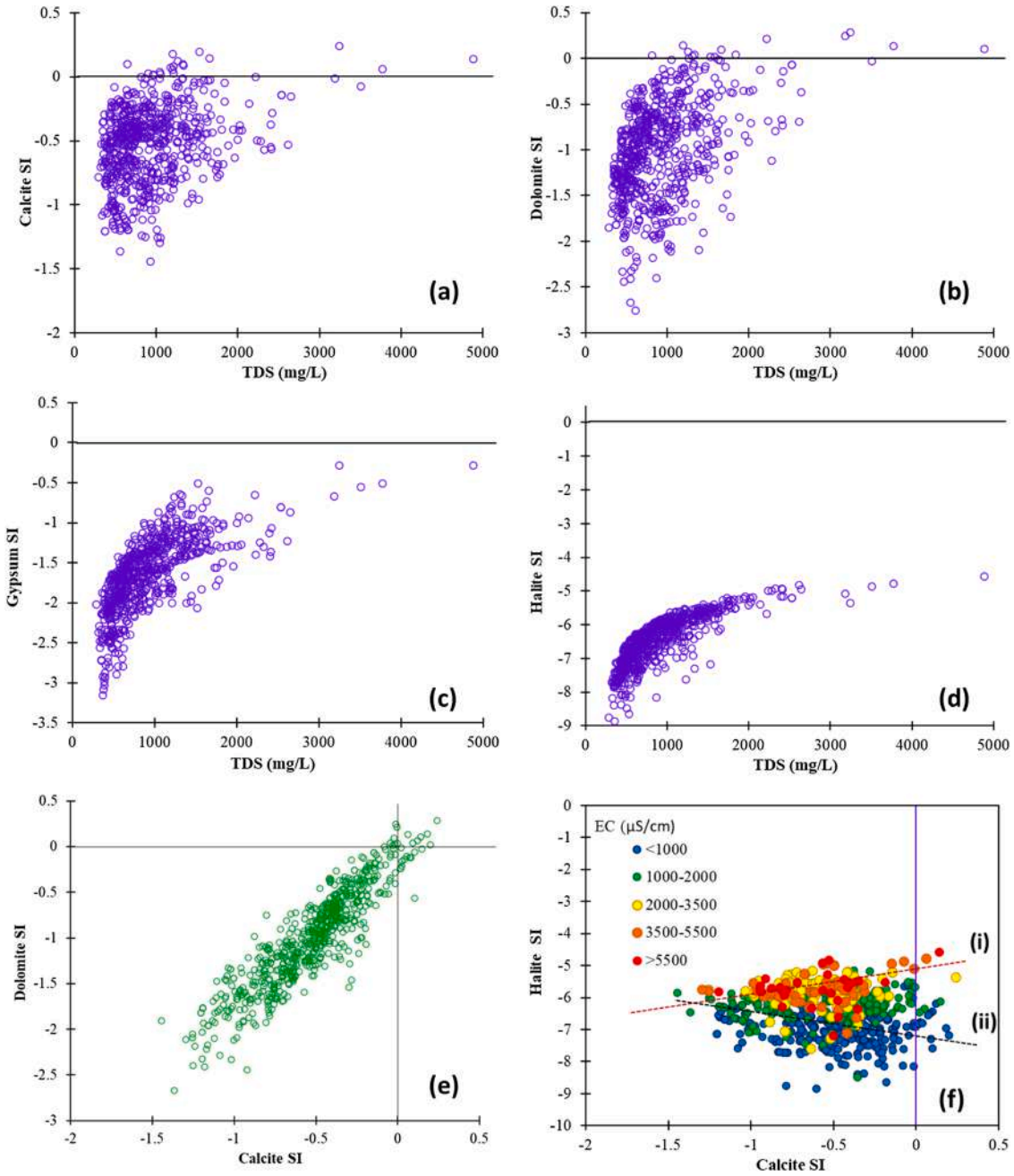

Fig. 5. Saturation Index (SI) for Calcite, Dolomite, Gypsum and Halite in groundwater samples.

irrigated agriculture in Razavi Khorasan province on which nitrogenous and animal-waste fertilizers containing high levels of nitrate are applied (Alighardashi et al., 2017).

The chromium model clearly indicates that ophiolite and ultramafic units are the main sources of chromium in groundwater. These ophiolite and ultramafic units usually consisting of peridotite, serpentinite, gabbro and chromite deposits (Shafaii Moghadam et al., 2014). Chromium is typically present as Cr(III) and Cr(VI), with Cr(VI) being very toxic and more soluble and mobile in groundwater (Coyte et al., 2019).

Cr(III) is found in minerals and can be oxidized and transformed to Cr(VI) in the existence of an oxides such as MnO_2 (Bertolo et al., 2011).

$$Cr(III) + 1.5\ MnO_2 + H_2O = HCr(VI)O_4^- + 1.5\ Mn^{2+} + H^+ \quad (6)$$

Groundwater arsenic in Razavi Khorasan is associated mainly with granitoid rocks (Fig. 7e). This is consistent with reported

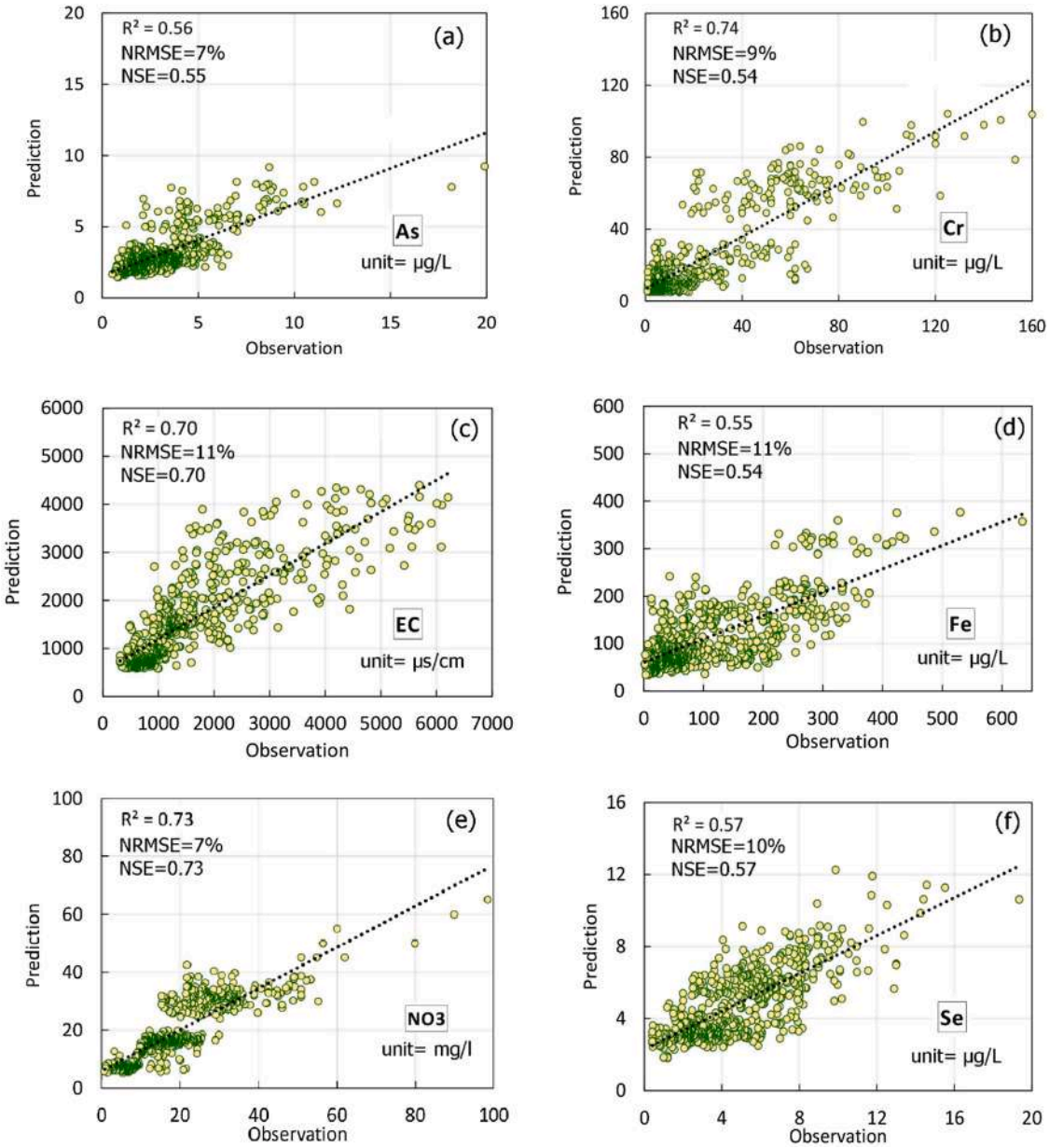

Fig. 6. Performance evaluation criteria and the plots of the predicted concentrations generated by the RF models against the observed concentrations; R^2: coefficient of determination, NRMSE: normalized root mean square error, NSE: Nash–Sutcliffe coefficient of efficiency.

geogenic arsenic-contaminated groundwater in Razavi Khorasan province (Hamidian et al., 2019), where arsenic release results from the weathering of sulfide minerals such as realgar, orpiment, and arsenopyrite in granitoid rocks (Ghasemzadeh et al., 2011; Alidadi et al., 2015; Alaminia et al., 2016; Taheri et al., 2016; Hamamipour et al., 2018).

Some possible reactions leading to the release of arsenic from sulfide minerals can be found by the following reactions (Chelsea et al., 2014):

orpiment dissolution:

$$0.5\ As_2S_3 + 3H_2O = H_3AsO_{3(aq)} + 1.5H_2S \quad (7)$$

arsenopyrite dissolution:

$$FeAsS(s) + 1.5H_2O + 2.75\ O_2(aq) = Fe_2^{2+} + H_3AsO_3\ (aq) + SO_4^{2-}\ (aq) \quad (8)$$

Fig. 7d shows that the presence of metal ore deposits is the dominant predictor of iron concentration in groundwater. Previous

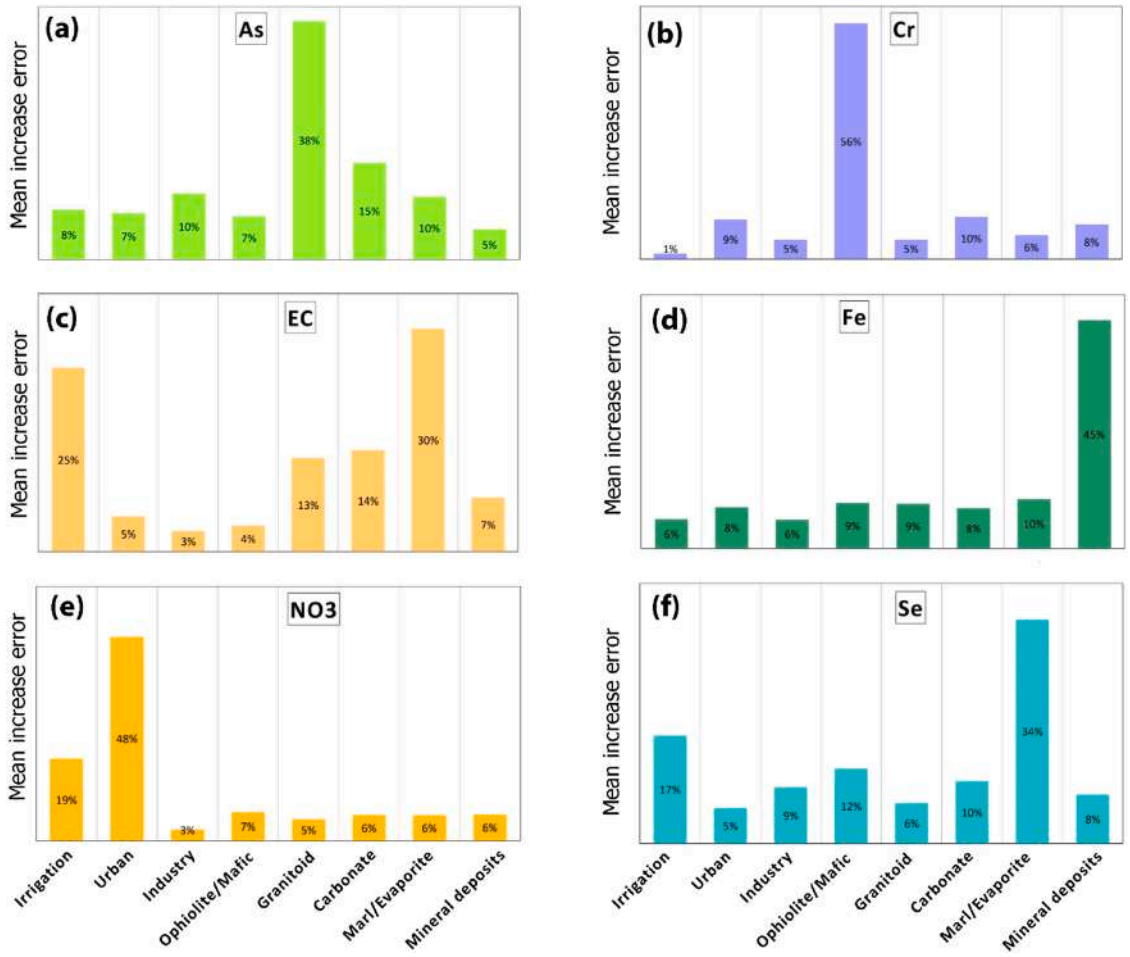

Fig. 7. Importance of the independent variables of the random forest models. The mean increase in error refers to the effect when a variable is randomly sorted.

studies indicated that iron can originate from trachyandesite and pyroclastic rocks in some parts of Razavi Khorasan province (Zirjanizadeh et al., 2016b; Taghadosi et al., 2018). Moreover, the well-known Sangan iron skarn deposit, which is located in the southeastern parts of the study area, is another well-known source of iron (Golmohammadi et al., 2015; Sepidbar et al., 2017).

The likely sources of groundwater contaminants based on the modeling results are summarized in Table 5.

3.4. Health risk assessment

A non-carcinogenic health risk assessment was conducted to estimate the probability of harmful effects of exposure to As, Cr, Cu, Fe, Pb, Se, V and Zn in groundwater used for drinking purposes.

The average hazard quotient (HQ) values indicate that As and Cr make up 53 % and 28 %, respectively, of the total non-carcinogenic risk (HI) due to groundwater constituents for the total population. HI ranges between 0.33 and 7.33 (average of 1.67) for children and between 0.13 and 3.01 (average of 0.65) for adults. Fig. 8 shows that areas with medium to high-risk values for

Table 5
Summary of main groundwater contamination sources as inferred from the random forest regression models.

Parameter	Source(s)	
As	Geology	granitoid rocks
Cr	Geology	ophiolites
EC	Geology/Agriculture	marl/evaporite/loess\groundwater-irrigated agriculture
Fe	Geology	metal ores
NO_3^-	Urban/Agriculture	waste water/fertilizer
Se	Geology	marl/evaporite/loess

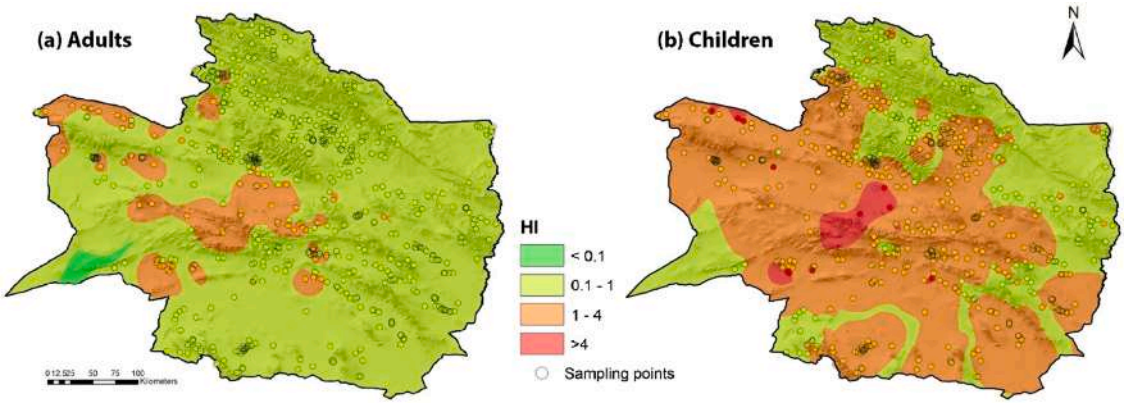

Fig. 8. Spatial distribution of non-carcinogenic hazard index (HI) for (a) adults and (b) children.

children largely coincide with zones of high As and Cr concentrations (Fig. 2).

In addition to causing adverse non-carcinogenic health effects, arsenic and chromium are categorized as carcinogenic substances (World Health Organization-WHO, 2017). The chronic consumption of As-contaminated water may cause skin, bladder or lung cancer (Polya and Middleton, 2017; World Health Organization-WHO, 2017), whereby chromium, especially Cr(VI), is known to cause DNA damage (Agency for Toxic Substances and Disease Registry (ATSDR), 2012; Wang et al., 2017).

4. Discussion

Despite there being separate alluvial aquifer systems in the study area separated by mountains, the results show that the dominant lithology of the mountains is responsible for controlling groundwater chemistry and increasing the concentration of some PTEs in groundwater, such as As, Cr, Fe and V, beyond the river-basin/aquifer boundaries. This can be conceptualized by two phenomena presented in Fig. 9.

If mountain block/front recharge exists, the chemistry of subsurface inflow directly affects the groundwater quality in alluvial aquifers (Fig. 9a) (Ajami et al., 2011; Joodavi et al., 2016). That is common in karst-alluvial aquifer systems in the northern parts of the study area where low salinity groundwater with Ca-Mg-HCO_3 water type can be found in alluvial aquifers. Moreover, it is possible that this mountain system recharge is responsible for high concentrations of arsenic in the western parts of the province where arsenic is released by weathering of sulfide minerals in granitoid rocks.

Even if the mountain block/front recharge component is not significant, the alluvial aquifers could contain particles from adjacent mountains (Fig. 9b) (Kaprara et al., 2014). The random forest model suggests that high Cr concentrations in groundwater are observed in the alluvial aquifers located not far from the ophiolitic rocks. While these rocks do not have a developed fractured storage system, the sediments of the alluvial aquifers originated from ophiolite and ultramafic units are likely the source of Cr in groundwater.

Furthermore, the geological map show that marl/evaporites are mainly found in the southern and western parts of the region. Hydrogeological studies have shown that these units form the bedrock of alluvial aquifers in these areas (Joodavi et al., 2009; Izady et al., 2015). The random forest model results confirm that groundwater resources in these areas are more saline.

The approach provided here identification of the sources of major ions and toxic elements in groundwater in regions lacking adequate monitoring programs and sampling data. Therefore, additional groundwater quality measurements and geochemical and mineralogical information as well as more information about the amount and chemistry of industrial wastewater would improve the robustness of the geostatistical models, especially in locations close to contamination sources such as industrial areas."

Another limitation of this study is that this method characterizes large-scale (macro-scale) spatial variation in the elements in groundwater. However, the chemical composition of groundwater samples may be affected by local hydrologic and hydrogeological factors. Future research will add consideration of these local factors such as residence time to accurately investigate the driving forces of groundwater quality.

5. Conclusion

Understanding the factors affecting and controlling groundwater quality is necessary to improve water security and public health through reducing water-related risks.

Although most hydrogeochemistry studies try to interpret geochemical reactions along groundwater flow paths in an aquifer or a watershed, this paper proposed an approach to identify the sources of salinity, nitrate and PTEs in groundwater in large-scale studies of broad geographical areas where there are large gaps in testing locations.

Integrated approaches of statistical analysis, conventional hydrogeochemical plots, and machine learning were employed in this study to characterize the groundwater chemistry in Razavi Khorasan province and identify likely sources of contamination. Hydrogeochemical controls on groundwater quality and human health risk from harmful elements in the province were identified from 676

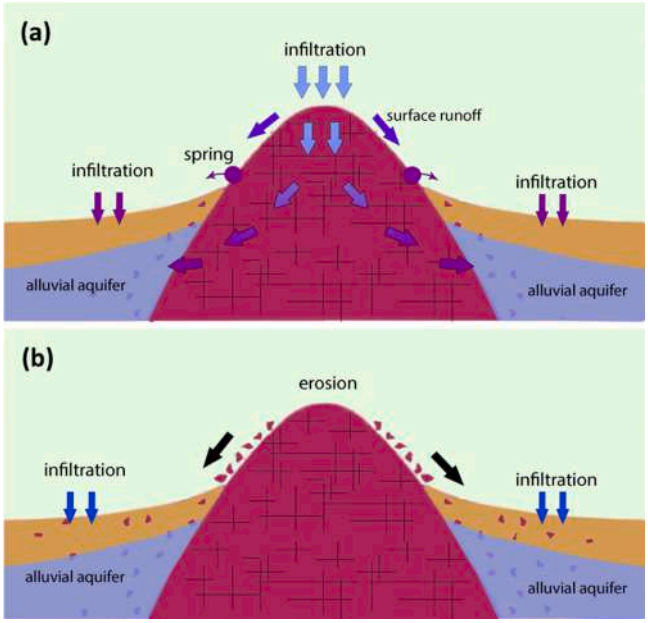

Fig. 9. Two conceptual models showing the effects of geology on groundwater quality beyond the river-basin/aquifer boundaries.

groundwater samples in the study area.

We found that the chemical composition of groundwater is determined predominantly by geology but also influenced by human activities. The Na-Cl water type along with high salinity levels in groundwater, Se and SO_4^{2-} can be related to the dissolution of salts from geological formations as well as evapotranspiration and irrigation return flow caused by groundwater-irrigated agriculture. Random forest regression modeling has also shown that high concentrations of chromium, arsenic and iron in groundwater are attributed to the presence of ophiolites, granitoid (intermediate to silicic volcanic) rocks and metal ores (formed in pyroclastic rocks and skarn deposits), respectively. Moreover, discharging sewage directly into aquifers and applying fertilizers in agricultural activities result in high levels of nitrate in groundwater. A non-carcinogenic health risk assessment of PTEs (As, Cr, Cu, Fe, Pb, Se, V, Zn) in groundwater indicates that As and Cr constitute 53 % and 28 % of the total risk, respectively.

The predictor variables used in the random forest modeling are readily available, making this integrated approach relevant for identifying potential regional groundwater contamination sources. The results can be used to develop cost-effective water quality monitoring programs for water resource planning and management in Razavi Khorasan province, Iran.

CRediT authorship contribution statement

Ata Joodavi: Conceptualization, Methodology, Writing - original draft. **Reza Aghlmand:** Data curation, Investigation. **Joel Podgorski:** Supervision, Writing - review & editing. **Reza Dehbandi:** Formal analysis, Validation. **Ali Abbasi:** Investigation, Writing - review & editing.

Declaration of Competing Interest

The authors declare that they have no known competing financial interests or personal relationships that could have appeared to influence the work reported in this paper.

Acknowledgments

This research was financially supported by Iran National Science Foundation (INSF), Grant Number 97008161 and the Swiss Agency for Development and Cooperation (project no. 7F-09963.01.01).

Appendix A. Supplementary data

Supplementary material related to this article can be found, in the online version, at doi:https://doi.org/10.1016/j.ejrh.2021.100885.

References

Addinsoft, 2020. XLSTAT Statistical and Data Analysis Solution. Boston, USA. https://www.xlstat.com.

Agency for Toxic Substances and Disease Registry (ATSDR), 2012. Toxicological Profile for Chromium. U.S. Department of Health and Human Services, Public Health Service, Atlanta, GA.

Ajami, H., Troch, P., Maddock, T., Meixner, T., Eastoe, C., 2011. Quantifying mountain block recharge by means of catchment-scale storage-discharge relationships. Water Resour. Res. 47 https://doi.org/10.1029/2010WR009598.

Alaminia, Z., Karimpour, M.H., Homam, S.M., 2016. Mineralization and trace element distribution in pyrite using EMPA in exploration drill holes from Cheshmeh Zard gold district, Khorasan Razavi Province. Iran. J. Econ. Geol. 7 (2), 203.

Alidadi, H., Ramezani, A., Davodi, M., Peiravi, R., Paydar, M., Dolatabadi, M., Rafe, S., 2015. Determination of total arsenic in water resources: a case study of Rivash in Kashmar City. J. Health Scope 4 (3). https://doi.org/10.17795/jhealthscope-25424.

Alighardashi, A., Mehrani, M.J., 2017. Survey and zoning of nitrate-contaminated groundwater in Iran. J. Mater. Environ. Sci. 8 (12), 4339–4348.

Amiri, V., Sohrabi, N., Dadgar, M.A., 2015. Evaluation of groundwater chemistry and its suitability for drinking and agricultural uses in the Lenjanat plain, central Iran. Environ. Earth Sci. 74, 6163–6176. https://doi.org/10.1007/s12665-015-4638-6.

Amiri, V., Kamrani, S., Ahmad, A., et al., 2021a. Groundwater quality evaluation using Shannon information theory and human health risk assessment in Yazd province, central plateau of Iran. Environ. Sci. Pollut. Res. 28, 1108–1130. https://doi.org/10.1007/s11356-020-10362-6.

Amiri, V., Li, P., Bhattacharya, P., et al., 2021b. Mercury pollution in the coastal Urmia aquifer in northwestern Iran: potential sources, mobility, and toxicity. Environ. Sci. Pollut. Res. 28, 17546–17562. https://doi.org/10.1007/s11356-020-11865-y.

Appelo, C., Postma, D., 2005. Geochemistry, Groundwater and Pollution, 2nd edition. Balkema, Rotterdam. https://doi.org/10.1201/9781439833544.

Ashraf, S., Nazemi, A., AghaKouchak, A., 2021. Anthropogenic drought dominates groundwater depletion in Iran. Sci. Rep. 11, 9135. https://doi.org/10.1038/s41598-021-88522-y.

Ayadi, R., Trabelsi, R., Zouari, K., et al., 2018. Hydrogeological and hydrochemical investigation of groundwater using environmental isotopes (18O, 2H, 3H, 14C) and chemical tracers: a case study of the intermediate aquifer, Sfax, southeastern Tunisia. Hydrogeol. J. 26, 983–1007. https://doi.org/10.1007/s10040-017-1702-1.

Baghvand, A., Nasrabadi, T., Nabi Bidhendi, G., Vosoogh, A., Karbassi, A., Mehrdadi, N., 2010. Groundwater quality degradation of an aquifer in Iran central desert. Desalination 260, 264–275.

Barbieri, M., Ricolfi, L., Vitale, S., et al., 2019. Assessment of groundwater quality in the buffer zone of Limpopo National Park, Gaza Province, Southern Mozambique. Environ. Sci. Pollut. Res. 26, 62–77. https://doi.org/10.1007/s11356-018-3474-0.

Bertolo, R., Bourotte, C., Hirata, R., Marcolan, L., Sracek, O., 2011. Geochemistry of natural chromium occurrence in a sandstone aquifer in Bauru Basin, São Paulo State, Brazil. Appl. Geochem. 26 (8), 1353–1363. https://doi.org/10.1016/j.apgeochem.2011.05.009.

Biau, G., Scornet, E., 2016. A random forest guided tour. TEST 25, 197–227. https://doi.org/10.1007/s11749-016-0481-7.

Breiman, L., 2001. Random forest. Mach. Learn. 45, 5–32. https://doi.org/10.1023/A:1010933404324.

Bretzler, A., et al., 2017. Groundwater arsenic contamination in Burkina Faso, West Africa: predicting and verifying regions at risk. Sci. Total Environ. https://doi.org/10.1016/j.scitotenv.2017.01.147.

Chelsea, W.N., Yang, Y.J., Schupp, D., Jun, Y.Sh., 2014. Water chemistry impacts on arsenic mobilization from arsenopyrite dissolution and secondary mineral precipitation: implications for managed aquifer recharge. Environ. Sci. Technol. 48 (8), 4395–4405. https://doi.org/10.1021/es405119q.

Coyte, R.M., McKinley, K.L., Jiang, S., Karr, J., Dwyer, G.S., Keyworth, A.J., Davis, C.C., Kondash, A.J., Vengosh, A., 2019. Occurrence and distribution of hexavalent chromium in groundwater from North Carolina, USA. Sci. Total Environ. https://doi.org/10.1016/j.scitotenv.2019.135135.

Dehbandi, R., Moore, F., Keshavarzi, B., Abbasnejad, A., 2017. Fluoride hydrogeochemistry and bioavailability in groundwater and soil of an endemic fluorosis belt, central Iran. Environ. Earth Sci. 76 (4), 177.

Dehbandi, R., Abbasnejad, A., Karimi, Z., Herath, I., Bundschuh, J., 2019. Hydrogeochemical controls on arsenic mobility in an arid inland basin, Southeast of Iran: the role of alkaline conditions and salt water intrusion. Environ. Pollut. 249, 910–922.

Esmaeili-Vardanjani, M., Rasa, I., Amiri, V., et al., 2015. Evaluation of groundwater quality and assessment of scaling potential and corrosiveness of water samples in Kadkan aquifer, Khorasan-e-Razavi Province, Iran. Environ. Monit. Assess. 187, 53. https://doi.org/10.1007/s10661-014-4261-0.

Fakhri, Y., Jafarzadeh, S., Moradi, B., et al., 2015. The non-carcinogenic risk of cadmium in bottled water in different age groups humans: Bandar Abbas City, Iran. Mater. Sociomed. 27 (Feb. (1)), 52–55. https://doi.org/10.5455/msm.2014.27.52-55.

Foster, S., Pulido-Bosch, A., Vallejos, Á., et al., 2018. Impact of irrigated agriculture on groundwater-recharge salinity: a major sustainability concern in semi-arid regions. Hydrogeol. J. 26, 2781–2791. https://doi.org/10.1007/s10040-018-1830-2.

Ghasemzadeh, F., Shafaroodi, A.A., 2011. Environmental impacts of arsenic in Cheshmeh Zard area, southwest of Neyshabour, Khorasan Razavi province. Iran. J. Crystallogr. Mineral. 19 (3), 545–556 (In Persian).

Ghorbani, M., 2013. Economic Geology of Iran, Mineral Deposits and Natural Resources of Iran. Springer Geology.

Golmohammadi, A., Karimpour, M.H., Malekzadeh Shafaroudi, A., Mazaheri, S.A., 2015. Alteration-mineralization, and radiometric ages of the source pluton at the Sangan Iron skarn deposit, Northeastern Iran. Ore Geol. Rev. 65, 545–563. https://doi.org/10.1016/j.oregeorev.2014.07.005.

Hamamipour, B., Tajeddin, H.A., Barahmand, L., 2018. Geology and mineralization of Sebandoon gold deposit, North of Bardeskan. J. Geosci. 27 (108), 155–168. https://doi.org/10.22071/gsj.2017.77437.1030.

Hamidian, A.H., Razeghi, N., Zhang, Y., Yang, M., 2019. Spatial distribution of arsenic in groundwater of Iran, a review. J. Geochem. Explor. 201, 88–98. https://doi.org/10.1016/j.gexplo.2019.03.014.

Heydarirad, L., Mosaferi, M., Pourakbar, M., et al., 2019. Groundwater salinity and quality assessment using multivariate statistical and hydrogeochemical analysis along the Urmia Lake coastal in Azarshahr plain, North West of Iran. Environ. Earth Sci. 78, 670. https://doi.org/10.1007/s12665-019-8655-8.

Hutchinson, M.F., 1989. A new procedure for gridding elevation and stream line data with automatic removal of spurious pits. J. Hydrol. 106, 211–232. https://doi.org/10.1016/0022-1694(89)90073-5.

Iran Water Resources Management Company, 2019. Iran Water Resources Management Company [Online]. Available: https://www.wrm.ir. (Accessed 23 December 2019).

Izady, A., Davary, K., Alizadeh, A., et al., 2015. Groundwater conceptualization and modeling using distributed SWAT-based recharge for the semi-arid agricultural Neishaboor plain, Iran. Hydrogeol. J. 23, 47–68. https://doi.org/10.1007/s10040-014-1219-9.

Joodavi, A., 2018. Effects of Geology on the Quality of Drinking Water Wells in Razavi Khorasan Province. Razavi Khorasan Water and Wastewater Company. In Farsi.

Joodavi, A., Zare, M., Etemadi, B., 2009. Hydrogeochemistry and sources of groundwater salinity in Feyz-Abad plane. In: Ahvaz, Iran12th Symposium of the Geological Society of Iran, 2, pp. 411–417. In Farsi.

Joodavi, A., Zare, M., Mahootchi, M., 2015. Development and application of a stochastic optimization model for groundwater management: crop pattern and conjunctive use consideration. Stochast. Environ. Res. Risk Assess. J. https://doi.org/10.1007/s00477-015-1049-x.

Joodavi, A., Zare, M., Raeisi, E., Ahmadi, M.B., 2016. A multi-compartment hydrologic model to estimate groundwater recharge in an alluvial-karst system. Arab. J. Geosci. 9, 195. https://doi.org/10.1007/s12517-015-2084-0.

Kaprara, E., Kazakis, N., Simeonidis, K., Coles, S., Zouboulis, A.I., Samaras, P., Mitrakas, M., 2014. Occurrence of Cr(VI) in drinking water of Greece and relation to the geological background. J. Hazard. Mater. 281, 2–11. https://doi.org/10.1016/j.jhazmat.2014.06.084.

Khanoranga, Khalid, S., 2019. An assessment of groundwater quality for irrigation and drinking purposes around brick kilns in three districts of Balochistan province, Pakistan, through water quality index and multivariate statistical approaches. J. Geochem. Explor. 197, 14–26. https://doi.org/10.1016/j.gexplo.2018.11.007.

Korehie, M.T., Ardebili, O., Dadashzadeh Ahari, H., Rezaei Shirzad, M., Fotovati, V., Ghalamghash, J., Kiani, T., Najafi, A., 2016. Atlas of Iran's Geology and Mineral Distribution with Maps on Scale 1:250.000. Geological Survey of Iran. In Farsi.

Lakshmanan, E., Kannan, R., Kumar, M.S., 2003. Major ion chemistry and identification of hydrogeochemical processes of ground water in a part of Kancheepuram district, Tamil Nadu, India. Environ. Geosci. 10 (4), 157–166.
Ledesma, R., Pasten-Zapata, E., Parra, R., Harter, T., Mahlknecht, J., 2014. Investigation of the geochemical evolution of groundwater under agricultural land: a case study in northeastern Mexico. J. Hydrol. 521, 410–423. https://doi.org/10.1016/j.jhydrol.2014.12.026.
Legates, D.R., McCabe, G.J., 1999. Evaluating the use of "goodness-of-fit" measures in hydrologic and hydroclimatic model validation. Water Resour. Res. 35 (1), 233–241.
McLean, W., Jankowski, J., Lavitt, N., 2000. Groundwater Quality and Sustainability in an Alluvial Aquifer, Australia Groundwater, Past Achievements and Future Challenges. A Balkema, Rotterdam, pp. 567–573.
Nematollahi, M.J., Ebrahimi, P., Razmara, M., et al., 2016. Hydrogeochemical investigations and groundwater quality assessment of Torbat-Zaveh plain, Khorasan Razavi, Iran. Environ. Monit. Assess. 188, 2. https://doi.org/10.1007/s10661-015-4968-6.
Parkhurst, D.L., Appelo, C.A.J., 2013. Description of Input and Examples for PHREEQC Version 3 - a Computer Program for Speciation, Batch-reaction, One-Dimensional Transport, and Inverse Geochemical Calculations: U.S. Geological Survey Techniques and Methods. book 6, chap. A43, 497 p., available only at. http://pubs.usgs.gov/tm/06/a43/.
Podgorski, J.E., Berg, M., 2020. Global threat of arsenic in groundwater. Science 368 (6493), 845–850. https://doi.org/10.1126/science.aba1510.
Polya, D.A., Middleton, D.R., 2017. Arsenic in drinking water: sources human exposure. In: Bhattacharya, P., Polya, D.A., Draganovic, D. (Eds.), Best Practice Guide on the Control of Arsenic in Drinking Water, 1st. International Water Association Publishing, London, UK. ISBN 9781843393856, Chapter 1.
Qasemi, M., Afsharnia, M., Farhang, M., Bakhshizadeh, A., Allahdadi, M., Zarei, A., 2018. Health risk assessment of nitrate exposure in groundwater of rural areas of Gonabad and Bajestan, Iran. Environ. Earth Sci. 77, 551.
Qasemi, M., Shams, M., Sajjadi, S.A., et al., 2019. Cadmium in groundwater consumed in the rural areas of Gonabad and Bajestan, Iran: occurrence and health risk assessment. Biol. Trace Elem. Res. 192, 106–115. https://doi.org/10.1007/s12011-019-1660-7.
Radfard, M., Yunesian, M., Nabizadeh, R., Biglari, H., Nazmara, Sh., Hadi, M., Yousefi, N., Yousefi, M., Abbasnia, A., Mahvi, A.H., 2019. Drinking water quality and arsenic health risk assessment in Sistan and Baluchestan, Southeastern Province, Iran. Hum. Ecol. Risk Assess. 25 (4), 949–965. https://doi.org/10.1080/10807039.2018.1458210.
Ravindra, K., Mor, S., 2019. Distribution and health risk assessment of arsenic and selected heavy metals in Groundwater of Chandigarh, India. Environ. Pollut. 250, 820–830.
Razavi Khorasan Management and Planning Organization, 2019. Spatial Planning Studies for Razavi Khorasan Province, Iran [In Farsi]. URL: https://khrazavi.mporg.ir/Portal/View/Page.aspx?PageId=6cd80675-0d18-43cc-9263-2ba794a490c1t=0 (Accessed: 23-Apr-2019).
Rezaei, A., Hassani, H., Hayati, M., et al., 2018. Risk assessment and ranking of heavy metals concentration in Iran's Rayen groundwater basin using linear assignment method. Stoch. Environ. Res. Risk Assess. 32, 1317–1336. https://doi.org/10.1007/s00477-017-1477-x.
Ricolfi, L., Barbieri, M., Muteto, P.V., et al., 2020. Potential toxic elements in groundwater and their health risk assessment in drinking water of Limpopo National Park, Gaza province, Southern Mozambique. Environ. Geochem. Health 42, 2733–2745. https://doi.org/10.1007/s10653-019-00507-z.
Sánchez-Martos, F., Pulido-Bosch, A., Molina-Sánchez, L., Vallejos-Izquierdo, A., 2002. Identification of the origin of salinization in groundwater using minor ions (Lower Andarax, Southeast Spain). Sci. Total Environ. 297 (1–3), 43–58. https://doi.org/10.1016/s0048-9697(01)01011-7.
Sepidbar, F., Mirnejad, H., Li, J.W., Wei, C., George, L.L., Burlinson, K., 2017. Mineral geochemistry of the Sangan skarn deposit, NE Iran: implication for the evolution of hydrothermal fluid. Geochemistry 77 (3), 399–419.
Shafaii Moghadam, H., Corfu, F., Chiaradia, M., Stern, R.J., Ghorbani, Gh., 2014. Sabzevar Ophiolite, NE Iran: progress from embryonic oceanic lithosphere into magmatic arc constrained by new isotopic and geochemical data. Lithos 210–211. https://doi.org/10.1016/j.lithos.2014.10.004.
Shojaat, B., Hassanipak, A.A., Mobasher, K., Ghazi, A.M., 2003. Petrology, geochemistry and tectonics of the Sabzevar Ophiolite, North Central Iran. J. Asian Earth Sci. 21 (9), 1053–1067. https://doi.org/10.1016/S1367-9120(02)00143-8.
Sohrabi, N., Kalantari, N., Amiri, V., et al., 2020. A probabilistic-deterministic analysis of human health risk related to the exposure to potentially toxic elements in groundwater of Urmia coastal aquifer (NW of Iran) with a special focus on arsenic speciation and temporal variation. Stoch. Environ. Res. Risk Assess. https://doi.org/10.1007/s00477-020-01934-6.
Statistical Center of Iran, 2019. Statistical Center of Iran [Online]. https://www.amar.org.ir/english. [Accessed: 23-Apr-2019].
Taghadosi, H., Malekzadeh Shafaroudi, A., 2018. Mineralogy, Alteration, geochemistry, and fluid inclusion studies of Fe oxide-copper mineralization of Namegh area, NE Kashmar. Iran. J. Crystallogr. Mineral. 26 (3), 541–554. https://doi.org/10.29252/ijcm.26.3.541.
Taheri, M., Mehrzad, J., Gharaie, M.H.M., Afshari, R., Dadsetan, A., Hami, S., 2016. High soil and groundwater arsenic levels induce high body arsenic loads, health risk and potential anemia for inhabitants of northeastern Iran. Environ. Geochem. Health 38 (2), 469–482.
Taherian, P., Joodavi, A., 2021. Hydrogeochemical characteristics and source identification of salinity in groundwater resources in an arid plain, northeast of Iran: implication for drinking and irrigation purposes. Acque Sotterranee - Italian J. Groundwater 10 (2), 21–31. https://doi.org/10.7343/as-2021-502.
Tahmasebi, P., Kamrava, S., Bai, T., Sahimi, M., 2020. Machine learning in geo- and environmental sciences: from small to large scale. Adv. Water Resour. 142, 103619 https://doi.org/10.1016/j.advwatres.2020.103619.
Tirkey, P., Bhattacharya, T., Chakraborty, S., Baraik, S., 2017. Assessment of groundwater quality and associated health risks: a case study of Ranchi city, Jharkhand, India. Groundw. Sustain. Dev. 5, 85–100. https://doi.org/10.1016/j.gsd.2017.05.002.
USEPA, 2020. Integrated Risk Information System (IRIS). Accessed date: 16 April 2020. http://www.epa.gov/iris/.
USEPA (US Environmental Protection Agency), 1999. A Risk Assessment-Multiway Exposure Spreadsheet Calculation Tool. United States Environmental Protection Agency, Washington D.C.
Vesali Naseh, M.R., Noori, R., Berndtsson, R., Adamowski, J., Sadatipour, E., 2018. Groundwater pollution sources apportionment in the Ghaen Plain, Iran. Int. J. Environ. Res. Public Health 15 (1), 172.
Wang, Y., Su, H., Gu, Y., Song, X., Zhao, J., 2017. Carcinogenicity of chromium and chemoprevention: a brief update. Onco. Ther. 10, 4065–4079. https://doi.org/10.2147/OTT.S139262.
World Health Organization-WHO, 2017. Guidelines for Drinking-Water Quality: Fourth Edition Incorporating the First Addendum. WHO, Geneva.
Wu, R., Podgorski, J., Berg, M., et al., 2020. Geostatistical model of the spatial distribution of arsenic in groundwaters in Gujarat State, India. Environ. Geochem. Health. https://doi.org/10.1007/s10653-020-00655-7.
Yousefi, M., Ghoochani, M., Mahvi, A.H., 2018. Health risk assessment to fluoride in drinking water of rural residents living in the Poldasht city, Northwest of Iran. Ecotoxicol. Environ. Saf. 148, 426–430. https://doi.org/10.1016/j.ecoenv.2017.10.057.
Zendehbad, M., Cepuder, P., Loiskandl, W., Stumpp, C., 2019. Source identification of nitrate contamination in the urban aquifer of Mashhad, Iran. J. Hydrol.: Regional Stud. 25, 100618 https://doi.org/10.1016/j.ejrh.2019.100618.
Zhou, P., Li, Z., Snowling, S., et al., 2019. A random forest model for inflow prediction at wastewater treatment plants. Stoch. Environ. Res. Risk Assess. 33, 1781–1792. https://doi.org/10.1007/s00477-019-01732-9.
Zirjanizadeh, S., Karimpour, M.H., 2016b. Mineralogy, geochemistry and petrography of intrusive volcanic rocks, Gonabad, Iran. Iran. J. Crystallogr. Mineral. 23 (4), 789–802. http://ijcm.ir/article-1-145-en.html.
Zirjanizadeh, S., Rocha, F., Santos, J.F., Samiee, S., 2016a. Origin of the Joumand fluorite and barite (Pb-Zn) veins of northwest Gonabad, Iran. Evidence from trace-element and stable (S) isotope data. Goldschmidt Conference Abstracts.

International Journal of
Environmental Research and Public Health

MDPI

Article

Evaluation of Chemical Parameters of Urban Drinking Water Quality along with Health Risk Assessment: A Case Study of Ardabil Province, Iran

Reza Aghlmand [1], Saeed Rasi Nezami [2] and Ali Abbasi [1,3,*]

[1] Department of Civil Engineering, Faculty of Engineering, Ferdowsi University of Mashhad, Mashhad 9177948974, Iran; rezaaghlmandcivil@gmail.com
[2] Department of Civil Engineering, Faculty of Engineering, University of Mohaghegh Ardabili, Ardabil 5619911367, Iran; rasinezami@uma.ac.ir
[3] Water Resources Section, Faculty of Civil Engineering and Geosciences, Delft University of Technology, 2628 CN Delft, The Netherlands
* Correspondence: aabbasi@um.ac.ir or a.abbasi@tudelft.nl; Tel.: +31-15-2781029

Abstract: In recent years, in addition to water resources' quantity, their quality has also received much attention. In this study, the quality of the urban water distribution network in northwestern Iran was evaluated using the water quality index (WQI) method. Then, some important trace elements were investigated, and finally, the health risk assessment was evaluated for both carcinogenic elements (Ni, Cd, Cr, Pb, and As) and non-carcinogenic elements (Ca, Mg, Na, K, F, NO_3, and Cu) using carcinogenic risk (CR) and hazard quotient (HQ), respectively. In the present study, the WQI was calculated based on both World Health Organization (WHO) and Iranian drinking water standards. Comparing the results of these standards revealed that the WQI based on the Iranian standard was slightly higher. Regarding the calculated WQI for the study region, the status of water quality for drinking consumption is in the good water quality class (25 < WQI < 50). It was observed that Cu and Cd have the highest and lowest concentrations in all sampling points, respectively. Hazard Index (HI) results showed that the non-carcinogenic substances studied had a low risk for both adults and children (<1.0). However, the CR results showed that Ni, Cd, and As were above the desired level for both children and adults. The results of this study can be applied for efficient water management and human health protection programs in the study area.

Keywords: health risk assessment; water quality index; Parsabad city; carcinogenic/non-carcinogenic risk; trace elements

Citation: Aghlmand, R.; Rasi Nezami, S.; Abbasi, A. Evaluation of Chemical Parameters of Urban Drinking Water Quality along with Health Risk Assessment: A Case Study of Ardabil Province, Iran. *Int. J. Environ. Res. Public Health* **2021**, *18*, 5179. https://doi.org/10.3390/ijerph18105179

Academic Editors: Jeffery Spickett and Giacomo Alessandro Gerosa

Received: 18 March 2021
Accepted: 10 May 2021
Published: 13 May 2021

1. Introduction

Access to clean drinking water is a fundamental human right, regardless of color, religion, nationality, wealth, or belief. Contaminated drinking water as well as poor sanitation are associated with the transmission of diseases such as diarrhea, polio, cholera, and dysentery. Globally, at least two billion people use fecal-contaminated drinking water sources [1,2]. The increasing need for energy, food, and housing as a result of population growth, urbanization, and modernization creates great pressure on water resources, especially water quality, as well as problems of sewage disposal and contamination of surface waters. Water quality, by definition, is a criterion for assessing the usability of water for different purposes (drinking, industry, agriculture, etc.) using various biological, physical, and chemical parameters [3,4].

Parsabad city is considered an agricultural hub in Ardabil province, Iran, that plays a key role in ensuring food security on a national scale, especially in northwestern Iran. Using chemical fertilizers and chemical pesticides in this area has caused serious water quality issues in the study area. As the effects of draining agricultural water on the quality

of drinking water in Parsabad have not been assessed so far, the results of the present study would be useful.

The Aras river is the only source of drinking water in Parsabad city. The lack of accurate identification of dangerous pollutants in this water source and subsequent lack of control in the drinking water treatment plant of this city can threaten the health of the inhabitants. Therefore, water quality monitoring through sampling from the water distribution network in critical points of the city is mandatory. These samples can be used to evaluate the water quality.

In this study, the water quality index (WQI) method has been used to evaluate the quality of drinking water in Parsabad city. The goal of this approach was to give a single value to water quality, which is calculated by considering a list of parameters and constituents [5]. The WQI method is widely used in assessing the quality of surface water and groundwater resources and plays a very important role in water resources' management [6]. In the present study, WQI was calculated in two ways: (a) using the World Health Organization (WHO) drinking water standard, and (b) using the Iranian drinking water standard. Then, the results of both were presented and compared.

Considering the importance of the drinking water resources used by local residents and the prevalence of various gastrointestinal cancers in the region, as one of the possible consequences of contaminated water consumption, it is necessary to identify different pollutants in the drinking water source. These results can lead to an accurate water quality evaluation in Parsabad city and, consequently, achievement of integrated and sustainable management of water resources in this region. In this study, the health risk assessment was evaluated from both approaches of carcinogenic and non-carcinogenic health risk assessment using carcinogenic risk (CR) and hazard quotient (HQ). In assessing health risk, both ingestion and dermal absorption effects were taken into account. Additionally, an attempt was made to localize health risk calculations; in other words, the parameters included in the health risk indices are consistent with the study area. Therefore, instead of using default values (as in previous studies) in the health risk calculations, we tried to use values calibrated based on the conditions and criteria of the study area.

2. Materials and Methods

2.1. Study Area and Sampling

Parsabad city, a border city in Ardabil province, northwest Iran, is located 230 km north of Ardabil city and along the Aras border river, from 39°12′ N to 39°42′ N latitude and 47°10′ E to 48°21′ E longitude, as shown in Figure 1. Surface water is the most important source of water in this region. The Aras river is the most important water source for Parsabad city. As one of the largest rivers in northern Iran, with a length of approximately 1072 km, the Aras river begins from Turkey and then crosses the common border of Iran with Armenia and Azerbaijan, and finally flows into the Caspian Sea. Parsabad city, with a population of about 177,601 people, is the second largest city in Ardabil province. This region is one of the most important agricultural hubs in Iran, with the production of more than 50 types of crops, which meet about 80% of Iran's need for corn seeds.

Therefore, due to the existence of large agricultural lands in the entire outskirts of the city and the use of chemical fertilizers in these lands, there is a possibility of contamination of the drinking water resources in this city, and therefore, the quality of the drinking water source in this area should be surveyed.

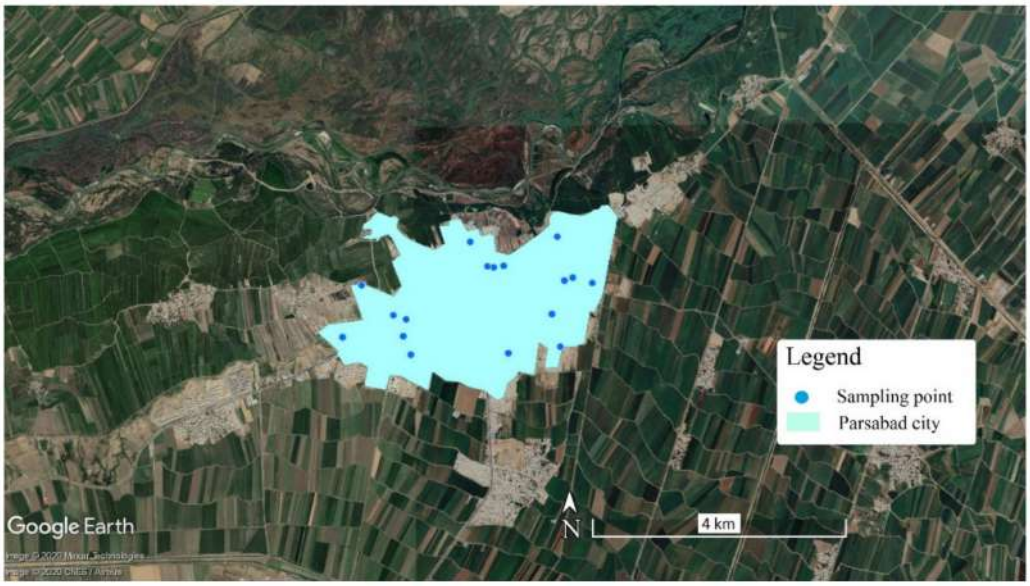

Figure 1. Location of urban drinking water sampling points in the study area.

2.2. Water Quality Index Method

Water quality indices have been used in recent years to evaluate the quality of water consumed by humans in various studies [7–12]. Water quality indices can be considered water quality models, as a simplified representation of a complex reality [13]. These indices provide a comprehensive picture of both surface water and groundwater quality for different purposes (e.g., domestic use and irrigation) [14]. In this study, a common and basic formula called the water quality index (WQI) was used [15–18]. To calculate the WQI, various water quality parameters measured in the year 2019, including pH, HCO_3, Cl, SO_4, NO_3, F, Ca, Mg, K, and Na, were used. It should be noted that the World Health Organization [19,20] and Iranian standards [21] for drinking purposes were considered to calculate the WQI. A minimum weight of 1 was assigned to low-significance parameters in the water quality assessment and a maximum weight of 5 was assigned to parameters with high importance (Table 1). In general, the WQI is computed using Equations (1)–(4) as follows:

$$\mathrm{W_i} = \frac{w_i}{\sum_{\mathrm{i}=1}^{n} w_i} \quad (1)$$

$$q_i = \frac{C_i}{S_i} \times 100 \quad (2)$$

$$\mathrm{SI}_i = W_i \times q_i \quad (3)$$

$$\mathrm{WQI} = \sum_{i=1}^{n} \mathrm{SI}_i \quad (4)$$

where W_i is the relative weight, w_i is the weight of each parameter, n is the number of parameters, q_i is the water quality rating, C_i is the measured concentration of each parameter, S_i indicates the drinking water standard for each parameter (mg/L), and SI_i is the sub-index of the i-th parameter.

Table 1. The weight (w_i), relative weight (W_i), and the standard value of each parameter for both Iranian and WHO standards applied in WQI calculation.

Parameter	Unit	WHO Standard	Iranian Standard	Weight (w_i)	Relative Weight (W_i)
pH	-	6.5–8.5	6.5–8.5	4	0.1176
HCO_3	mg/L	300	-	3	0.0882
Cl	mg/L	200–600	250–400	2	0.0588
SO_4	mg/L	400	250–400	4	0.1176
NO_3	mg/L	50	50	5	0.1471
F	mg/L	1.5	-	5	0.1471
Ca	mg/L	75–200	300	3	0.0882
Mg	mg/L	50–150	30	3	0.0882
Na	mg/L	200	200	3	0.0882
K	mg/L	10	-	2	0.0588
				$\sum w_i = 34$	$\sum W_i = 1$

The classification of water quality based on the WQI value is represented in Table 2. Accordingly, water quality is divided into five general classes, which include excellent quality, good quality, poor quality, very poor quality, and unsuitable for drinking purposes [22,23].

Table 2. Water quality classification based on WQI values [23,24].

WQI Value	Water Quality Status	Possible Usage
0–25	Excellent	Drinking, irrigation, and industrial
26–50	Good	Drinking, irrigation, and industrial
51–75	Poor	Irrigation and industrial
76–100	Very poor	Irrigation
Above 100	Unsuitable	Proper treatment required

2.3. GIS Application

To estimate the value of required parameters in ungauged areas, sampling points should be used through interpolation. In the present study, geographic information system (GIS) software was used for the spatial interpolation of various water quality parameters and for the preparation of distribution maps for each parameter in the study area. The results of comparing different interpolation methods in GIS show that the kriging method, particularly regression kriging, has a much better performance than other methods, such as inverse distance weighting (IDW) and spline [25]. Therefore, in this study, the kriging method in GIS software was used to prepare spatial distribution maps of water quality parameters.

2.4. Health Risk Assessment

Trace elements, particularly some heavy metals, are non-degradable, resistant, and often recycled through biological and physicochemical processes that can pose a significant threat to human health by damaging the nervous system and other internal organs [26]. In recent years, many researchers have tried to assess the potential hazard of trace elements in water to human health using existing methods [27]. In general, human exposure to trace elements can occur through three main pathways: direct ingestion, inhalation through the mouth and nose, and dermal absorption. In the water environment, ingestion and dermal absorption are more important and common [28], and the exposure dose from the two mentioned pathways can be calculated using Equations (5) and (6), which are adapted from the risk assessment guidance by the United States Environmental Protection Agency [29,30].

$$ADD_{ingestion} = \frac{C_w \times IR \times EF \times ED}{BW \times AT} \quad (5)$$

$$ADD_{dermal} = \frac{C_w \times SA \times K_P \times ET \times EF \times ED \times 10^{-3}}{BW \times AT} \quad (6)$$

where $ADD_{ingestion}$ and ADD_{dermal} are the average daily exposure doses through ingestion and dermal absorption of water (mg/kg/day or µg/kg/day), respectively; C_w is the average concentration of trace elements in water (mg/L or µg/L); IR is the ingestion rate (L/day); EF is the exposure frequency (day/year); ED is the exposure duration (year); SA is the exposed skin area (cm^2); K_P is the dermal permeability coefficient in water (cm/h)—in this study, 0.0001 for Pb [26], 0.002 for Cr, 0.001 for As, Cd, Cu, Ca, Mg, Na, K, F, and NO_3, and 0.0002 for Ni [29,31]; ET is the exposure time (h/day); BW is the body weight (kg); and AT is the averaging time (day). The default values assigned for the above variables are shown in Table 3 [30,32,33].

Table 3. Default values in the calculation of average daily exposure dose (ADD) through ingestion and dermal absorption.

Variable	Adults	Children
IR (L/day)	2	0.64
EF (day/year)	350	350
ED (year)	30	6
BW (kg)	70	15
AT (day)	10,950	2190
SA (cm^2)	18,000	6600
ET (h/day)	0.58	1

In this study, in order to characterize carcinogenic and non-carcinogenic risk, Equations (7)–(9) were used [26]. The potential non-carcinogenic and carcinogenic risks were evaluated using hazard quotient (HQ) and carcinogenic risk (CR), respectively. The Hazard Index (HI) represents the total non-carcinogenic risks of trace elements from all applicable pathways (e.g., ingestion and dermal absorption). If HQ or HI < 1, the non-carcinogenic health risk is low, but if HQ or HI > 1, non-carcinogenic effects should be considered. The acceptable range of CR according to the United States Environmental Protection Agency (USEPA) is 10^{-6} to 10^{-4} [30].

$$\text{Hazard Quotient (HQ)} = \frac{ADD}{RfD} \quad (7)$$

$$\text{Hazard Index (HI)} = \sum_{i=1}^{n} \left(HQ_{ingestion} + HQ_{dermal} \right) \quad (8)$$

$$\text{Carcinogenic Risk (CR)} = ADD \times CSF \quad (9)$$

where ADD is the average daily exposure dose through ingestion or dermal absorption (mg/kg/day or µg/kg/day); RfD is the reference dose (mg/kg/day or µg/kg/day); CSF is the cancer slope factor of a carcinogen/trace element, $(\mu g/kg/day)^{-1}$ or $(mg/kg/day)^{-1}$. CSF values were extracted from previous studies [34–40]. In this study, unlike previous studies in this field, the values of $RfD_{ingestion}$ and RfD_{dermal} for the study area have been localized/specialized. The equations used to calculate $RfD_{ingestion}$ and RfD_{dermal} are as follows:

$$RfD_{ingestion} = \frac{C_{IS}}{W_m} \times P_{ingestion} \quad (10)$$

$$RfD_{ingestion} = \frac{C_{IS}}{W_m} \times P_{dermal} \quad (11)$$

where C_{IS} is the Iranian standard value for each parameter, W_m is the mean weight of a person, $P_{ingestion}$ indicates the total per capita water consumption for cooking and drinking in Iran, P_{dermal} shows the total per capita water consumption for bathing, showering,

washing, and sanitation in Iran. The average $P_{ingestion}$ in Iran is about 11 L/day and the average P_{dermal} is about 87.5 L/day [41]. In this study, W_m was considered to be 45 kg.

3. Results and Discussion

The spatial distribution maps of different water quality parameters are shown in Figure 2. It can be observed that the parameters of K, Mg, Na, HCO_3, SO_4, Cr, and Cl are higher mainly in the eastern part of the study area. The values of the other parameters are distributed generally unbalanced all over the desired area, which can be seen in Figure 2.

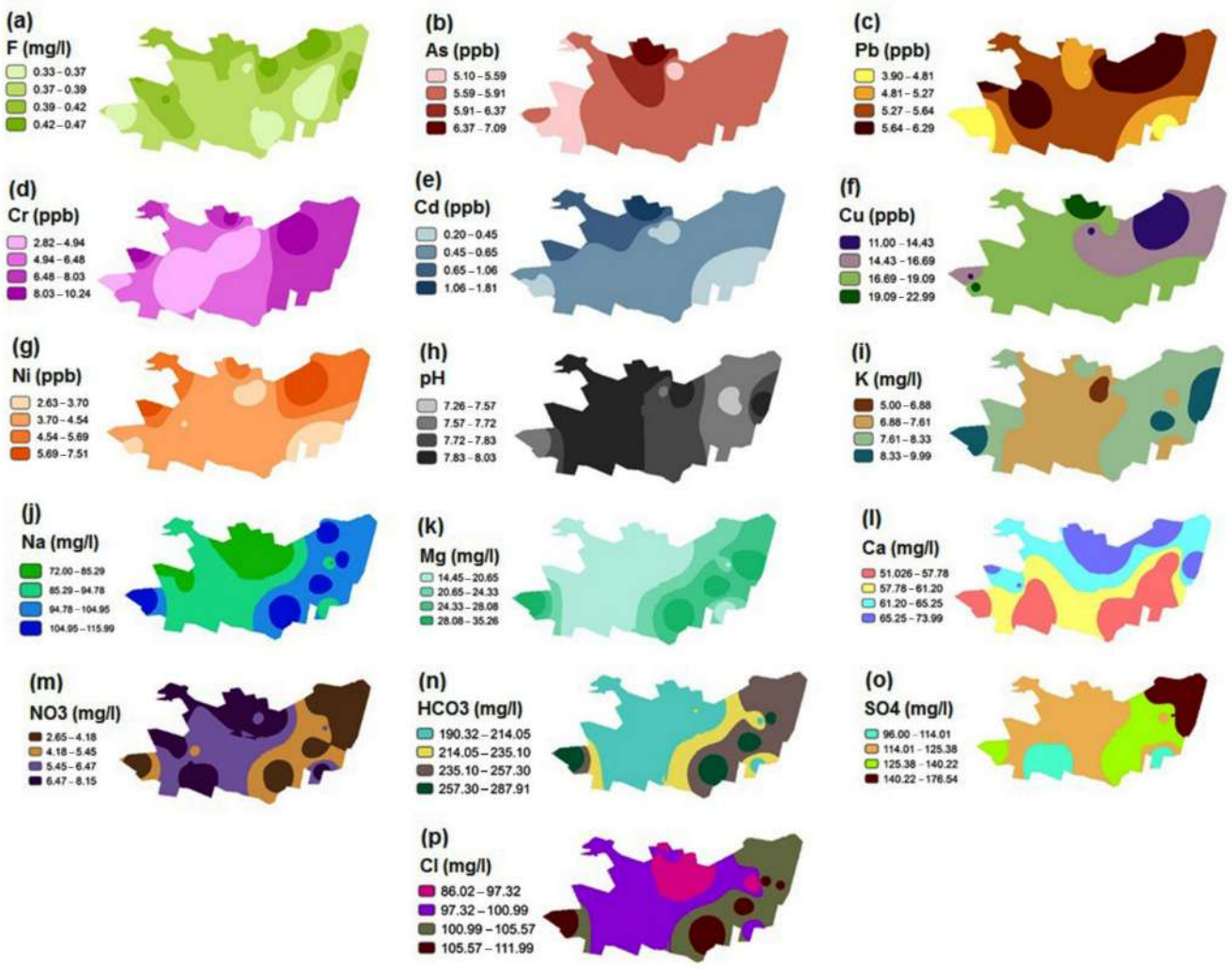

Figure 2. Spatial distribution maps of the various hydrochemical parameters in the study area. (**a**) Fluoride; (**b**) arsenic; (**c**) lead; (**d**) chromium; (**e**) cadmium; (**f**) copper; (**g**) nickel; (**h**) pH; (**i**) potassium; (**j**) sodium; (**k**) magnesium; (**l**) calcium; (**m**) nitrate; (**n**) bicarbonate; (**o**) sulphate; (**p**) chloride.

The WQI was calculated to evaluate the suitability of the urban water quality of the study area for drinking purposes. In this study, the physical and chemical parameters considered in the WQI calculations are pH, calcium, magnesium, sodium, potassium, chloride, sulfate, nitrate, bicarbonate, and fluoride. To calculate the WQI, data from 17 sampling points were used. The WQI was examined based on two standards (i.e., WHO and Iranian standards), the results of which are shown in Figures 3 and 4. The results of the WQI show that by entering the Iranian standard values in the WQI calculations compared to those of the WHO, the WQI in the whole study area is higher. However, there is not much difference between the WQI results when entering the two mentioned standards in the calculations, and according to the classification in Table 2, the WQI value in the whole

study region (in both standards) is in the "Good" water quality class (26 < WQI < 50). The spatial distribution maps of the WQI were prepared using the calculation of the WQI at the sampling points of the urban water distribution network followed by interpolation using the kriging method in the GIS environment.

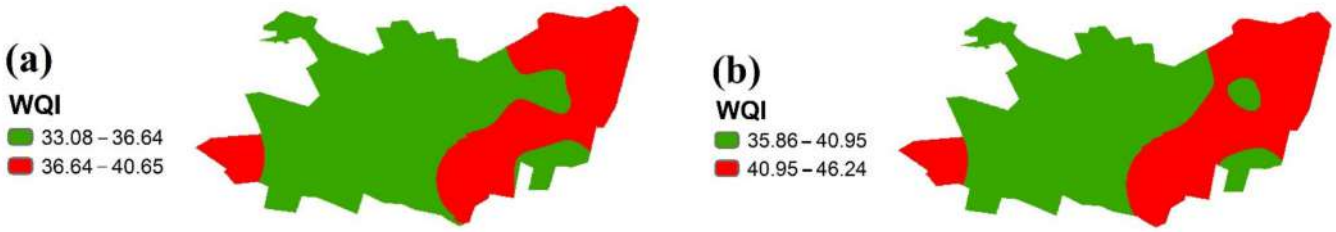

Figure 3. WQI values in the study area using (**a**) the WHO standard and (**b**) the Iranian standard.

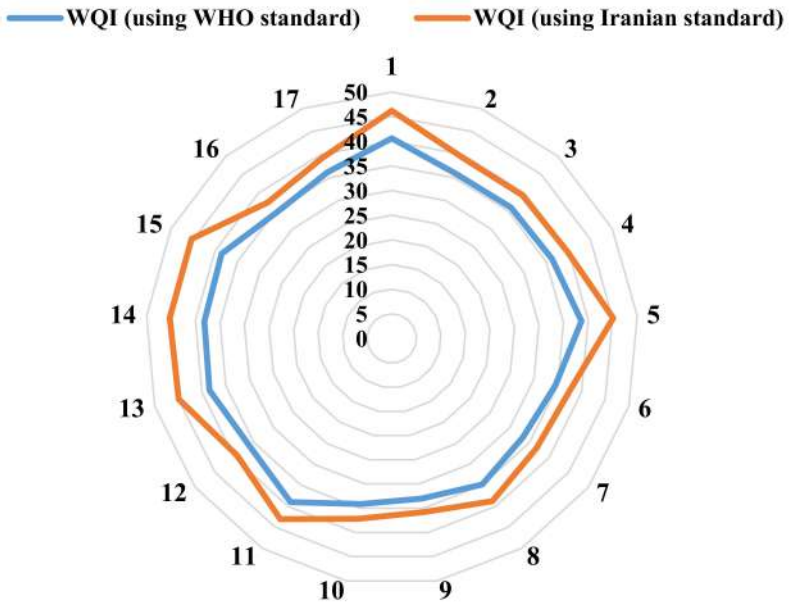

Figure 4. Water quality index (WQI) values in the sampling points.

As shown in Figure 3, generally, in the eastern half of the study area, the WQI value is higher than that in the western half, but it is not high enough to change the status of the water quality according to Table 2. It can be observed that the WQI value using the Iranian standard in all sampling points is higher than the WQI value using the WHO standard, according to Figure 4.

The total concentrations of the trace elements in the sampling points ranged from 31.34 to 51.01 µg/L, with a mean value of 39.43 µg/L (Figure 5). It was observed that copper (Cu) has the highest concentration in all sampling points. After Cu, the next highest concentrations belong to Cr, As, Pb, and Ni in the study area. In addition, cadmium (Cd) has the lowest concentration. In the present study, due to the lack of trace elements data in some sampling points, only nine sampling points' data were used.

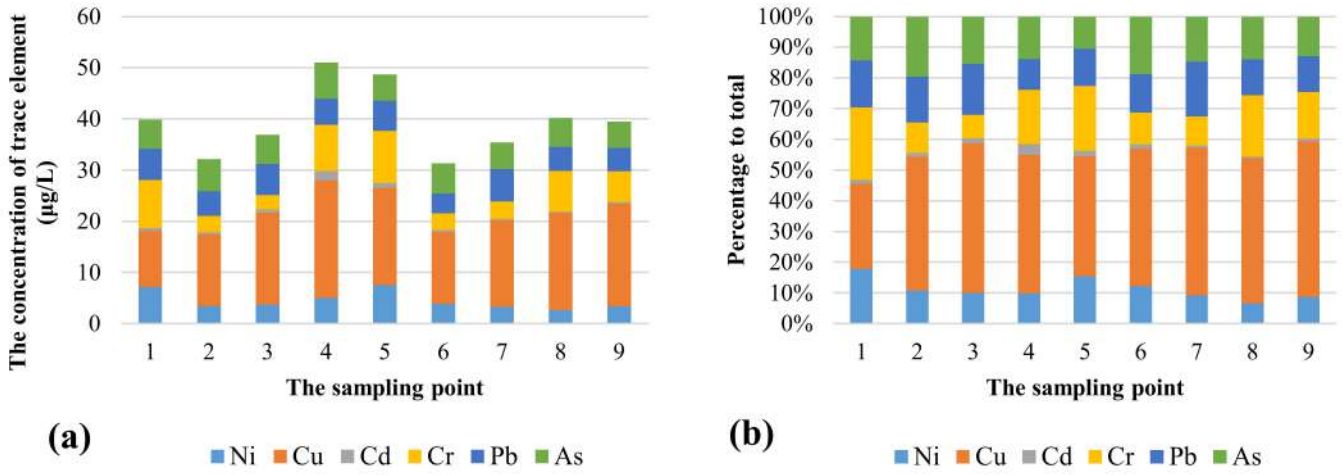

Figure 5. (**a**) Total concentrations of the trace elements at the sampling points (µg/L); (**b**) percentage of various trace elements out of the total concentrations at each sampling point.

In general, 44% of the total concentration of trace elements belonged to Cu, 16% to Cr, 15% to As, 13% to Pb, 11% to Ni, and 2% to Cd. As shown in Figure 5a, sampling points 4 (51.01 µg/L) and 5 (48.69 µg/L) showed the highest total concentrations of trace elements. In this study, in order to assess non-carcinogenic and carcinogenic risk, hazard quotient (HQ) and carcinogenic risk (CR) were used, respectively. The parameters considered in the non-carcinogenic risk calculations were Ca, Mg, Na, K, F, NO_3, and Cu; the parameters used in the carcinogenic risk assessment included As, Cr, Pb, Ni, and Cd. The results of HQ and HI and those of CR are shown in Tables 4 and 5, respectively.

Table 4. Reference dose (RfD) (mg/kg/day), average daily exposure dose (ADD) (mg/kg/day), hazard quotient (HQ), and hazard index (HI) for health risk assessment of non-carcinogenic trace elements (subscript "ing": ingestion; subscript "der": dermal).

	RfD_{ing}	RfD_{der}	Adult					Child				
			ADD_{ing}	ADD_{der}	HQ_{ing}	HQ_{der}	HI	ADD_{ing}	ADD_{der}	HQ_{ing}	HQ_{der}	HI
Ca	73.33	583.33	1.67	0.0088	0.0229	1.5×10^{-5}	0.0229	2.5077	0.0259	0.0342	4.43×10^{-5}	0.0342
Mg	7.33	58.33	0.61	0.0032	0.0838	5.5×10^{-5}	0.0839	0.9181	0.0095	0.1252	1.62×10^{-4}	0.1254
Na	48.88	388.88	2.56	0.0134	0.0524	3.43×10^{-5}	0.0524	3.8242	0.0394	0.0782	1.01×10^{-4}	0.0783
K	2.44	19.44	0.21	0.0011	0.0870	5.71×10^{-5}	0.0871	0.3177	0.0033	0.1300	1.68×10^{-4}	0.1301
NO_3	12.22	97.22	0.14	0.00078	0.0122	8.02×10^{-6}	0.0122	0.3048	0.0023	0.0249	2.37×10^{-5}	0.0250
Cu	0.24	1.94	0.00047	2.46×10^{-6}	0.0019	1.27×10^{-6}	0.0019	0.00070	7.26×10^{-6}	0.0029	3.74×10^{-6}	0.0029
F	0.36	2.91	0.0109	5.67×10^{-5}	0.0297	1.95×10^{-5}	0.0297	0.0162	0.00016	0.0443	5.74×10^{-5}	0.0444

Table 5. Cancer slope factor (CSF) $(mg/kg/day)^{-1}$, average daily exposure dose (ADD) (mg/kg/day), and carcinogenic risk (CR) for health risk assessment of carcinogenic trace elements (subscript "ing": ingestion; subscript "der": dermal).

	CSF	Adult					Child				
		ADD_{ing}	ADD_{der}	CR_{ing}	CR_{der}	CR_{total}	ADD_{ing}	ADD_{der}	CR_{ing}	CR_{der}	CR_{total}
Ni	0.84	1.21×10^{-4}	1.26×10^{-7}	1.02×10^{-4}	1.06×10^{-7}	1.02×10^{-4}	1.81×10^{-4}	3.73×10^{-7}	1.52×10^{-4}	3.13×10^{-7}	1.52×10^{-4}
Cd	6.3	1.66×10^{-5}	8.69×10^{-8}	1.05×10^{-4}	5.47×10^{-7}	1.05×10^{-4}	2.48×10^{-5}	2.56×10^{-7}	1.57×10^{-4}	1.61×10^{-6}	1.58×10^{-4}
Cr	0.5	1.68×10^{-4}	1.75×10^{-6}	8.42×10^{-5}	8.78×10^{-7}	8.50×10^{-5}	2.51×10^{-4}	5.18×10^{-6}	1.26×10^{-4}	2.59×10^{-6}	1.28×10^{-4}
Pb	0.0085	1.44×10^{-4}	7.54×10^{-8}	1.23×10^{-6}	6.41×10^{-10}	1.23×10^{-6}	2.15×10^{-4}	2.22×10^{-7}	1.84×10^{-6}	1.89×10^{-9}	1.84×10^{-6}
As	1.5	1.57×10^{-4}	8.22×10^{-7}	2.36×10^{-4}	1.23×10^{-6}	2.37×10^{-4}	2.35×10^{-4}	2.42×10^{-6}	3.53×10^{-4}	3.63×10^{-6}	3.56×10^{-4}

The results show that the HI values for all parameters considered in the health risk assessment of non-carcinogenic trace elements are lower than one, and therefore, there is

little risk associated with ingestion and dermal absorption in the study area. However, the results of the health risk assessment of carcinogenic trace elements show that nickel, cadmium, and arsenic exceeded the acceptable threshold (1.0×10^{-4}) for both adults and children. In addition, chromium is at an acceptable level for adults (8.50×10^{-5}), but not for children (1.28×10^{-4}), and lead is within the acceptable limits for both children and adults.

In this study, it was observed that the general water quality based on the WQI in the study area was good, while the results of the CR index showed that three out of five trace elements are above the defined threshold. This does not indicate conflict in the results, because the nature and purpose of the two mentioned indices are completely different. The purpose of using the WQI is to achieve a general interpretation of water quality, while the purpose of the CR index is to examine the amounts of cancerous substances in the water and whether the amounts of these substances are suitable for children and adults. This study showed that the use of a simple water quality index (e.g., WQI) cannot be a criterion for water quality planning and management. Rather, for the correct and efficient management of water quality, a wide range of quality parameters should be used. In other words, to judge the water quality of an area accurately, it needs to be evaluated from different perspectives by using various water quality indices.

4. Conclusions

In this study, the water quality of Parsabad city in Ardabil province, Iran, was evaluated using the water quality index method. To calculate the WQI, the WHO and Iranian standards were used and then compared. The WQI results were similar for both standards and showed that the water quality in the whole study area is in the good water quality class. However, the use of the Iranian standard in the calculation of the WQI led to relatively higher values, but not high enough to change the status of the water quality. The results also showed that Cu and Cd have the highest and lowest concentrations at all sampling points among the studied trace elements, respectively. Then, the health risk assessment of carcinogenic and non-carcinogenic parameters was performed using two indices, HQ (or HI) and CR. The HI results showed that the non-carcinogenic substances studied had a low risk for both adults and children (<1.0). However, the CR results showed that Ni, Cd, and As were above the desired level for both children and adults. Cr was only in the safe range for adults, and Pb was in the safe range for both groups (adults and children). It should be noted that only the amount of CR related to ingestion is high, and the risk associated with dermal absorption is low for all elements. Therefore, water managers in the study area should make more efforts in planning and managing water quality in Parsabad city to reduce the health risk of the mentioned elements. The results of the present study showed that in order to understand and make accurate judgments about the water quality in an area, water quality should be considered comprehensively from different perspectives and using various indices.

Author Contributions: Conceptualization, R.A. and S.R.N.; methodology, R.A. and S.R.N.; software, R.A.; validation, R.A., S.R.N. and A.A.; formal analysis, R.A. and S.R.N.; investigation, R.A., S.R.N. and A.A.; resources, R.A. and S.R.N.; data curation, R.A. and S.R.N.; writing—original draft preparation, R.A.; writing—review and editing, R.A. and A.A.; visualization, R.A., S.R.N. and A.A.; supervision, S.R.N. and A.A.; project administration, S.R.N. and A.A.; funding acquisition, A.A. All authors have read and agreed to the published version of the manuscript.

Funding: This research received no external funding.

Institutional Review Board Statement: Not applicable.

Informed Consent Statement: Not applicable.

Data Availability Statement: Data available on request due to privacy and ethical restrictions.

Acknowledgments: The authors would like to thank the Ardabil Regional Water Company, Ardabil, Iran, for providing the required data and information.

Conflicts of Interest: The authors declare no conflict of interest.

References

1. Li, P.; Wu, J. Drinking Water Quality and Public Health. *Expo. Health* **2019**, *11*, 73–79. [CrossRef]
2. Drinking Water. Available online: https://www.who.int/en/news-room/fact-sheets/detail/drinking-water (accessed on 7 December 2020).
3. Giri, S.; Qiu, Z. Understanding the relationship of land uses and water quality in Twenty First Century: A review. *J. Environ. Manag.* **2016**, *173*, 41–48. [CrossRef] [PubMed]
4. Bhateria, R.; Jain, D. Water quality assessment of lake water: A review. *Sustain. Water Resour. Manag.* **2016**, *2*, 161–173. [CrossRef]
5. Abbasi, T.; Abbasi, S.A. *Water Quality Indices*; Elsevier: Amsterdam, The Netherlands, 2012; ISBN 978-0-444-54304-2.
6. Wu, Z.; Wang, X.; Chen, Y.; Cai, Y.; Deng, J. Assessing river water quality using water quality index in Lake Taihu Basin, China. *Sci. Total Environ.* **2018**, *612*, 914–922. [CrossRef] [PubMed]
7. Varnosfaderany, M.N.; Mirghaffary, N.; Ebrahimi, E.; Soffianian, A. Water quality assessment in an arid region using a water quality index. *Water Sci. Technol.* **2009**, *60*, 2319–2327. [CrossRef] [PubMed]
8. Lobato, T.C.; Hauser-davis, R.A.; Oliveira, T.F.; Silveira, A.M.; Silva, H.A.N.; Tavares, M.R.M.; Saraiva, A.C.F. Construction of a novel water quality index and quality indicator for reservoir water quality evaluation: A case study in the Amazon region. *J. Hydrol.* **2015**, *522*, 674–683. [CrossRef]
9. Hamlat, A.; Guidoum, A. Assessment of groundwater quality in a semiarid region of Northwestern Algeria using water quality index (WQI). *Appl. Water Sci.* **2018**, *8*, 220. [CrossRef]
10. Gharibi, E.; Ghalit, M.; Taupin, J.D.; Patris, N.; Kouotou, D. Assessment of the quality of Moroccan bottled water by application of quality indices. *J. Water Supply Res. Technol. AQUA* **2018**, *67*, 576–585. [CrossRef]
11. Ewaid, S.H.; Abed, S.A.; Al-Ansari, N.; Salih, R.M. Development and evaluation of a water quality index for the Iraqi rivers. *Hydrology* **2020**, *7*, 67. [CrossRef]
12. Tian, Y.; Jiang, Y.; Liu, Q.; Dong, M.; Xu, D.; Liu, Y.; Xu, X. Using a water quality index to assess the water quality of the upper and middle streams of the Luanhe River, northern China. *Sci. Total Environ.* **2019**, *667*, 142–151. [CrossRef]
13. Kachroud, M.; Trolard, F.; Kefi, M.; Jebari, S.; Bourrié, G. Water Quality Indices: Challenges and Application Limits in the Literature. *Water* **2019**, *11*, 361. [CrossRef]
14. Ravikumar, P.; Mehmood, M.A.; Somashekar, R.K. Water quality index to determine the surface water quality of Sankey tank and Mallathahalli lake, Bangalore urban district, Karnataka, India. *Appl. Water Sci.* **2013**, *3*, 247–261. [CrossRef]
15. Sahu, P.; Sikdar, P.K. Hydrochemical framework of the aquifer in and around East Kolkata Wetlands, West Bengal, India. *Environ. Geol.* **2008**, *55*, 823–835. [CrossRef]
16. Vasanthavigar, M.; Srinivasamoorthy, K.; Vijayaragavan, K.; Rajiv Ganthi, R.; Chidambaram, S.; Anandhan, P.; Manivannan, R.; Vasudevan, S. Application of water quality index for groundwater quality assessment: Thirumanimuttar sub-basin, Tamilnadu, India. *Environ. Monit. Assess.* **2010**, *171*, 595–609. [CrossRef] [PubMed]
17. Tiwari, A.; Singh, P.; Mahato, M. GIS-Based Evaluation of Water Quality Index of Groundwater Resources in West Bokaro coalfield, India. *Curr. World Environ.* **2014**, *9*, 843–850. [CrossRef]
18. Rakib, M.A.; Sasaki, J.; Matsuda, H.; Quraishi, S.B.; Mahmud, M.J.; Bodrud-Doza, M.; Ullah, A.K.M.A.; Fatema, K.J.; Newaz, M.A.; Bhuiyan, M.A.H. Groundwater salinization and associated co-contamination risk increase severe drinking water vulnerabilities in the southwestern coast of Bangladesh. *Chemosphere* **2020**, *246*, 125646. [CrossRef]
19. WHO. *Guidelines for Drinking-Water Quality: Fourth Edition Incorporating the First Addendum*; World Health Organization: Geneva, Switzerland, 2017; ISBN 978-92-4-154995-0.
20. Karunanidhi, D.; Aravinthasamy, P.; Subramani, T.; Muthusankar, G. Revealing drinking water quality issues and possible health risks based on water quality index (WQI) method in the Shanmuganadhi River basin of South India. *Environ. Geochem. Health* **2021**, *43*, 931–948. [CrossRef]
21. ISIRI. *Drinking Water: Physical and Chemical Specifications (ISIRI No. 1053)*, 5th ed.; Institute of Standards and Industrial Research of Iran (ISIRI): Tehran, Iran, 2010; p. 26.
22. Brown, R.M.; McClelland, N.I.; Deininger, R.A.; O'Connor, M.F. A Water Quality Index—Crashing the Psychological Barrier. In *Indicators of Environmental Quality*; Springer: Boston, MA, USA, 1972; pp. 173–182.
23. Lkr, A.; Singh, M.R.; Puro, N. Assessment of water quality status of Doyang River, Nagaland, India, using Water Quality Index. *Appl. Water Sci.* **2020**, *10*, 1–13. [CrossRef]
24. Bora, M.; Goswami, D.C. Water quality assessment in terms of water quality index (WQI): Case study of the Kolong River, Assam, India. *Appl. Water Sci.* **2017**, *7*, 3125–3135. [CrossRef]
25. Meng, Q.; Liu, Z.; Borders, B.E. Assessment of regression kriging for spatial interpolation - Comparisons of seven GIS interpolation methods. *Cartogr. Geogr. Inf. Sci.* **2013**, *40*, 28–39. [CrossRef]
26. Zeng, X.; Liu, Y.; You, S.; Zeng, G.; Tan, X.; Hu, X.; Hu, X.; Huang, L.; Li, F. Spatial distribution, health risk assessment and statistical source identification of the trace elements in surface water from the Xiangjiang River, China. *Environ. Sci. Pollut. Res.* **2015**, *22*, 9400–9412. [CrossRef]
27. Ustaoğlu, F.; Tepe, Y.; Taş, B. Assessment of stream quality and health risk in a subtropical Turkey river system: A combined approach using statistical analysis and water quality index. *Ecol. Indic.* **2020**, *113*, 105815. [CrossRef]

28. Wu, B.; Zhao, D.Y.; Jia, H.Y.; Zhang, Y.; Zhang, X.X.; Cheng, S.P. Preliminary risk assessment of trace metal pollution in surface water from Yangtze River in Nanjing section, China. *Bull. Environ. Contam. Toxicol.* **2009**, *82*, 405–409. [CrossRef] [PubMed]
29. USEPA. *Risk Assessment Guidance for Superfund Volume I: Human Health Evaluation Manual (Part E, Supplemental Guidance for Dermal Risk Assessment)*; U.S. Environmental Protection Agency: Washington, DC, USA, 2004.
30. Rodriguez-Proteau, R.; Grant, R.L. Toxicity Evaluation and Human Health Risk Assessment of Surface and Ground Water Contaminated by Recycled Hazardous Waste Materials. In *Water Pollution*; Springer: Berlin/Heidelberg, Germany, 2005; pp. 133–189.
31. Yu, G.; Wang, J.; Liu, L.; Li, Y.; Zhang, Y.; Wang, S. The analysis of groundwater nitrate pollution and health risk assessment in rural areas of Yantai, China. *BMC Public Health* **2020**, *20*, 1–6. [CrossRef] [PubMed]
32. Wang, J.; Liu, G.; Liu, H.; Lam, P.K.S. Multivariate statistical evaluation ofdissolved trace elements and awater quality assessment in the middle reaches ofHuaihe River, Anhui, China. *Sci. Total Environ.* **2017**, *583*, 421–431. [CrossRef] [PubMed]
33. Liang, B.; Han, G.; Liu, M.; Yang, K.; Li, X.; Liu, J. Distribution, sources, and water quality assessment of dissolved heavy metals in the Jiulongjiang river water, southeast China. *Int. J. Environ. Res. Public Health* **2018**, *15*, 2752. [CrossRef]
34. Mohammadi, A.A.; Zarei, A.; Majidi, S.; Ghaderpoury, A.; Hashempour, Y.; Saghi, M.H.; Alinejad, A.; Hosseingholizadeh, N.; Ghaderpoori, M. Carcinogenic and non-carcinogenic health risk assessment of heavy metals in drinking water of Khorramabad, Iran. *MethodsX* **2019**, *6*, 1642–1651. [CrossRef]
35. Nkpaa, K.W.; Amadi, B.A.; Wegwu, M.O. Hazardous metals levels in Groundwater from Gokana, Rivers State, Nigeria: Non-cancer and Cancer Health Risk Assessment. *Hum. Ecol. Risk Assess.* **2018**, *24*, 214–224. [CrossRef]
36. Kusin, F.M.; Azani, N.N.M.; Hasan, S.N.M.S.; Sulong, N.A. Distribution of heavy metals and metalloid in surface sediments of heavily-mined area for bauxite ore in Pengerang, Malaysia and associated risk assessment. *Catena* **2018**, *165*, 454–464. [CrossRef]
37. Yuswir, N.S.; Praveena, S.M.; Aris, A.Z.; Syed Ismail, S.N.; de Burbure, C.; Hashim, Z. Heavy Metal Contamination in Urban Surface Soil of Klang District (Malaysia). *Soil Sediment Contam.* **2015**, *24*, 865–881. [CrossRef]
38. Yang, X.; Duan, J.; Wang, L.; Li, W.; Guan, J.; Beecham, S.; Mulcahy, D. Heavy metal pollution and health risk assessment in the Wei River in China. *Environ. Monit. Assess.* **2015**, *187*, 1–11. [CrossRef] [PubMed]
39. Zeng, F.; Wei, W.; Li, M.; Huang, R.; Yang, F.; Duan, Y. Heavy Metal Contamination in Rice-Producing Soils of Hunan Province, China and Potential Health Risks. *Int. J. Environ. Res. Public Health* **2015**, *12*, 15584–15593. [CrossRef] [PubMed]
40. Luo, X.; Ding, J.; Xu, B.; Wang, Y.; Li, H.; Yu, S. Incorporating bioaccessibility into human health risk assessments of heavy metals in urban park soils. *Sci. Total Environ.* **2012**, *424*, 88–96. [CrossRef] [PubMed]
41. *Bases & Design Criteria for Domestic Water Supply Projects (Standard No. 117-3)*; Ministry of Energy: Tehran, Iran, 1993.

water

MDPI

Article

Evaluation of Integrating SWAT Model into a Multi-Criteria Decision Analysis towards Reliable Rainwater Harvesting Systems

Shahab Doulabian [1], Erfan Ghasemi Tousi [2], Reza Aghlmand [3], Babak Alizadeh [4], Alireza Ghaderi Bafti [3] and Ali Abbasi [3,5,*]

1 Department of Civil Engineering, Shahrood University of Technology, Shahrood, Semnan 3619995161, Iran; doulabian@gmail.com
2 Department of Civil & Architectural Engineering and Mechanics, The University of Arizona, Tucson, AZ 85721, USA; erfang@email.arizona.edu
3 Department of Civil Engineering, Faculty of Engineering, Ferdowsi University of Mashhad, Mashhad 9177948974, Iran; rezaaghlmandcivil@gmail.com (R.A.); ghaderibafti.alireza@mail.um.ac.ir (A.G.B.)
4 Department of Civil Engineering, The University of Texas at Arlington, Arlington, TX 76019, USA; babak.alizadeh@mavs.uta.edu
5 Faculty of Civil Engineering and Geosciences, Water Resources Section, Delft University of Technology, 2628 CN Delft, The Netherlands
* Correspondence: aabbasi@um.ac.ir or a.abbasi@tudelft.nl; Tel.: +31-15-2781029

Abstract: Rainwater harvesting (RWH) has been recognized as one of the most reliable and efficient methods for water supply, especially in arid and semi-arid regions (ASARs) facing freshwater scarcity. Nevertheless, due to the inherent uncertainty of input data and subjectivity involved in the selection of influential parameters, the identification of RWH potential areas is a challenging procedure. In this study, two approaches for locating potential RWH sites were implemented. In the first approach, a frequently-used method of the multi-criteria decision analysis and geographic information system (MCDA-GIS) was utilized, while, in the second approach, a novel strategy of integrating the soil and water assessment tool (SWAT) model as a hydrology model into an MCDA-GIS method was proposed to evaluate its performance in locating potential RWH sites. The Mashhad Plain Basin (MPB) was selected as a case study area. The developed potential RWH maps of the two approaches indicated similar patterns for potential RWH areas; in addition, the correlation coefficient (CC) between the two obtained maps were relatively high (i.e., CC = 0.914) revealing that integration of SWAT as a comprehensive hydrologic model does not necessarily result in very different outputs from the conventional method of MCDA-GIS for RWH evaluation. The overlap of developed maps of the two approaches indicated that 3394 km^2 of the study area, mainly located in the northern parts, was identified as high-potential RWH areas. The performed sensitivity analysis indicated that rainfall and slope criteria, with weights of 0.329 and 0.243, respectively, had the greatest sensitivity on the model in the first approach while in the second approach, the criterion of runoff coefficient (with weights of 0.358) had the highest impact. Based on results from the identification of the potential locations for conventional RWH techniques, pond and pan techniques are the most proper options, covering high-potential areas of RWH more effectively than other techniques over MPB.

Keywords: rainwater harvesting; multi-criteria decision analysis; geospatial techniques; SWAT model; arid and semi-arid regions

Citation: Doulabian, S.; Ghasemi Tousi, E.; Aghlmand, R.; Alizadeh, B.; Ghaderi Bafti, A.; Abbasi, A. Evaluation of Integrating SWAT Model into a Multi-Criteria Decision Analysis towards Reliable Rainwater Harvesting Systems. *Water* **2021**, *13*, 1935. https://doi.org/10.3390/w13141935

Academic Editor: Ryan Bailey

Received: 14 June 2021
Accepted: 9 July 2021
Published: 13 July 2021

1. Introduction

Freshwater scarcity has become a pivotal issue in sustainable development [1–3], especially in arid and semi-arid regions (ASARs) where communities are encountering water scarcity problems, not only in agricultural and industrial sectors, but also for satisfying domestic water demands [4–7]. Most countries in North Africa and the Middle

East are facing water scarcity and its related consequences [8]. Moreover, various factors, such as accelerated climate change, population growth, intensive agricultural activities, and industrialization, as well as continuous pollution of water resources, will exacerbate freshwater scarcity and shortages in the future [9,10]. Therefore, more studies are needed in order to focus more specifically on water conservation planning and management, and the sustainable use of potential water resources [5,8,11].

Rainwater harvesting (RWH) can be considered as one of the most cost-effective and environmentally-friendly water conservation methods, especially in ASARs, which simultaneously address water scarcity issues and alleviates groundwater over-extraction [2,12–14]. From a historical perspective, archeological evidence found in Southwest Asia revealed that RWH has been practiced since the Neolithic Age (around 10,000 BC to 4500 BC) [11,15]. Moreover, examples of RWH structures were discovered in Tunisia, Greece, China, and historical Palestine, tracing back thousands of years [2,16]. In general, all schemes for collecting and storing rainwater to supply safe and inexpensive water for different purposes, such as domestic, industrial, and agricultural purposes are identified as RWHs [17–19].

In developing countries, where domestic water utilization is low, RWH can meet a large amount of water demand [20,21]. Furthermore, harvested water can be managed and diverted for other purposes, such as groundwater recharge, downstream flood mitigation, soil moisture improvement, irrigation, and livestock purposes [1,22,23]. However, identifying RWH potential areas/zones could be challenging, since several criteria need to be considered, including hydrology, climatic condition, topography, and soil parameters, to maximize water availability, particularly in ASARs [24,25].

Many methods have been applied to incorporate contributing RWH factors to locate potential RWH areas. In this regard, the integrated application of multi-criteria decision analysis (MCDA) and geographic information systems (GIS) has been frequently used for a wide range of objectives in water resource research, including potential RWH assessment [26–28]. In Saudi Arabia, geospatial and MCDA methods were implemented for identifying potential areas for some RWH structures [29]. In Egypt, potential RWH and storage areas were determined using remote sensing and decision support systems [30]. In South Africa, in-field RWH and ex-field RWH suitability maps were developed by combining ecological, physical, and socio-economic factors [20]. There are other studies that have been done in which assessment of potential RWHs was conducted through the incorporation of biophysical factors (e.g., slope, soil type, land use) [31,32].

As a multi-criteria decision-making (MCDM) system, the analytical hierarchy process (AHP) was introduced by Saaty [33,34]. It is a favorable decision-supporting technique for solving multiplex problems [35]. Particularly, it has been recognized as the most applicable decision method for the identification of potential RWH areas, along with the GIS platform [36]. In the AHP technique, based on the knowledge of experts and mathematics, decisions are organized and analyzed in a structured procedure. The primary idea behind AHP is to use hierarchical symbols to represent the components of any issue and show links between them [35]. Many studies have made extensive use of AHP in order to identify possible RWH sites [37].

The majority of related studies indicate that the utilization of practical approaches, as well as the selection of proper/suitable criteria, are the two main factors in the successful implementation of geospatial and MCDA methods in mapping potential RWH areas [29,38]. In this study, an assessment of potential RWH through the incorporation of biophysical parameters into MCDA, within a GIS environment, as a frequently used approach, is conducted. Furthermore, the novel approach of integration of SWAT as a hydrological model with MCDA and GIS is adopted to evaluate potential RWHs. The integrated approach of hydrological modeling with MCDA and GIS toward the identification of potential RWH areas in ASARs has already been addressed in numerous studies [25,39–41]. The primary reason for utilizing a hydrological model is to obtain, either the potential runoff generation depth and coefficient map, or to incorporate the obtained layer into MCDA to enhance the RWH site selection criteria. Additionally, studies revealed that the

combination of SWAT with GIS and MCDA reduces the likelihood of inherent biases in GIS-based MCDA.

The runoff coefficient is considered as one of the most influential parameters in RWH assessment, accounting for major contributing factors, such as rainfall, topography, land use, and soil texture and structure [29,42]. Meanwhile, in most studies, a runoff coefficient map is generated by utilizing the widely-used method known as the soil conservation service-curve number (SCS-CN) method [43–45]. The SCS-CN method calculates runoff depth based on land cover, hydrologic soil group, and antecedent soil moisture content. While the SCS-CN method is simple, easily applicable, and conceptually stable, it is constrained by some factors, such as the basin area (less than 8 km^2), low infiltration capacity, and high rainfall depth [44,46].

On the other hand, in ungagged basins, the SWAT model [47] can be considered as a suitable option for hydrological simulations, particularly in developing countries lacking rainfall and runoff records [48–50]. Data availability for most parts of the world, along with other advantageous features, including ease of representation, use of spatially available data, and capability of result presentation through GIS, increase the potential of integrating SWAT with the MCDA-GIS approach for the identification of potential RWH areas [51,52]. Moreover, the SWAT model, which requires a higher number of inputs, is more comprehensive compared to the SCS-CN, and its application can lead to a more accurate runoff coefficient map. In addition, the SWAT model includes, not only all factors used in the SCS-CN method, but also the independent interaction of influential factors, including infiltration and evaporation in rainfall–runoff modeling, which enables capturing more variability rather than relying on a single CN as a lumped parameter [48].

This paper evaluates the impact of incorporating a hydrological model on improving the identification of suitable RWH locations. To enable the evaluation, two approaches, one including hydrological model and the other one excluding the hydrological model, are examined. The integrated MCDA-GIS approach was used as the first approach. The second approach, which incorporates hydrological modeling, was the combination of the SWAT model with MCDA and GIS. MPB is located in northeast Iran and struggles with water supply, especially in recent years. A parameters sensitivity analysis was performed to reduce the subjectivity of parameters selected using expert judgment [48]. In addition, it identified the most sensitive criteria for locating potential RWH zones in MPB. In the end, the most applied RWH structures in ASARs were evaluated for MPB to find the best practices for high-potential areas for RWH.

The inclusive objectives of this research are to: (1) develop and compare the MCDA-GIS approach with the MCDA-GIS integrated with SWAT approach to identify potential RWH zones in the MPB; (2) implement sensitivity analyses on the two approaches to identify the most contributing criteria for potential RWH zone selection; (3) identify the potential location for three conventional RWH techniques (i.e., ponds and pans, terracing, and percolation tank) over MPB. The combined approach of the SWAT model, MCDA, and GIS was evaluated for the first time in ASARs. This paper is categorized as follows: in Section 2, we describe the study basin and the data and methods used in this study. Section 3 presents the results of the evaluation. Section 4 describes conclusions and recommendations for future studies.

2. Materials and Methods

2.1. Study Framework

In this study, a GIS-based MCDA framework has been developed and implemented at a large basin scale for the identification of potential RWH areas. Figure 1 represents the conceptual methodological framework of this study. In the present study, two approaches were developed and compared. In the first approach, five biophysical factors: rainfall, slope, land use, soil type, and soil depth, were incorporated into an MCDA for the evaluation of potential RWH zones. While in the second approach, four factors: slope, rainfall, and soil type, along with the runoff coefficient map derived from the SWAT model were used.

The selected criteria in both approaches were weighted using AHP and then normalized and reclassified using GIS techniques. Afterward, different sub-criteria were scored and rasterized. Then, weighted linear combination (WLC) was used in the GIS environment to develop the final potential RWH maps.

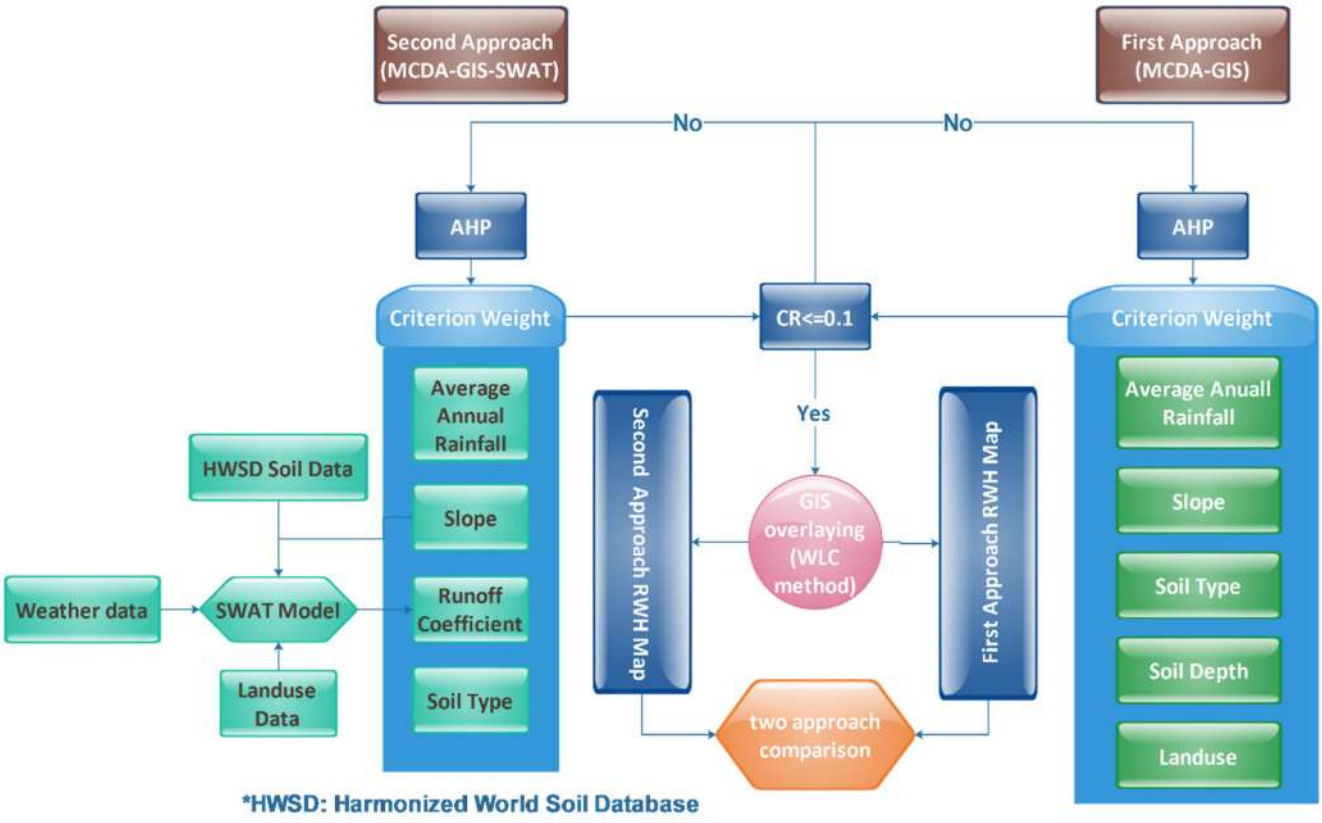

Figure 1. Conceptual methodology framework used in this research.

2.2. Study Area and Data Collection

The methodology was applied to MPB, located in the northeast of Iran, with an area of 9762 km^2, between 35°59′ N to 37°03′ N latitude and 60°06′ to 58°22′ E longitude (Figure 2). The climate of the study area is semi-arid to arid, and the average monthly temperature ranges from 11.6 to 26.7 °C [48]. A review of 19 rain gauge stations during 30 years (1979–2010) indicated an annual average rainfall of 303 mm, which varies from 166 to 486 mm [53]. In general, a V-shaped monthly rainfall pattern is observed. January, February, and March are the wettest months, while the rainfall trend decreases until July, the driest month of the year, and increases again until December. Climate change has increased the temperature trend, while no considerable changes in rainfall patterns are observed [54]. The annual average evapotranspiration ranges from 236 to 310 mm [55]. In addition, the mean elevation of the basin is 1487 m above sea level (ASL), which varies from 856 to 3247 m ASL; and the average land slope in the study area is 16.2%. From the geological point of view, the main constituents of the study area are ultramafic, granitic, and metamorphic rocks. In addition, the northern parts of the study area are sedimentary zones, mainly comprised of limestone, conglomerate, dolomite, and gypsiferous marls, and the higher parts of the MPB include discontinuous loess deposits [56].

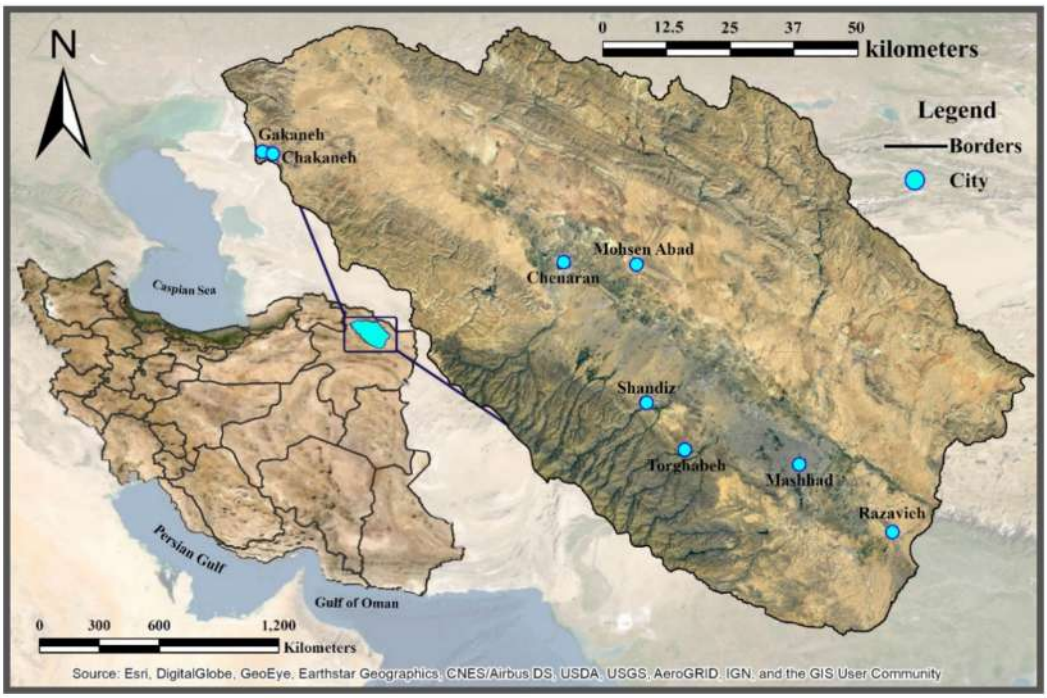

Figure 2. Mashhad Plain Basin in Northeastern Iran.

2.3. Data Collection

The available data were obtained from various governmental organizations and other direct sources, such as field surveys and RS (i.e., satellite imagery) data; data collection focused on the main influential factors to identify potential RWH areas, including maps of rainfall, soil, and land use. Furthermore, data processing and an assortment of supporting techniques were conducted to perform the data analysis. All the generated/available data (GIS layers) were geo-referenced to the MPB geographical coordinate system (WGS_1984_UTM_ Zone_40N).

2.4. Data Processing and Analysis

2.4.1. Criteria Map Generation

Slope map generation was performed using the ASTER DEM surface and the 3D Analyst tool in the ArcGIS environment. The hydrological soil map was reclassified into three soil groups, according to the soil texture and characteristics (infiltration and soil grading). The land use data were merely descriptive and were not readily available to be incorporated directly into the model; the geological field mapping along with the satellite images were used for better land-use data preparation.

The SWAT model was used due to model compatibility for regions lacking proper available data. The SWAT model incorporates various contributing factors in the runoff process and lessens the inherent biases involved in the MCDA-GIS approach [48].

ASTER DEM was utilized in the SWAT model to delineate basin, sub-basins, and hydrological response units (HRUs). Then, weather data for the period of 1981 to 2010 (i.e., CFSR (climate forecast system reanalysis), daily rainfall, minimum and maximum temperature collected from the GSMaP (global satellite mapping of precipitation)) was imported to build the basin model and enable hydrological simulation. Calibration and validation processes were neglected for two main reasons; the first reason is the inadequacy of observed runoff data to examine the model simulations and the comparative and/or relative survey of the results because in the comparative environment, calibration and validation processes are obviously not necessary. Therefore, the non-calibrated model does not have any impact on the relative runoff coefficient and the optimal locations for RWH. After calculating the annual average rainfall for each station, it was interpolated using the

kriging method in ArcGIS, which was later averaged over each sub-basin. With the mean runoff depth obtained from the SWAT model, and the average rainfall over each sub-basin, a mean runoff coefficient was determined for all 43 sub-basins within the study area.

After preparing the selected criteria and assigning normalized scores to each sub-criterion, the final map for each criterion was generated and classified into three classes. For all the criteria, except soil depth, soil type, and land use, the classification method of Jenks natural breaks was applied [57,58]. The Jenks natural breaks method, which is considered a conventional method of classification, has been frequently used by previous studies [30,59,60]. Natural break classes are based on natural groupings inherent in the data. Class breaks are identified such that similar values are grouped and the differences between the mean values of classes maximized [57]. It should be noted that the classification of soil depth, soil type, and land use was done based on the literature and expert judgment.

2.4.2. Comparison of Approaches

To compare the potential RWH maps resulting from the two approaches, the correlation coefficient (CC) between the two maps was calculated using the band collection statistics tool in ArcGIS [61]. The correlation between two grid datasets was calculated as the covariance of two grids divided by-product of standard deviations of two grids, as follows:

$$CC = \frac{Cov_{ij}}{\sigma_i \sigma_j} \quad (1)$$

where σ_i and σ_j are the standard deviation of grid i and j, which here can refer to the resulting potential RWH maps of approach 1 and 2, respectively; Cov_{ij} is the covariance between all pairs of cells of the two grids, calculated as follows:

$$Cov_{ij} = \frac{\sum_{k=1}^{N} (V_{ik} - \mu_i)(V_{jk} - \mu_j)}{N - 1} \quad (2)$$

where V is the cell value, μ is the mean value of each grid, N is the total number of cells in each grid, and k denotes a particular cell in the grid. The CC ranges between -1 to 1, such that CC equal to 1 and -1 showing a fully positive and negative correlation between two grids, respectively.

2.5. Multi-Criteria Decision Analysis

2.5.1. Analytic Hierarchy Process (AHP)

To produce the potential RWH map, AHP was selected as an MCDA technique [62]. AHP has been widely used due to its simple interpretation and implementation, as well as the consistency of its results [59,63–65]. However, the main challenge with the MCDA method is how to select the criteria and relative weights, considering the judgment of experts. Therefore, through the use of expert knowledge and extensive review of RWH articles, effective criteria were selected and proper weights and scores were assigned [16,25,66]. Each of the mentioned criteria had different feature classes; the appropriate score for each feature class of the layers was determined and then normalized. Proper scores were assigned to selected thematic layers on a scale of 1–9, proposed by Saaty [67]. A pair-wise comparison of the assigned weights matrices was made using the Saaty AHP approach to determining the weights of the criteria. Subsequently, these desired priority vectors were computed using the eigenvector technique [62] and finally the assigned weights were tested for consistency by computing the consistency ratio as follows [67]:

$$\text{Consistency Ratio (CR)} = (\lambda_{max} - n)/((n - 1) \times RI) \quad (3)$$

where λ_{max} is the principal eigenvalue computed by the eigenvector technique, n is the number of criteria, and RI denotes random index. More details about the eigenvector technique are provided by Saaty (1980) [67].

It is worth mentioning that the AHP method requires independence between each criterion; while the parameters used in approach 2 (i.e., runoff coefficient, soil type, and slope) are interrelated. Nevertheless, the aims of selecting and including criteria into AHP are two-fold. The selected area for RWH should have, first, the potential of runoff generation and, second, the potential of runoff harvesting. Two areas having the same runoff coefficient and the same amount of rainfall do not necessarily provide the same chance of RWH; the area with a gentler slope and less pervious soil provides a better opportunity for RWH. The runoff coefficient is a key parameter in RWH in the second approach that shows the percent of water that can be available for RWH and has the highest weight compared to the other factors. Rainfall, slope, and soil type are, accordingly, other parameters that determine the feasibility of harvesting rainwater, having lower effective weights in the second approach, respectively.

2.5.2. Rainwater Harvesting Potential Index (RWHPI)

In this study, for each of the two approaches mentioned in previous sections, different criteria were used, as listed in Table 1. These criteria were selected based on their proven effectiveness in locating potential RWH zones in ASARs, as documented in a literature review [16,25]. All thematic layers, along with their normalized weights were integrated using ArcGIS software to map the potential RWH zones for both approaches. The total normalized weights of different features were overlaid in the integrated raster layer using the weighted linear combination (WLC) as Equations (4) and (5), which were used for the first and second approaches, respectively.

$$\mathrm{RWHPI} = (\mathrm{R})_c(\mathrm{R})_s + (\mathrm{S})_c(\mathrm{S})_s + (\mathrm{ST})_c(\mathrm{ST})_s + (\mathrm{SD})_c(\mathrm{SD})_s + (\mathrm{LU})_c(\mathrm{LU})_s \quad (4)$$

$$\mathrm{RWHPI} = (\mathrm{R})_c(\mathrm{R})_s + (\mathrm{RC})_c(\mathrm{RC})_s + (\mathrm{S})_c(\mathrm{S})_s + (\mathrm{ST})_c(\mathrm{ST})_s \quad (5)$$

where RWHPI is rainwater harvesting potential index, subscript c shows the normalized weight of each criterion, and subscript s denotes the normalized score of a feature class of each criterion. RWHPI is a dimensionless indicator that is useful for finding the high-potential RWH zones within the study area.

Table 1. The criteria used in RWHPI.

Thematic Layer	Abbreviation	1st Approach	2nd Approach
Runoff Coefficient	RC	-	√
Soil Type	ST	√	√
Slope	S	√	√
Rainfall	R	√	√
Land Use	LU	√	-
Soil Depth	SD	√	-

2.6. Sensitivity Analysis

It is very important to check the reliability and robustness of the methodology used in this study and the results should be validated to evaluate the impact and importance of each of the factors affecting the model. Sensitivity analysis was performed to obtain insights into the dependence of model outputs on certain model variables [68]. These analyses, in addition to determining the impact of each variable on the RWH analysis, reduce the subjective aspects of the various criteria. The most sensitive identified criteria are ranked as the first priority for future analyses, to ensure more accurate measurements due to their high weights in the analysis. Single parameter analysis introduced by Napolitano et al. [69] was used to estimate the contamination vulnerability of aquifers in several studies [70,71]. In addition, single parameter sensitivity analysis manages the over-parameterization that commonly occurs in hydrological modeling [48,49,72]. The sensitivity analysis method

replaces the initial criteria weight used for the AHP with "effective weights" calculated using Equation (6):

$$W_i = \sum_{j=1}^{n} \frac{F_i \times S_{ij}}{V_j} \times 100/n \quad (6)$$

where W_i is the effective weight of each factor, F_i indicates the initial weight of criterion, S_{ij} is the value score of ith criterion in jth pixel of the raster map, and V_j is the value of the applied index (i.e., RWHPI) and n is the number of pixels in the raster map of the case study. The sensitivity analysis was applied to both approaches.

After performing the sensitivity analysis, the effective weights were applied to obtain the modified RWHPI. The modified RWHPI assumes the same class scoring and parameters as the base RWHPI but using effective weight values obtained from Equation (6), (i.e., W). The modified RWHPI is obtained considering the effective weight of each criterion rather than the initial assigned weight, which reduces the initial subjectivity of the assigned weights selected by using expert judgment.

2.7. Identification of Suitable Sites for Different RWH Techniques

After identifying potential RWH areas and also discarding unsuitable areas for RWH, different RWH techniques for the potential areas were evaluated. For this purpose, the most common techniques used in ASARs for agricultural and domestic applications were considered, including percolation tanks, terracing, and pond and pan [25]. The suitability map for each RWH technique was generated based on common local practice criteria, as well as a comprehensive review of previous studies. The most common parameters applied for the development, planning, and implementation of such techniques are listed in Table 2 [25]. In the following sections, some explanations about several RWH techniques are provided.

Table 2. The common techniques and criteria used for RWH site selection in ASARs.

RWH Techniques	Rainfall (mm)	Slope%	Soil Type	Land Use/Cover	Reference
Pond and Pan	>200	<5	Silty loam, sandy clay loam	Planting forests, low-density pasture, semi-dense pasture, woodland and scrubland, high-density pasture, irrigated cropland and pasture, dry farming	[24,31,73–76]
Terracing	200–1000	5–30	Clay loam, sandy clay, sandy loam	Semi-dense forest, low-density pasture, woodland and scrubland, planting forests, dry farming, semi-dense pasture, rock protrusions, high-density pasture	[37,77,78]
Percolation tank	<1000	<10	Clay loam, silt loam	Semi-dense pasture, woodland and scrubland, low-density pasture, rock protrusions, high-density pasture, dry farming	[74,76,79]

3. Results

3.1. Selected Criteria in MCDA

In the present study, two approaches for locating potential RWH zones were implemented and compared to examine the effect of incorporating SWAT as a hydrological model to the frequently used approach of MCDA-GIS [24,25,31,75]. In the calculation of RWHPI and generating RWH potential maps, the highest harvesting possibilities of rainwater, as well as runoff generation, were considered. The RWHPI for the first and second approaches were calculated using Equations (4) and (5), respectively. To guarantee the consistency of the analyses, the procedure of weighting thematic layers in AHP was set such that the consistency ratio for all of the obtained thematic layers would be less than the limit of 0.10 [67]. The selected RWH criteria, as well as the assigned corresponding weights, are shown in Table 3. Their selection was based on expert knowledge and extensive literature reviews over several RWH publications for ASARs.

Table 3. Weights of the thematic layers (criteria) and their features (sub-criteria).

Thematic Layer	Feature Class	Assigned Score	Layers Relative Weights	
			Approach 1	Approach 2
Runoff Coefficient	0.031–0.041	2	-	0.387
	0.042–0.058	4		
	0.059–0.087	6		
	0.088–0.12	8		
	0.13–0.18	9		
Rainfall (mm/year)	161–202	2	0.380	0.275
	203–272	4		
	273–331	6		
	332–395	8		
	396–466	9		
Slope (%)	0–5	9	0.234	0.198
	5–10	8		
	10–15	7		
	15–30	5		
	>30	3		
Soil Type	Silt loam or loam	5	0.179	0.140
	Sandy clay loam	7		
	Clay loam or clay	9		
Soil depth	Water bodies	9	0.107	-
	Very shallow	8		
	Shallow	7		
	Relatively deep	5		
	Deep	3		
Land use	Semi-dense forest	2	0.100	-
	Woodland and scrubland	3		
	Planting forests	4		
	Scatter forest	5		
	Dry farming, irrigated cropland	6		
	High density pasture	7		
	Low and semi-dense pasture	8		
	Urban and built-up land, water bodies	9		

Most of the selected biophysical criteria in this study have been widely used in previous studies in ASARs. Adham et al. [25] showed that, in 48 studies regarding the potential RWH evaluation through GIS, land cover/use (75% of studies), soil type (75% of studies), rainfall (56% of studies), and slope (83% of studies), were used as influential criteria. The rainfall data are one of the necessities/prerequisites to identify potential RWH zones and technically more rainfall in an area means a higher-potential RWH [80]. In ASARs, in terms of the practical effectiveness of RWH techniques, a minimum available rainfall of 200 mm/year was recommended [81,82]. Daily global rainfall CFSR data for 30 years (1981 to 2010) were used and mean annual rainfall data over the sub-basins were obtained. According to the rainfall map shown in Figure 3b, the annual rainfall ranges from 161 to 466 mm, and over 60% of rainfall occurs during December, February, March, April, and May. The northern sub-basins receive a higher amount of rainfall (about 400 mm/year), while less rainfall (around 161–202 mm/year) is received in the southern sub-basins. The rainfall received in the middle parts of the study area ranges from around 203 to 395 mm/year. In this study, direct consideration of evaporation was ignored due to a lack of data and simplification. However, in the second approach, evaporation was indirectly considered. This is because of the fact that the runoff coefficient map utilized as a biophysical criterion was obtained from a SWAT model, which considers evaporation in the process.

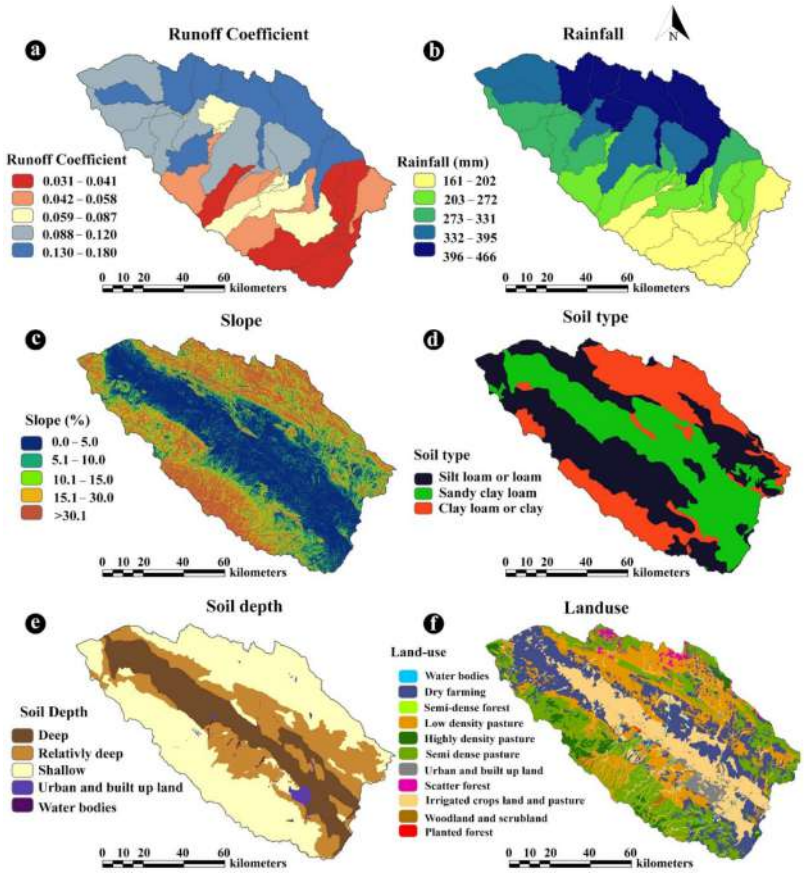

Figure 3. Layers and corresponding feature classes. (**a**) Runoff coefficient, (**b**) rainfall, (**c**) slope, (**d**) soil type, (**e**) soil depth, and (**f**) land use.

The slope is another criterion for the mapping of potential RWH zones. As the percentage of slope increases, the runoff generation increases, while the harvesting opportunity of rainwater for most RWH techniques decreases—this results in less suitability for RWH [29,77]. Hilly areas respond to rainfall events in the way that a high amount of rainwater rapidly runs off and becomes unavailable, even if the mean amount of rainfall is fairly noticeable. That is the case, particularly in the peak domestic and agricultural demand periods [77]. On the other hand, milder areas retain water for a longer time and facilitate groundwater recharge. Moreover, a large amount of earthwork along with implementing erosion control measures are required for constructing RWH systems on hilly areas, which undermines the economic aspect of building RWH systems in areas with a high degree of slope [31,42]. Typically, areas with higher slopes (>5%) are more prone to erosion due to the uneven distribution of runoff over the area [83]. A slope map is shown in Figure 3c. All around the study area, except for the southeastern border, is surrounded by mountains (high elevation areas), while central portions of the study area are located at lower elevations. The slope ranges between 0 and 1% in almost 37% of the study area and the slope of 9.1% of the study area is in the range of 1 to 3%. Steep areas (>15%) cover 4.1% of the basin. The rest of the desired region is divided into three almost equal portions (around 16% of the study area) that have slope ranges of 3–5%, 5–10%, and 10–15%.

Another important criterion for RWH planning and selecting optimal locations for implementing RWH techniques is the soil type [84,85]. Soil characteristics determine the infiltration capacity rate, water holding capacity, and runoff generation potential [78,85–87]. The textural features of soil are determined by the percentage of sand, silt, and clay. Naturally, a higher sand portion in the soil implies a higher infiltration rate, lower water storage capacity, and lower runoff generation potential, while the reverse of these properties is the case when the soil consists of a higher clay percentage [78,86,88]. A soil map is shown

in Figure 3d. Sandy clay loam with low infiltration rates forms about 25.4% of the soil in the study area; besides, silt loam, or loam with a moderate infiltration rate forms about 49.3% of the study area. The rest of the basin (almost 25.3%) consists of clay/clay loam with a low infiltration capacity rate and consequently higher runoff potential. There are several factors (e.g., vegetation coverage, soil texture) involved in the amount of runoff that is generated from rainfall events which are reflected in a runoff coefficient [87,89]. Since most of the influential factors in runoff generation are considered in SWAT's structure, the resultant runoff coefficient map reasonably represents case study characteristics.

The runoff coefficient map (Figure 3a) indicates the average runoff coefficient of each sub-basin over 30 years (1981–2010). The runoff coefficient map values range from 0.03 to 0.18. The northern parts indicate higher values while lower runoff coefficients are shown in the southern sub-basins. Typically, a higher runoff coefficient denotes a higher runoff potential; nevertheless, it should be mentioned that successful RWH is not exclusively the function of high runoff potential, but the potential of harvesting the generated runoff should also be considered, which itself is a function of other criteria to ascertain potential RWH.

Land use characteristics dictate the quantitative and qualitative relations between captured rainfall by the basin, groundwater recharge, evapotranspiration loss, and the remaining water running off a basin [88]. Infiltration is lower in urban and pasture-covered areas, which results in higher overland flow. While, as the vegetation coverage becomes intense, water abstraction, interception, and infiltration are increased and its consequences in less generated runoff [40,48,84]. The land use map (Figure 3f) shows that dominated land covers of low-density pasture, semi-dense pasture, irrigated agriculture, and dry farming constitute 23%, 24%, 19%, and 25% of the study area, respectively. It is worth mentioning that due to the incorporation of the runoff coefficient map, the land use layer was not directly included in the second approach. This is because the runoff coefficient map is highly dependent on land use and SWAT requires a land-use map as an input. Thus, the impact of different land uses on RWH is intrinsically reflected in a runoff coefficient map.

The classification of the soil depth map (Figure 3e) based on FAO suggestions (Food and Agriculture Organization of the United Nations) [90] includes very shallow (<30 cm), shallow (30–50 cm), moderately deep (50–100 cm), and deep (100–150 cm). The soil depth map (Figure 3e) indicates that central portions of the study area are mainly covered by deep soils (20.9%), while outer areas are mostly shallow soils (46%). The rest of the basin (27.6%) has relatively deep soil. Areas with shallow soils are potentially more suitable for RWH than areas with deep soils (with some exceptions, such as terrace (earthwork)) due to lower permeability and higher water generation [91]. In other words, a runoff coefficient is higher in areas with a shallower soil depth. The soil depth layer was not directly included in the second approach due to the high dependency of runoff coefficient on soil depth. A runoff coefficient is interrelated to the soil depth and assumed as its proper representative in the second approach.

3.2. Rainwater Harvesting Potential Maps

RWH Potential maps were produced by integrating the selected layers (Table 3) of each approach using the WLC technique in ArcGIS Spatial Analyst Tools. Afterward, RWHPI was computed using Equations (4) and (5) for the first and second approaches, respectively, to generate the potential RWH maps, shown in Figure 4a,b. The output maps of both approaches were classified into three categories of "low", "moderate", and "high" RWH potential. The same classification method of Jenks natural breaks was implemented to classify both potential RWH maps to facilitate the comparison of the two approaches. The RWHPI for both approaches ranged in almost the same intervals for all RWH potential classes, as shown in Figure 4a,b. The low classes ranged in 0.083–0.181 and 0.102–0.193, moderate classes ranged in 0.182–0.253 and 0.194–0.242, and the interval of high classes were 0.254–0.352 and 0.243–0.337 for the first and second approaches, respectively. According to Figure 4a,b, although there are some discrepancies between the two developed maps, the general patterns of both maps are almost identical. The areas with high potential RWH

are located in the northern parts of the case study area, while a lesser potential RWH was predicted by both approaches for the southern parts. The northwestern and central parts of the study area had moderate RWH potential.

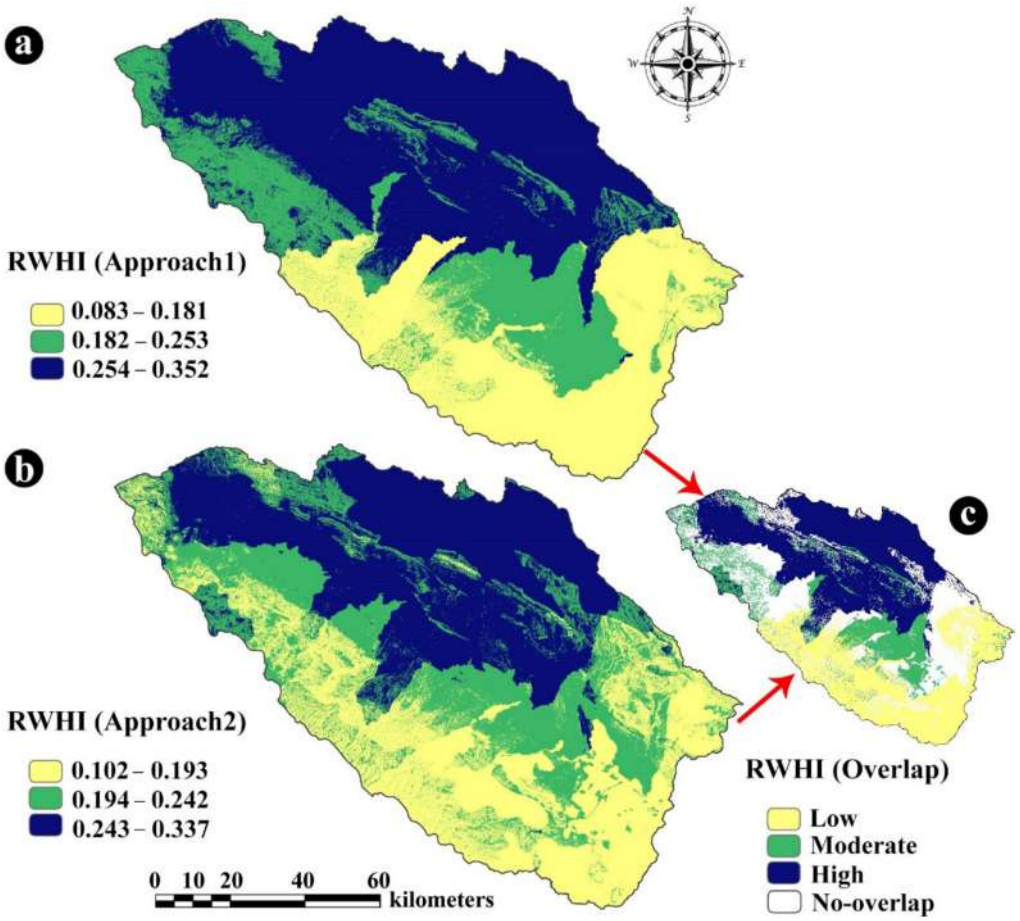

Figure 4. RWH potential map of the study area for the first and second approaches and for the overlap of the two approaches.

Apart from the almost identical potential RWH area distributions of both approaches over the case study area, the coverage areas of each class are also analogous (Table 4). Moreover, the overlapping map of both approaches is shown in Figure 4c, where navy blue color shows a high overlap and the white-colored areas indicate no overlap. The overlap percentage of each RWH potential class is also provided in Table 4.

Table 4. Three classes of potential RWH using two approaches.

RWH Potential Classes	Approach 1	Approach 2	Percentage of Overlap of the Two Approaches (%)
	The Portion of Study Area (%)	The Portion of Study Area (%)	
Low	29.9	34	32.9
Moderate	24.3	30.5	19.1
High	45.8	35.5	48.0

According to Table 4, the low potential RWH class comprises almost 30% of the study area in both approaches, such that 80.4% of the area is in common between the two developed maps. This fact shows the conformity of the two approaches in discriminating areas with less potential for RWH. Areas with high RWH potential cover 45.8% and 35.5% of the study area in the first and second approaches, respectively. While there is a noticeable difference in the percentages of the coverage area, 76.5% of the high potential RWH areas are overlapped in both maps. These areas that encompass 3394 km^2 (Figure 4c) are mainly

located in the northern part of the study area and are considered the most promising sites for RWH since they are obtained by both approaches. In addition, high potential overlap areas can be listed as top priority zones for RWH interventions by decision-makers. The models' agreement on their high potential RWH increases their credibility. The moderate class comprises almost the same portions (24.3% and 30.5% for the first and second approach, respectively) of the basin; nevertheless, there is less agreement between the two models in this class and the overlapping coverage is 57.4%. The moderate class in the first approach is located in a more concentrated way, while there are more scatterings in the second approach. To more thoroughly compare implemented approaches, the correlation between the two obtained potential RWH maps was evaluated utilizing the Spearman method. The calculated correlation coefficient is 0.914, which indicates that the two maps are strongly correlated, and both approaches yield almost the same results. Based on the high correlation coefficient, percentages of overlapped area for each of the classes (Table 4), and the general pattern of the two potential RWH maps (Figure 4a,b), the following conclusion is obtained.

3.3. Sensitivity Analysis

Criteria weights and sub-criteria scores have a vital impact on the evaluation of the obtained results. Given that their determination is generally made through expert interpretation, the selection of potential RWH zones can be sensitive to weight changes in criteria-related decision weights [92,93]. For example, considering a feature in which the distribution of feature classes is rather homogeneous, this would have a fairly equal influence on the whole study area. Solving this problem requires sensitivity analysis in such a way that the weight values constantly change to check the amount of change in the final results. At first, as an initial weight, the runoff coefficient was considered as the dominant parameter. The next considered significant parameters included rainfall, slope, soil type, soil depth, and land use, respectively.

The results of the sensitivity analyses (Figure 5) showed that the least sensitive factor in approach 1 was land use (with the mean value of 0.075), which was expected due to the weight factors assigned (Table 3). Additionally, in approach 2, the least sensitive parameter was slope (with the mean value of 0.207). Performed comparison of the RWHI map produced from the sensitivity analyses of approach 1 and approach 2 indicates that these two approaches are well comparable in general, therefore it would be rational to conclude that the assumed weight was fairly suitable and the results are reliable as both weights and final results were rather similar.

The result of sensitivity analysis for both approaches revealed that the effective influence of the assumed weights for rainfall and runoff coefficient layers would be less in reality (Table 5). This can be attributed to the rather homogeneous distribution of rainfall and runoff coefficient layers and the fact that they were averaged for each sub-basin (see Figure 3a,b). Revising the initial weight of criteria with the effective weight obtained from sensitivity analysis, Equation (6), slightly increased the overall overlap of the two approaches with a previous study. The overlap of approaches 1 and 2 after sensitivity analysis were, thus, 47.9 and 37.7%, respectively. To be more specific, using sensitivity analysis decreases the sensitivity of features by minimizing the difference between the estimated weights and their real influence. Examining the results of the sensitivity analysis of approach 1, it is observed that the parameters of rainfall and slope, both had the greatest impact on the model, in other words, have the highest sensitivity. In approach 2, the runoff coefficient parameter had the highest sensitivity. According to the RWH overlap map of the two approaches, about 50% of the study area has a high potential RWH, about 28% moderate, and about 22% low potential RWH (Table 6). Generally, the northern half of MPB has a high potential RWH; however, the southern half of the study area has a moderate to low potential RWH.

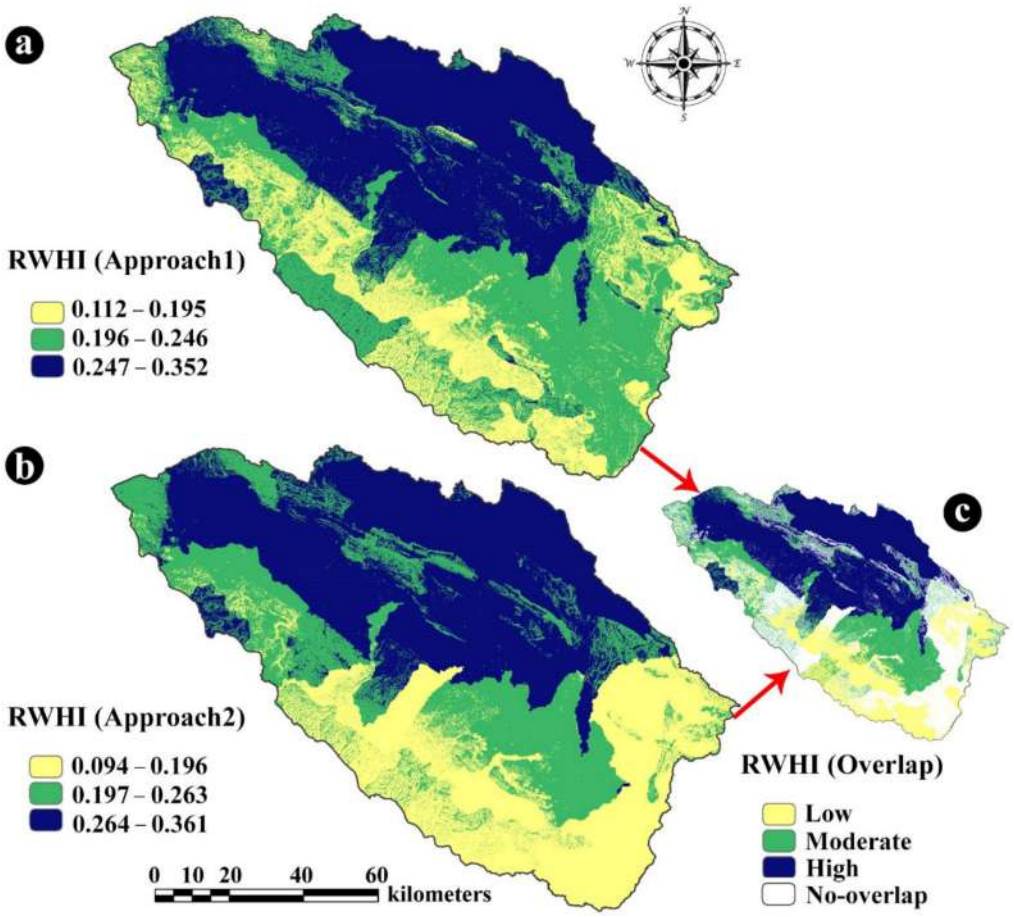

Figure 5. Potential RWH map of the study area for the first and second approaches after sensitivity analyses.

Table 5. Statistics of the effective weights from sensitivity analysis.

Approach 1					
Parameter	**Initial Weight (W), (AHP)**	**Min (W_i)**	**Max (W_i)**	**Mean (μ)**	**SD (σ)**
Rainfall	0.380	0.105	0.639	0.329	0.126
Slope	0.234	0.030	0.475	0.243	0.126
Soil Type	0.179	0.134	0.565	0.265	0.083
Soil Depth	0.107	0.033	0.261	0.088	0.035
Land Use	0.100	0.014	0.197	0.075	0.023
Approach 2					
Parameter	**Initial Weight (W), (AHP)**	**Min (W_i)**	**Max (W_i)**	**Mean (μ)**	**SD (σ)**
Runoff Coefficient	0.387	0.133	0.580	0.358	0.100
Rainfall	0.275	0.071	0.441	0.226	0.073
Slope	0.198	0.023	0.473	0.207	0.119
Soil Type	0.140	0.099	0.555	0.209	0.087

Table 6. Three classes of potential RWH in the two approaches after sensitivity analysis.

RWH Potential Classes	Approach 1	Approach 2	Percentage of Overlap of the Two Approaches (%)
	The Portion of Study Area (%)	The Portion of Study Area (%)	
Low	21.9	30.3	22.1
Moderate	28.4	28.2	27.8
High	39.7	41.4	50.1

In conclusion, using CFSR data does not result in an identical output as using observed data due to the high sensitivity of locating potential RWH areas according to rainfall data; however, the global availability of CFSR data enables RWH analysis all over the world. Thus, more attention should be paid to data quality and also to the fact that the high uncertainty associated with them should not be neglected. In the next step/section, after identifying the high-potential RWH areas, the feasibility of different RWH structures in the study area is assessed.

3.4. Potential Zones for RWH Techniques

After identifying the most suitable areas for RWH, various RWH techniques were determined. As mentioned earlier, the most common RWH techniques are ponds and pans, terracing, and percolation tanks. Figure 6 shows the suitable locations for various RWH techniques from the perspective of both approaches 1 and 2. The whole study area is divided into low, medium, high, and unsuitable classes in terms of suitability for different techniques. The suitability map of the study area from the perspective of different techniques was prepared using criteria related to each technique for both approaches 1 and 2 in the ArcGIS environment, the results of which are according to Table 7. As presented in Table 7, the most suitable areas among the various techniques studied are related to ponds and pans, in which the total area with low, moderate, and high potential for this type of technique is about 44% (or about 4295 km^2). After ponds and pans, the most suitable areas, respectively, are tanks with about 30% (about 2928 km^2) and terracing with about 20% (about 1952 km^2).

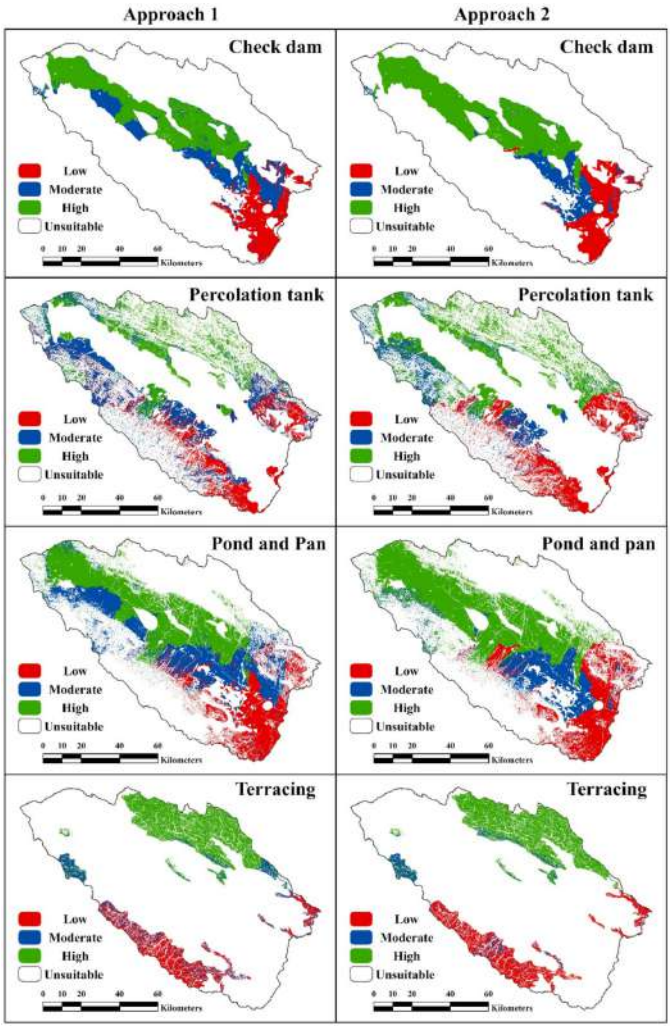

Figure 6. Suitable areas for various RWH techniques, as obtained from the two approaches.

Table 7. The total potential area of the various RWH techniques in the study area as percentages.

RWH Techniques	Class	Approach 1		Approach 2	
		Without Sensitivity Analysis	With Sensitivity Analysis	Without Sensitivity Analysis	With Sensitivity Analysis
Terracing	Poor	5.7	2.2	6.8	6.1
	Moderate	3.3	5.6	1.9	2.2
	Very Good	11.1	12.3	11.3	11.8
	Total	20.0	20.0	20.0	20.0
Percolation Tank	Poor	8.9	7.4	9.8	9.5
	Moderate	11.8	12.8	7.1	10.4
	Very Good	9.2	9.7	13.1	10.0
	Total	29.9	29.9	29.9	29.9
Pond and Pan	Poor	10.3	4.0	10.7	10.9
	Moderate	15.3	19.3	9.1	11.4
	Very Good	18.2	20.5	24.0	21.4
	Total	43.7	43.7	43.7	43.7

3.5. Potential of RWH in MBP Water Management

MPB has been struggling with water scarcity and shortage problems for decades. Currently, surface water supplies about 22% of the water demand in Khorasan Razavi Province, encompassing the MPB, and the rest is provided through groundwater resources. Of the total capacity of the large dams in Khorasan Razavi Province (1549 million cubic meters, MCM), most dams operate at only about 34% of their total capacity. On average, about 6404 MCM are extracted annually from groundwater sources, about 85% of which is exploited through wells, about 9% through qanats, and 6% through springs. However, groundwater recharge potential is only 5300 MCM, which indicates an average annual groundwater shortage of 1100 MCM. Groundwater over-extraction and the low operating capacity of existing dams have eventuated the province's water crisis. Mashhad, as the center of the province, with an average annual water consumption (industrial, agricultural and domestic water consumption) of 26.46 MCM, has the highest over-exploitation of renewable water in the province (Khorasan Razavi Regional Water Authority [55]).

Nevertheless, based on the demonstrated results (Figure 5), the study area has a high RWH potential. An annual rainfall of 2946 MCM falls on the whole study area of which 1505 and 1569 MCM are on the high potential RWH class, and 952 and 780 MCM is received by the moderate class in the first and second approaches, respectively. Moreover, the rainfall received by the overlap of high potential RWH areas in both approaches is 1436 MCM. The resulting surface runoff within a catchment is one of the decent water resources, once it is managed efficiently, and can be utilized to supply a high portion of water (domestic and agricultural) demands. The results indicate the high potential of the case study area in harvesting rainwater and alleviating the existing water crisis. Finding and implementing efficient water management strategies at a basin/sub-basin scale is an urgent requirement of the MBP. Water shortages will continue to be a major problem in the study area unless efforts are made to achieve sustainable and efficient use of potential RWHs.

4. Conclusions

RWHs are recognized as an applicable and favorable method of water supply, as it conserves existing water resources, while contributes to water scarcity alleviation, particularly in ASARs. Nevertheless, identification of potential RWH areas is challenging due to the inherent uncertainty of input data and the subjectivity involved in selection of influential parameters. In the present study, two approaches for locating potential RWH areas were implemented. In the first approach, a frequently used MCDA-GIS method was utilized, while in the second approach, the SWAT model was included in the analysis in order to

examine the effect of incorporating SWAT as a hydrological model into an MCDA-GIS method for RWH assessment. In this study, the SWAT model, as a more comprehensive hydrological model compared to the SCS curve number method was employed for generating the runoff coefficient map.

The resultant potential RWH maps of the two approaches indicated a similar pattern for potential RWH areas. In both potential RWH maps, the northern parts of the study area were categorized as the high potential areas, whereas less harvesting potential of rainwater was demonstrated for the southern areas of the case study. In addition, the overlap of the resultant maps of the two approaches indicated that 3394 km^2 of the study area is considered a high-potential RWH area. These areas, mainly located in the northern parts of the study area receiving an average annual rainfall of 1366 MCM. Meanwhile, the total capacity of the large dams of Khorasan Razavi Province, where the study area is located, is 1549 MCM. Accordingly, there is high RWH potential in the study area that, if be managed and utilized efficiently, could contribute to water supply and ensure long-term water security.

The high value of the calculated correlation coefficient between the two resultant potential RWH maps (i.e., CC = 0.914), along with provided results, demonstrated that both approaches yield almost identical results. Therefore, it can be stated that the inclusion of SWAT as a hydrological model under the described methodology does not necessarily result in different outputs from conventional MCDA-GIS for RWH evaluation purposes, whereas it demands a higher degree of effort to run the hydrological models. On the other hand, the inclusion of hydrological models can be considered as an efficient strategy to reduce uncertainties embedded in RWH assessment using MCDA. Additionally, there would be less uncertainty associated with the overlapping high-potential RWH areas, since these areas are suggested by a combination of the two approaches, rather than a single conventional MCDA-GIS method.

Moreover, the results of the conducted sensitivity analyses indicate that the rainfall and slope criteria (with weights of 0.329 and 0.243, respectively) have the highest impact on the model in approach 1 whereas the criterion of runoff coefficient (with weights of 0.358) has the highest sensitivity in approach 2. The most-sensitive identified criteria could be ranked as the first priority for future data augmentation to ensure more accurate measurements due to their high weight in the analysis.

Based on the discussed results, a suitability map of the study area from the perspective of three different techniques was developed using various criteria related to each technique for both approaches 1 and 2, and for both models, with and without sensitivity analyses. Results indicate that the ponds and pans technique is the most suitable option for MPB, covering more areas with a high potential of RWH than the two other techniques for both approaches (21% of the study area on average). After that, terracing and percolation tank cover 11.6% and 10.5% of the study area with high potential for RWH on average, respectively.

It should be noted that the modeling cost, data availability and accuracy, and efficiency of these methods can vary significantly from basin to basin. In more developed countries, data can be obtained with minimal effort and have a high accuracy. On the other hand, the cost of developing a hydrologic model may defeat the purpose of integrating the hydrologic model with the MCDA-GIS approach. The abovementioned cost-benefit analysis is clearly beyond the scope of this project. It is recommended that the above approach be considered in other case studies where the flow of data is readily available and the SWAT model parameters can be calibrated. Therefore, the findings of this research can be compared against those of other areas and the reliability of these results can be further investigated.

Moreover, applying hydrologic models as comprehensive as SWAT are usually demanding in terms of data, time, and effort and their advantages need to justify their application. Meanwhile, since in this study generated maps from two approaches that were highly correlated which may not justify its application. This may be because of the fact that we intended to evaluate the efficiency of the model for areas suffering from data

scarcity and, consequently, we did not calibrate the SWAT model. Considering this, we recommend applying this approach for areas with sufficient in situ data in order to calibrate the SWAT model and to assess the results from two approaches to check the justification for using a hydrologic model. It is possible that other hydrologic models result in a different conclusion than those drawn in this research and justify the use of hydrologic models for RWH. It is recommended that a group of different hydrologic models be considered to compare two approaches and further evaluate the use of hydrologic modeling in RWH. Moreover, the comparison between the two approaches might be impacted by the utilized MCDA method. It is recommended that a similar analysis be considered using other MCDA methods, such as ANP, and assess possible impacts. In the end, the identified high-potential RWH areas are based on the initial assessment of this study area. More specific and comprehensive studies are required to consider impacts of other hydrological processes, including evapotranspiration, to estimate the actual harvestable rainwater in these areas and fine-tune the water resources management of MPB.

Results of this research can potentially be helpful for further studies for populated areas in a developing country, such as Iran. While there are many technical issues for implementing RWH techniques in a populated area, such as MPB, it is an inevitable need to help satisfy the ever-increasing demand for domestic water. Consequently, it is well within expectations that this approach, or any other comparable one, be considered for application in the near future.

Author Contributions: Conceptualization, E.G.T.; methodology, E.G.T., S.D., R.A., and B.A.; software, E.G.T., and S.D.; validation, E.G.T., S.D., R.A., B.A., and A.A.; formal analysis, E.G.T., R.A., B.A., and A.G.B.; investigation, E.G.T., R.A., B.A., A.G.B., and A.A.; resources, S.D., E.G.T., R.A., B.A., and A.A.; data curation, S.D., E.G.T., R.A., B.A., and A.G.B.; writing—original draft preparation, E.G.T., R.A., B.A., and A.A.; writing—review and editing, E.G.T., R.A., B.A., A.G.B., and A.A.; visualization, S.D., E.G.T., R.A., B.A., and A.A.; supervision, A.A.; project administration, A.A.; funding acquisition, A.A. All authors have read and agreed to the published version of the manuscript.

Funding: This research received no external funding.

Institutional Review Board Statement: Not Applicable.

Informed Consent Statement: Not Applicable.

Data Availability Statement: Data available on request due to privacy and ethical restrictions.

Acknowledgments: The authors would like to express their sincere gratitude to Amirhossein Shadmehri Toosi who provided insight and expertise that greatly assisted the research.

Conflicts of Interest: The authors declare no conflict of interest.

References

1. Hafizi Md Lani, N.; Yusop, Z.; Syafiuddin, A. A review of rainwater harvesting in Malaysia: Prospects and challenges. *Water* **2018**, *10*, 506. [CrossRef]
2. Musayev, S.; Burgess, E.; Mellor, J. A global performance assessment of rainwater harvesting under climate change. *Resour. Conserv. Recycl.* **2018**, *132*, 62–70. [CrossRef]
3. Khorshidi, M.S.; Nikoo, M.R.; Sadegh, M.; Nematollahi, B. A Multi-Objective Risk-Based Game Theoretic Approach to Reservoir Operation Policy in Potential Future Drought Condition. *Water Resour. Manag.* **2019**, *33*, 1999–2014. [CrossRef]
4. Adham, A.; Sayl, K.N.; Abed, R.; Abdeladhim, M.A.; Wesseling, J.G.; Riksen, M.; Fleskens, L.; Karim, U.; Ritsema, C.J. A GIS-based approach for identifying potential sites for harvesting rainwater in the Western Desert of Iraq. *Int. Soil Water Conserv. Res.* **2018**, *6*, 297–304. [CrossRef]
5. WWAP (United Nations World Water Assessment Programme). *The United Nations World Water Development Report 2015: Water for a Sustainable World*; UNESCO: Paris, France, 2015.
6. Samadi, F.; Kruzic, A.; Prabakar, S. Effect of Various Inline Injection and Mixing Conditions on Degree of Mixing of Chlorine and Ammonia. In Proceedings of the World Environmental and Water Resources Congress 2018: Water, Wastewater, and Stormwater, Urban Watershed Management, Municipal Water Infrastructure, and Desalination and Water Reuse, Minneapolis, MN, USA, 3–7 June 2018; pp. 159–170.
7. Deb, P.; Kiem, A.S.; Willgoose, G. Mechanisms influencing non-stationarity in rainfall-runoff relationships in southeast Australia. *J. Hydrol.* **2019**, *571*, 749–764. [CrossRef]

8. UN Water. *Coping with Water Scarcity: Challenge of the Twenty-First Century*; UN Water: Geneva, Switzerland, 2007.
9. Alizadeh, B. Improving Post Processing of Ensemble Streamflow Forecast for Short-to-long Ranges: A Multiscale Approach. Ph.D. Dissertation, The University of Texas at Arlington, Arlington, TX, USA, 2019. Available online: http://hdl.handle.net/10106/28663 (accessed on 16 January 2021).
10. Alipour, M.H.; Kibler, K.M.; Alizadeh, B. Flow alteration by diversion hydropower in tributaries to the Salween river: A comparative analysis of two streamflow prediction methodologies. *Int. J. River Basin Manag.* **2020**, 1–11. [CrossRef]
11. Pandey, D.N.; Gupta, A.K.; Anderson, D.M. Rainwater harvesting as an adaptation to climate change. *Curr. Sci.* **2003**, *85*, 46–59.
12. Khorrami, M.; Alizadeh, B.; Ghasemi Tousi, E.; Shakerian, M.; Maghsoudi, Y.; Rahgozar, P. How Groundwater Level Fluctuations and Geotechnical Properties Lead to Asymmetric Subsidence: A PSInSAR Analysis of Land Deformation over a Transit Corridor in the Los Angeles Metropolitan Area. *Remote Sens.* **2019**, *11*, 377. [CrossRef]
13. Khorrami, M.; Abrishami, S.; Maghsoudi, Y.; Alizadeh, B.; Perissin, D. Extreme subsidence in a populated city (Mashhad) detected by PSInSAR considering groundwater withdrawal and geotechnical properties. *Sci. Rep.* **2020**, *10*. [CrossRef]
14. Aghlmand, R.; Abbasi, A. Application of MODFLOW with Boundary Conditions Analyses Based on Limited Available Observations: A Case Study of Birjand Plain in East Iran. *Water* **2019**, *11*, 1904. [CrossRef]
15. Varma, H.; Tiwari, K. *Current Status and Prospects of Rainwater Harvesting. Indian National Committee on Hydrology*; Report No INCOH/SAR-3/95, INCOH Secretariat; National Institute of Hydrology: Roorkee, India, 1995; p. 47.
16. Campisano, A.; Butler, D.; Ward, S.; Burns, M.J.; Friedler, E.; DeBusk, K.; Fisher-Jeffes, L.N.; Ghisi, E.; Rahman, A.; Furumai, H. Urban rainwater harvesting systems: Research, implementation and future perspectives. *Water Res.* **2017**, *115*, 195–209. [CrossRef]
17. Nikvar Hassani, A.; Farhadian, H.; Katibeh, H. A comparative study on evaluation of steady-state groundwater inflow into a circular shallow tunnel. *Tunn. Undergr. Sp. Technol.* **2018**, *73*, 15–25. [CrossRef]
18. Hassani, A.N.; Katibeh, H.; Farhadian, H. Numerical analysis of steady-state groundwater inflow into Tabriz line 2 metro tunnel, northwestern Iran, with special consideration of model dimensions. *Bull. Eng. Geol. Environ.* **2016**, *75*, 1617–1627. [CrossRef]
19. Petit-Boix, A.; Devkota, J.; Phillips, R.; Vargas-Parra, M.V.; Josa, A.; Gabarrell, X.; Rieradevall, J.; Apul, D. Life cycle and hydrologic modeling of rainwater harvesting in urban neighborhoods: Implications of urban form and water demand patterns in the US and Spain. *Sci. Total Environ.* **2018**, *621*, 434–443. [CrossRef]
20. Kahinda, J.M.; Lillie, E.; Taigbenu, A.; Taute, M.; Boroto, R. Developing suitability maps for rainwater harvesting in South Africa. *Phys. Chem. Earth Parts A/B/C* **2008**, *33*, 788–799. [CrossRef]
21. Senay, G.; Verdin, J. Developing index maps of water-harvest potential in Africa. *Appl. Eng. Agric.* **2004**, *20*, 789. [CrossRef]
22. Tiwari, K.; Goyal, R.; Sarkar, A. GIS-based methodology for identification of suitable locations for rainwater harvesting structures. *Water Resour. Manag.* **2018**, *32*, 1811–1825. [CrossRef]
23. Goyal, R. Rooftop rainwater harvesting: Issues & challenges. *Indian Plumb. Today* **2014**, *125*, 148–161.
24. IsIioye, O.A.; Shebe, M.W.; Momoh, U.O.; Bako, C.N. A multi criteria decision support system (MDSS) for identifying rainwater harvesting site(s) in Zaria, Kaduna state, Nigeria. *Int. J. Adv. Sci. Eng. Technol. Res.* **2012**, *1*, 53–71.
25. Ammar, A.; Riksen, M.; Ouessar, M.; Ritsema, C. Identification of suitable sites for rainwater harvesting structures in arid and semi-arid regions: A review. *Int. Soil Water Conserv. Res.* **2016**, *4*, 108–120. [CrossRef]
26. Melville-Shreeve, P.; Ward, S.; Butler, D. Rainwater harvesting typologies for UK houses: A multi criteria analysis of system configurations. *Water* **2016**, *8*, 129. [CrossRef]
27. Jozaghi, A.; Alizadeh, B.; Hatami, M.; Flood, I.; Khorrami, M.; Khodaei, N.; Ghasemi Tousi, E. A Comparative Study of the AHP and TOPSIS Techniques for Dam Site Selection Using GIS: A Case Study of Sistan and Baluchestan Province, Iran. *Geosciences* **2018**, *8*, 494. [CrossRef]
28. Shafieardekani, M.; Hatami, M. Forecasting Land Use Change in suburb by using Time series and Spatial Approach; Evidence from Intermediate Cities of Iran. *Eur. J. Sci. Res.* **2013**, *116*, 199–208.
29. Jha, M.K.; Chowdary, V.M.; Kulkarni, Y.; Mal, B.C. Rainwater harvesting planning using geospatial techniques and multicriteria decision analysis. *Resour. Conserv. Recycl.* **2014**, *83*, 96–111. [CrossRef]
30. Mahmoud, S.H.; Alazba, A. The potential of in situ rainwater harvesting in arid regions: Developing a methodology to identify suitable areas using GIS-based decision support system. *Arabian J. Geosci.* **2015**, *8*, 5167–5179. [CrossRef]
31. Al-Adamat, R.; Diabat, A.; Shatnawi, G. Combining GIS with multicriteria decision making for siting water harvesting ponds in Northern Jordan. *J. Arid Environ.* **2010**, *74*, 1471–1477. [CrossRef]
32. Mahmoud, W.H.; Elagib, N.A.; Gaese, H.; Heinrich, J. Rainfall conditions and rainwater harvesting potential in the urban area of Khartoum. *Resour. Conserv. Recycl.* **2014**, *91*, 89–99. [CrossRef]
33. Saaty, T.L. A scaling method for priorities in hierarchical structures. *J. Math. Psychol.* **1977**, *15*, 234–281. [CrossRef]
34. Saaty, T.L. How to make a decision: The analytic hierarchy process. *Interfaces* **1994**, *24*, 19–43. [CrossRef]
35. Balkhair, K.S.; Ur Rahman, K. Development and assessment of rainwater harvesting suitability map using analytical hierarchy process, GIS and RS techniques. *Geocarto Int.* **2019**, *36*, 421–448. [CrossRef]
36. Wu, R.S.; Molina, G.L.L.; Hussain, F. Optimal sites identification for rainwater harvesting in northeastern Guatemala by analytical hierarchy process. *Water Resour. Manag.* **2018**, *32*, 4139–4153. [CrossRef]
37. Krois, J.; Schulte, A. GIS-based multi-criteria evaluation to identify potential sites for soil and water conservation techniques in the Ronquillo watershed, northern Peru. *Appl. Geogr.* **2014**, *51*, 131–142. [CrossRef]

38. Jha, M.K.; Peiffer, S. *Applications of Remote Sensing and GIS Technologies in Groundwater Hydrology: Past, Present and Future*; BayCEER: Bayreuth, Germany, 2006.
39. Weerasinghe, H.; Schneider, U.; Löw, A. Water harvest-and storage-location assessment model using GIS and remote sensing. *Hydrol. Earth Syst. Sci. Discuss.* **2011**, *8*, 3353–3381. [CrossRef]
40. Kadam, A.K.; Kale, S.S.; Pande, N.N.; Pawar, N.; Sankhua, R. Identifying potential rainwater harvesting sites of a semi-arid, basaltic region of Western India, using SCS-CN method. *Water Resour. Manag.* **2012**, *26*, 2537–2554. [CrossRef]
41. Shadmehri Toosi, A.; Ghasemi Tousi, E.; Ghassemi, S.A.; Cheshomi, A.; Alaghmand, S. A multi-criteria decision analysis approach towards efficient rainwater harvesting. *J. Hydrol.* **2020**, *582*, 124501. [CrossRef]
42. Critchley, W.; Siegert, K.; Chapman, C.; Finket, M. *Water Harvesting: A Manual for the Design and Construction of Water Harvesting Schemes for Plant Production*; Scientific Publishers: Jodhpur, India, 2013.
43. Rallison, R.E. Origin and evolution of the SCS runoff equation. In Proceedings of the Symposium on Watershed Management, Boise, ID, USA, 21–23 July 1980; pp. 912–924.
44. US SCS. *National Engineering Handbook, Section 4: Hydrology*; US Soil Conservation Service, USDA: Washington, DC, USA, 1985.
45. Chow, V.T.; Maidment, D.R.; Mays, L.W. *Applied Hydrology*, 1st ed.; McGraw-Hill: New York, NY, USA, 1988.
46. Sorrell, R.C. *Computing Flood Discharges for Small Ungaged Watersheds*; Michigan Department of Environment, Great Lakes, and Energy (EGLE): Lansing, MI, USA, 2010. Available online: https://www.michigan.gov/documents/deq/wrd-scs_558239_7.pdf (accessed on 25 September 2020).
47. Arnold, J.G.; Srinivasan, R.; Muttiah, R.S.; Williams, J.R. Large area hydrologic modeling and assessment part I: Model development. *JAWRA J. Am. Water Resour. Assoc.* **1998**, *34*, 73–89. [CrossRef]
48. Shadmehri Toosi, A.; Calbimonte, G.H.; Nouri, H.; Alaghmand, S. River basin-scale flood hazard assessment using a modified multi-criteria decision analysis approach: A case study. *J. Hydrol.* **2019**, *574*, 660–671. [CrossRef]
49. Kundu, S.; Khare, D.; Mondal, A. Past, present and future land use changes and their impact on water balance. *J. Environ. Manag.* **2017**, *197*, 582–596. [CrossRef] [PubMed]
50. Deb, P.; Kiem, A.S. Evaluation of rainfall–runoff model performance under non-stationary hydroclimatic conditions. *Hydrol. Sci. J.* **2020**, *65*, 1667–1684. [CrossRef]
51. Ouessar, M.; Sghaier, M.; Mahdhi, N.; Abdelli, F.; De Graaff, J.; Chaieb, H.; Yahyaoui, H.; Gabriels, D. Assessment. An integrated approach for impact assessment of water harvesting techniques in dry areas: The case of Oued Oum Zessar watershed (Tunisia). *Environ. Monit. Assess.* **2004**, *99*, 127–140. [CrossRef] [PubMed]
52. Gary, G. *Design of Individual and Community-Scale Rainwater Harvesting Systems for Domestic Water Use in Austin, Texas*; Department of Civil, Architectural, and Environmental Engineering, The University of Texas at Austin: Arlington, TX, USA, 2013.
53. IRIMO. Iran Metrological Organization. Available online: https://www.irimo.ir/eng/index.php (accessed on 12 January 2021).
54. Rahimi, J.; Malekian, A.; Khalili, A. Climate change impacts in Iran: Assessing our current knowledge. *Theor. Appl. Climatol.* **2019**, *135*, 545–564. [CrossRef]
55. KHRW. Regional Water Company of Khorasan Razavi. Available online: http://www.khrw.ir (accessed on 2 February 2021).
56. Karimi, A.; Haghnia, G.H.; Ayoubi, S.; Safari, T. Impacts of geology and land use on magnetic susceptibility and selected heavy metals in surface soils of Mashhad plain, northeastern Iran. *J. Appl. Geophys.* **2017**, *138*, 127–134. [CrossRef]
57. Jenks, G.F. The data model concept in statistical mapping. *Int. Yearb. Cartogr.* **1967**, *7*, 186–190.
58. Chen, Y.; Yu, J.; Khan, S. The spatial framework for weight sensitivity analysis in AHP-based multi-criteria decision making. *Environ. Model. Softw.* **2013**, *48*, 129–140. [CrossRef]
59. Kazakis, N.; Kougias, I.; Patsialis, T. Assessment of flood hazard areas at a regional scale using an index-based approach and Analytical Hierarchy Process: Application in Rhodope–Evros region, Greece. *Sci. Total Environ.* **2015**, *538*, 555–563. [CrossRef]
60. Kourgialas, N.N.; Karatzas, G.P. A flood risk decision making approach for Mediterranean tree crops using GIS; climate change effects and flood-tolerant species. *Environ. Sci. Policy* **2016**, *63*, 132–142. [CrossRef]
61. Snedecor, G.W.; Cochran, W.G. *Statistical Methods*; Iowa State University Press: Ames, IA, USA, 1967.
62. Saaty, T.L.; Vargas, L.G. *Models, Methods, Concepts & Applications of the Analytic Hierarchy Process*, 1st ed.; Springer: New York, NY, USA, 2001.
63. Oikonomidis, D.; Dimogianni, S.; Kazakis, N.; Voudouris, K. A GIS/remote sensing-based methodology for groundwater potentiality assessment in Tirnavos area, Greece. *J. Hydrol.* **2015**, *525*, 197–208. [CrossRef]
64. Junior, R.V.; Varandas, S.; Fernandes, L.S.; Pacheco, F.A.L. Environmental land use conflicts: A threat to soil conservation. *Land Use Policy* **2014**, *41*, 172–185. [CrossRef]
65. Spiliotis, M.; Skoulikaris, C. A fuzzy AHP-outranking framework for selecting measures of river basin management plans. *Desalin. Water Treat* **2019**, *167*, 398–411. [CrossRef]
66. Adham, A.; Wesseling, J.G.; Riksen, M.; Ouessar, M.; Ritsema, C.J. A water harvesting model for optimizing rainwater harvesting in the wadi Oum Zessar watershed, Tunisia. *Agric. Water Manag.* **2016**, *176*, 191–202. [CrossRef]
67. Saaty, T.L. *The Analytic Hierarchy Process: Planning. Priority Setting. Resource Allocation*; MacGraw-Hill: New York, NY, USA, 1980.
68. Munoz-Carpena, R.; Parsons, J.E.; Gilliam, J.W. Modeling hydrology and sediment transport in vegetative filter strips. *J. Hydrol.* **1999**, *214*, 111–129. [CrossRef]
69. Napolitano, P.; Fabbri, A.G. Single-parameter sensitivity analysis for aquifer vulnerability assessment using DRASTIC and SINTACS. *IAHS Publ.-Ser. Proc. Rep. Int. Assoc. Hydrol. Sci.* **1996**, *235*, 559–566.

70. Bordbar, M.; Neshat, A.; Javadi, S. A new hybrid framework for optimization and modification of groundwater vulnerability in coastal aquifer. *Environ. Sci. Pollut. Res.* **2019**, *26*, 21808–21827. [CrossRef] [PubMed]
71. Nazzal, Y.; Howari, F.M.; Iqbal, J.; Ahmed, I.; Orm, N.B.; Yousef, A. Investigating aquifer vulnerability and pollution risk employing modified DRASTIC model and GIS techniques in Liwa area, United Arab Emirates. *Groundw. Sustain. Dev.* **2019**, *8*, 567–578. [CrossRef]
72. Box, G.E.; Jenkins, G.M.; Reinsel, G.C. *Time Series Analysis: Forecasting and Control*; Holden-Day: San Francisco, CA, USA, 1970.
73. Durbude, D.G.; Venkatesh, B. Site suitability analysis for soil and water conservation structures. *J. Indian Soc. Remote Sens.* **2004**, *32*, 399–405. [CrossRef]
74. Ramakrishnan, D.; Bandyopadhyay, A.; Kusuma, K. SCS-CN and GIS-based approach for identifying potential water harvesting sites in the Kali Watershed, Mahi River Basin, India. *J. Earth Syst. Sci.* **2009**, *118*, 355–368. [CrossRef]
75. Girma, M. Identification of Potential Rainwater Harvesting Areas in the Central Rift Valley of Ethiopia Using a GIS Based Approach. Master's Thesis, Wageningen University, Wageningen, The Netherlands, 2009.
76. Al-Adamat, R.; AlAyyash, S.; Al-Amoush, H.; Al-Meshan, O.; Rawajfih, Z.; Shdeifat, A.; Al-Harahsheh, A.; Al-Farajat, M. The combination of indigenous knowledge and geo-informatics for water harvesting siting in the Jordanian Badia. *J. Geogr. Inf. Syst.* **2012**, *4*, 366–376. [CrossRef]
77. De Winnaar, G.; Jewitt, G.P.W.; Horan, M. A GIS-based approach for identifying potential runoff harvesting sites in the Thukela River basin, South Africa. *Phys. Chem. Earth Parts A/B/C* **2007**, *32*, 1058–1067. [CrossRef]
78. Mbilinyi, B.; Tumbo, S.; Mahoo, H.; Mkiramwinyi, F. GIS-based decision support system for identifying potential sites for rainwater harvesting. *Phys. Chem. Earth Parts A/B/C* **2007**, *32*, 1074–1081. [CrossRef]
79. Mati, B.; De Bock, T.; Malesu, M.; Khaka, E.; Oduor, A.; Meshack, M.; Oduor, V. Mapping the potential of rainwater harvesting technologies in Africa. A GIS overview on development domains for the continent and ten selected countries. *Tech. Man.* **2006**, *6*, 126.
80. Al-Adamat, R. GIS as a decision support system for siting water harvesting ponds in the Basalt Aquifer/NE Jordan. *J. Environ. Assess. Policy Manag.* **2008**, *10*, 189–206. [CrossRef]
81. Prinz, D. Water Harvesting—Past and Future. In *Sustainability of Irrigated Agriculture*; Pereira, L.S., Feddes, R.A., Gilley, J.R., Lesaffre, B., Eds.; Springer: Dordrecht, The Netherlands, 1996; pp. 137–168.
82. Tumbo, S.; Mbillinyi, B.; Mahoo, H.; Mkiramwinyi, F. *Determination of Suitability Levels for Important Factors for Identification of Potential Sites for Rainwater Harvesting*; Sokoine University of Agriculture: Morogoro, Tanzania, 2016.
83. Hatibu, N.; Mahoo, H.F.; Gowing, J.W.; Kajiru, G.; Lazaro, E.; Mzirai, O.; Rockstrom, J.; Rwehumbiza, F.; Senkondo, E. *Rainwater Harvesting for Natural Resources Management: A Planning Guide for Tanzania*; Sida's Regional Land Management Unit: Nairobi, Kenya, 2000.
84. Jasrotia, A.; Majhi, A.; Singh, S. Water balance approach for rainwater harvesting using remote sensing and GIS techniques, Jammu Himalaya, India. *Water Resour. Manag.* **2009**, *23*, 3035–3055. [CrossRef]
85. Selvam, S.; Magesh, N.; Chidambaram, S.; Rajamanickam, M.; Sashikkumar, M.C. A GIS based identification of groundwater recharge potential zones using RS and IF technique: A case study in Ottapidaram taluk, Tuticorin district, Tamil Nadu. *Environ. Earth Sci.* **2015**, *73*, 3785–3799. [CrossRef]
86. Adham, A.; Riksen, M.; Ouessar, M.; Ritsema, C.J.W. A methodology to assess and evaluate rainwater harvesting techniques in (semi-) arid regions. *Water* **2016**, *8*, 198. [CrossRef]
87. Alaghmand, S.; Beecham, S.; Hassanli, A. Impacts of vegetation cover on surface-groundwater flows and solute interactions in a semi-arid Saline floodplain: A case study of the lower Murray river, Australia. *Environ. Process.* **2014**, *1*, 59–71. [CrossRef]
88. NSWRI. National Soil and Water Research Institute of Iran Ministry of Agriculture. Available online: https://www.maj.ir/ (accessed on 18 March 2020).
89. Bathrellos, G.D.; Skilodimou, H.D.; Chousianitis, K.; Youssef, A.M.; Pradhan, B. Suitability estimation for urban development using multi-hazard assessment map. *Sci. Total Environ.* **2017**, *575*, 119–134. [CrossRef] [PubMed]
90. FAO. *Guidelines for Soil Description*, 3rd ed.; Food and Agriculture Organization of United Nations: Rome, Italy, 1990.
91. Steenhuis, T.S.; Winchell, M.; Rossing, J.; Zollweg, J.A.; Walter, M.F. SCS runoff equation revisited for variable-source runoff areas. *J. Irrig. Drain. Eng.* **1995**, *121*, 234–238. [CrossRef]
92. Fernández, D.; Lutz, M. Urban flood hazard zoning in Tucumán Province, Argentina, using GIS and multicriteria decision analysis. *Eng. Geol.* **2010**, *111*, 90–98. [CrossRef]
93. Chang, N.-B.; Parvathinathan, G.; Breeden, J.B. Combining GIS with fuzzy multicriteria decision-making for landfill siting in a fast-growing urban region. *J. Environ. Manag.* **2008**, *87*, 139–153. [CrossRef]